

EDITORS

David Stein (Editor-in-Chief)
LTV Aerospace & Defense Co.
P.O. Box 530685
Grand Prairie, TX 75053-0685

Richard W. Adler, Managing Editor
Naval Postgraduate School
Code 62AB
Monterey, CA 93943

Michael Thorburn, Advertising Editor
Oregon State University
Dept. of Electrical & Computer Engineering
34788 Riverside Drive SW
Albany, OR 97321-9409

Virgil Arens
Arens Applied Electromagnetics
Gaithersburg, MD

James Logan
Naval Oceans Systems Center
San Diego, CA

Robert Bevensee (Editor Emeritus)
Lawrence Livermore Nat'l Lab
Livermore, CA

Ronald Marhefka
Ohio State University
Columbus, OH

Robert Brown
Grumman Corporation
Bethpage, NY

Kenneth Siarkiewicz
Rome Air Development Center
Griffiss AFB, NY

Dawson Coblin
Lockheed Missiles & Space Co.
Sunnyvale, CA

Chris Smith
Kaman Sciences Corp.
Colorado Springs, CO

Edgar Coffey
Advanced Electromagnetics
Albuquerque, NM

Wan-xian Wang
University of Florida
Gainesville, FL

Stanley Kubina
Concordia University
Montreal, Quebec, Canada

THE APPLIED COMPUTATIONAL ELECTROMAGNETICS SOCIETY
JOURNAL and NEWSLETTER

Vol. 2 Number 2

Fall 1987

* FROM THE EDITOR	5
* PRESIDENT'S CORNER	7
* THE NEWSLETTER	
* ACES NEWS	10
* AVAILABLE SOFTWARE by Ted Roach, Editor	14
"Two New MININEC3 Service Programs", by Robert T. Hart	19
"Evaluation of Antenna Programs Written by R. G. Fitzgerrell", by J. K. Breakall	26
* EM MODELING NOTES by Gerald Burke	30
"Comparative Performance of MININEC for Various Computers and Languages", by C. C. Smith	45
* PANDORA'S BOX by Dawson Coblin, Editor	47
"A Comparison of NEC and MININEC on the Stepped Radius Problem", by J. K. Breakall and R. W. Adler	47
* THE JOURNAL	
"Backscattering from a Cube", by Art Ludwig	55
"A Numerical Example of a 2-D Scattering Problem Using a Subgrid, by John C. Kashner and Kane S. Yee	75
"Modeling by NEC of an HF Log-Periodic Antenna", by G. R. Haack	103
"The Computational Expressions of Spheroidal Eigenvalues", by Wan-xian Wang	112
"Near-Fields of a Log-Periodic Dipole Antenna; NEC Modeling and Comparison with Measurements", by K. T. Wong and P. S. Excell ...	122
"The Application of the Conjugate Gradient Method to the Solution of Operator Equations -- an Unconventional Perspective", by Tapan Sarker ..	131
* INSTITUTIONAL MEMBERS	136

©1987, The Applied Computational Electromagnetics Society

**APPLIED COMPUTATIONAL ELECTROMAGNETICS SOCIETY
OFFICERS AND COMMITTEE CHAIRMEN**

OFFICERS:

Edmund Miller
President (1988)
Box 1085
Thousand Oaks, CA 91365

Office (805)373-4297
Home (805)527-6051

James C. Logan
Vice President (1988)
NOSC, Code 822 (T)
271 Catalina Blvd.
San Diego, CA 92152

Richard Adler
Secretary (1988)
Naval Postgraduate School
Code 62AB
Monterey, CA 93943

Office (408)646-2352
Home (408)649-1234

James K. Breakall
Treasurer (1988)
Lawrence Livermore Nat'l Lab
P.O. Box 5504, L-156
Livermore, CA 94550

Office (415)422-8196
Home (415)447-9738

Robert Bevensee
AD COM (1989)
Lawrence Livermore Nat'l Lab
P.O. Box 5504, L-156
Livermore, CA 94550

Office (415)422-6787

Donn Campbell
AD COM (1988)
TRW MIL ELEX DIV
RC2/266 7X
San Diego, CA 92128

Office (619)592-3245

Janet McDonald
AD COM (1988)
US Army
USAISEIC/ASBI-STS
Ft. Huachuca, AZ 85613-7300

Office (602)538-7639
or 538-7680

Ted Roach, Chairman
SOFTWARE EXCHANGE COMMITTEE
Microcube Corp.
Box 488
Leesburg, VA 22075

Office (703)777-7157
Home (703)777-4138

Robert Bevensee, Chairman
CONFERENCE COMMITTEE
Lawrence Livermore Nat'l Lab
P.O. Box 5504, L-156
Livermore,CA 94550

Office (415)422-6787

Janet McDonald, Chairman
NOMINATIONS COMMITTEE
US Army
USAISEIC/ASBI-STS
Ft. Huachuca, AZ 85613-7300

Office (602)538-7639
or 538-7680

David Stein, Chairman
PUBLICATIONS COMMITTEE
P.O. Box 530685
Grand Prairie, TX 75053-0685

Office (214)266-4958
Home (214)641-2404

Welcome to the Fall 1987 issue, which is the first issue published under our new name, the ACES Journal and Newsletter. From among several proposed names (including our former name, which was considered for retention), the Editorial Board chose this one. We decided to act for two reasons. First, several of you indicated that a name change was long overdue, inasmuch as the issue was raised last March at the Third Annual Review. (Although one member indicated that the issue should be decided at the Fourth Annual Review in March 1988, we received no other requests for a decision by membership vote, as offered in our letter of 4 September 1987). Second, our ongoing promotional efforts, which cannot be deferred until March 1988, are better supported by our new name.

We believe that we have selected a name with which almost all of you will be pleased. Nonetheless, if you feel otherwise, then we shall reconsider the issue during the business meeting at the Fourth Annual Review. Please keep in mind, however, that at least two segments of the computational electromagnetics community have manifested themselves within ACES. There are those who wish to share their experiences in applied computational electromagnetics on an informal basis, without stringent criteria for review and publication. These people are best served by a "newsletter". Others, who prefer a more prestigious, established, or formal publication, are better served by a refereed "journal". Our new name recognizes both segments of the community and is therefore "neutral". It is imperative that we not alienate either segment by name or by deed.

Meanwhile, we have identified new opportunities to promote the ACES Journal and Newsletter, so that we may better serve both community segments. We shall capitalize on these opportunities by publishing one or more special issues in the months ahead, beginning in mid-1988. Each special issue will feature papers on a single topic, and some will also feature special guest editors. Your recommendations for special topics are needed -- immediately. The topic for the first special issue will be announced at the Fourth Annual Review in March 1988. (The special issues are in addition to the regular issues).

Other promotional activities have placed your Publications Committee in a unique role -- that of "filling in" for certain other committees. In an effort to include committee reports in this issue, we learned that only three other committees are active: Software, Nominations, and Conferences. While the Membership Committee and Publicity Committee do not appear to exist, they exist in spirit. As we expand the circulation and authorship base of the ACES Journal and Newsletter, we also attract new members. The Publications Committee was instrumental in revising the ACES brochure which is sent to prospective members. The revised version, recently completed, is now being sent to university electrical engineering departments and to people involved in the development of electromagnetic modeling codes. At the same time, we are promoting technical activities by publishing (and in some cases, "recruiting") certain types of papers. You will notice that various papers in this issue validate computational results against other data, computed as well as measured. Another paper, tentatively scheduled for the next issue, bridges some gaps between low- and high-frequency computational methods, in terms of fundamental mechanisms. Of course, we can never be a complete

substitute for any of these committees, nor is this our intent. (However, if you would like to assist in membership, publicity, or technical activities, let the Publications Committee know. Until your committee of interest is functioning autonomously, consider working with us).

Of our other accomplishments to date, two may not yet be apparent. First, our new Advertising Editor, Michael Thorburn, is completing arrangements for advertising. You will observe the results of his efforts in the Spring 1988 and subsequent issues. Secondly, the editorial review has now involved almost every editor. If we were ever a "one-person effort", those days are over.

None of our accomplishments are ends unto themselves. Instead, they enable us to better achieve our existing goals as well as new ones -- one of which is to address long-standing needs in computational electromagnetics. We shall address these needs, primarily by seeking and publishing the appropriate material. There is a place for each of you in this effort, not only to assist but also to be a driving force if you wish. Some of you can submit papers which promote the state-of-the-art in computational electromagnetics. Similarly, papers dealing with inter-disciplinary studies in computational electromagnetics are welcome. Furthermore, we need papers which present solutions to general-interest problems. These papers will help eliminate the need to "re-invent the wheel". (A number of electrical engineers and physicists do not like to waste time solving for themselves an already-solved computational problem. In addition to the waste, there is another consequence -- the proliferation of similar codes, each used by only a few people. Standardization efforts then become more difficult). Let's not forget the need for additional papers dealing with code validation and performance analysis. And remember -- even we do not think of everything!

David E. Stein
Editor-in-Chief

PRESIDENT'S CORNER

E. K. Miller

Where has the year gone? Here it is, almost the end of 1987 and we're finalizing plans for the Spring 1988 Meeting of ACES. This will be our fourth annual review about which you will find more information elsewhere in this Newsletter.

The topic of this column is related to one of the panel discussions planned for the '88 Meeting, the problem of software validation. We are fortunate that Professor Stanley J. Kubina (Concordia University, Electrical Engineering Department, 7141 Sherbrooke Street West, Montreal, Quebec, Canada H4B 1R6, Tel. (514) 848-3093) has agreed to organize and chair this particular panel, as he has been actively involved in this area for some time. If you have any input for panel consideration or would like to participate on the panel, please contact Stan as soon as possible.

The ideas discussed here are extracted from various articles that I've written on modeling in the past. Since they are relevant to the basic issue of validation, I've tried to integrate them into one package. Thus, if some of what follows sounds familiar, the explanation is that you might have seen portions of it before. I should also add that software validation will be the topic of a workshop to be held following the URSI/AP-S Meeting at Syracuse University next June. As mentioned in the December 1987 "PCs for AP" column in the AP-S Newsletter, Prof. Leo Felsen has agreed to serve as co-organizer of that workshop. With the proliferation of modeling codes and computational resources, the importance of facing up to the problem of validation can only increase.

SOFTWARE VALIDATION--Software validation is a complex process the outcome of which establishes the accuracy or reliability of a particular modeling code. In order to place the issue of accuracy into a broader context, we note that modeling software has three principal attributes, accuracy, efficiency and utility, of which accuracy must be considered to be the most important. Above all else, a modeling computation must possess acceptable, preferably known, and better yet "dialable", accuracy. This is an attribute to which all others, however desirable, must be considered to be secondary, for invalid results have no value and can even cause harm.

Therefore, one of the most time consuming and long lasting of the tasks associated with any model development is that of validation to establish the code's accuracy for the various kinds of problems for which it has been designed. Long after work on the model has been completed questions will continue to arise about whether a given result is valid or whether the model can be applied to a given problem. There are essentially two kinds of validation procedures that can be considered to answer such questions, which are:

Internal Validation--A check that can be made concerning solution validity within the model itself.

External Validation--A check that utilizes information from other sources which could be analytical, experimental or numerical.

Existing computer models often do not perform internal checks on the results they produce, but instead leave that as an exercise to the user. For example, NEC (Numerical Electromagnetics Code) one of the more widely used models, could provide and indeed has been exercised to give various kinds of checks relating to power balance, reciprocity and boundary-condition matching. But the software to do this is not an integral part of the code, generally being "patched in" by the user (most often Gerry Burke) for a particular problem and check. It would seem to be of extremely great potential value if a variety of such

checks could be built into the code and exercised as desired by the modeler or determined to be needed by the code itself.

As a particular example of the use to which internal checks could be put, consider the case when a problem new to the modeler is being implemented and the initial results are obtained. Present practice usually involved "eye-balling" the data to see if it feels right, perhaps having first run some documented test cases to verify code performance. Since these test cases would not be likely to closely resemble the new problem, their successful solution would not provide much insight concerning the new results. If however, a series of checks built into the code could then be exercised at the modeler's discretion to verify that conditions necessary for a valid solution of Maxwell's Equations are satisfied, confidence in the model's reliability could increase. These checks might range from being as exhaustive as boundary-condition matching would be, to being fairly simple, such as checking for reciprocity and power conservation. They could only be viewed as necessary but not sufficient conditions for solution validity, and could only involve such behavioral aspects as are not implicit in the model already (e.g., some formulations produce symmetric matrices so that bi-static scattering and transmit-receive reciprocity are assured). It would seem feasible to develop a figure-of-merit from the results of such checks that would provide in a single number a "quality factor" for the solution.

The second kind of check involves use of independent data from other sources. Perhaps the most convincing overall is experimental data, but analytical or numerical results should be comparably useful. Indeed, one of the most convenient computational checks would be provided by a code that permits two different models to be developed for the same problem, for example by incorporating user-selectable basis and weight functions. For greatest utility, such checks ideally should not be of single-point nature, for example to compare results for input impedance at a single frequency. Experience shows that computer models produce results that exhibit slight frequency shifts, angle shifts or spatial shifts in field quantities with respect to "exact" solutions, or even other computer models. Consequently, global comparisons are usually more meaningful, but even then may not be straightforward. If the shifts mentioned are observed, it would seem appropriate to develop a correlation measure to establish the minimum squared difference between the two results as they are shifted along the axis of the common variable. For other models and applications, the results may be even less directly comparable, as is the case for IE and DE modeling approaches. Some work is needed in the general area of how results from two different representations of the same problem can be most meaningfully compared.

ERROR TYPES IN CEM--Finally, the issue of what kinds of errors can occur in CEM deserves discussion and analysis. It is helpful for initial consideration to categorize the various kinds of errors that can render CEM uncertain according to:

Level 0 errors--These are the kinds of errors that keep a program from running to conclusion, and can arise from a variety of causes. They are therefore the most obvious when they occur, but not necessarily the easiest to correct.

Level 1 errors--Errors in this category are those that occur when a program runs to conclusion, where the requested output is produced but it contains obviously incorrect results. A fairly common example is that of obtaining a negative input resistance for an antenna.

Level 2 errors--It is this category of error that is generally most insidious, for a level-2 error is the kind that is probably most difficult to identify and correct. It occurs when the program runs and produces what appear to be physically plausible results, but which are invalid for the problem being modeled. The source of a level-2 error might be a numerical modeling error which arises from obtaining insufficiently accurate numerical results for the model that has been selected, one example being non-converged results. On the other hand, it could be a physical modeling error which arises from an inadequate "match" between the physical reality of interest and the numerical model that has been used.

Level 3 errors--This category of error is user dependent, as it occurs when the modeler mis-interprets or otherwise mis-uses the results produced by the computation. It is reasonably

well accepted for example, that computer models produce results that are generally more accurate on a relative than on an absolute basis. Although the nulls and peaks of a radiation pattern or a transfer function can be shifted between and computation and measurement, as is often the case, the utility of the computer model may be unaffected for purposes of practical application.

Modeling uncertainties or errors of level-3 type can be assigned to two basic error categories, a physical modeling error ϵ_p , and a numerical modeling error ϵ_N . The former is due to the fact that for most problems of practical interest varying degrees of approximation are needed in developing a simplified or idealized problem representation that will be compatible with the computer code to be used for the modeling computations. The latter is due to the fact that the numerical results obtained are almost invariably only approximate solutions to that idealized representation. We note that although an analytical expression may in principle represent a formally exact solution, the process of obtaining numerical results in that case is still one which inevitably involves finite-precision evaluation of the formal solution.

By its very nature, the physical modeling error requires some kind of measurement for its determination, except for those few problems whose analytical solution in principle involves no physical idealization nor subsequent numerical approximation. One example of such problems is that of determining the scattering or radiating properties of the perfectly conducting or dielectric sphere.

The numerical modeling error is itself comprised of two components in general, the determination of which would normally involve one or more kinds of computation. The first and generally more important of these components is the solution error which arises because the computer model used, even if solved exactly, would not provide an exact solution for the idealized problem representation. The solution error arises essentially due to the fact that the computer model is solved using a finite number of unknowns. The other, generally less important contributor to the numerical modeling error is the equation error which arises because the numerical results obtained from the computer model used may not numerically satisfy the modeling equations. The equation error may be caused both by round-off due to the computer word size as well as the solution algorithm employed, as in the case of iteration, for example. The impact of equation error can be expected to increase with increasing condition number of the direct matrix.

CANONICAL BENCHMARKS--Without essentially "exact" results to serve as benchmarks, there will always be some lingering doubts regarding the validity, let alone accuracy, of computer models. Unfortunately, as is well known, there are few closed-form, exact solutions available from classical electromagnetics. For a 3D computer model to match results for a spherical body is hardly convincing anymore that the same model will work as well for a more arbitrary body geometry. But without reference solutions to provide benchmark results, quantification of computer-model accuracy and validity will remain an open question for the most part.

Therefore, some attention must be given to identifying treatments and problems that might be viewed as "primary standards" for comparison purposes, much in the same way that the United States National Bureau of Standards has established standards for various metrological applications. If a set of standards were to be developed for checking computer models using a prescribed methodology, more confidence could eventually be placed in a model that satisfied certain testing criteria.

The idea of test standards might be somewhat novel in the computer world, but it has been used for years in experimentation. Radar scattering ranges, for example, have routinely employed a metal sphere as a target for calibration purposes. Even if the RCS of the sphere were unknown, the measured results could have been calibrated with respect to this basic target. Since the sphere was the first 3D target whose cross section could be quantified in absolute terms, it enabled absolute results to be inferred for unknown targets being measured. What has worked so well in the experimental world is worth examining for how it might contribute to the calibration and validation of computed results.

Discussions dealing with all of the above issues as well as others relevant to "software validation" will be held during the Panel Discussion at the ACES '88 Meeting. We hope to see and hear from you there.

ACES NEWS

1. The 4th Annual Review of Progress in Applied Computational Electromagnetics is scheduled for Tuesday 22 March through Thursday 24 March 1988 at the Naval Postgraduate School, Monterey, CA. Everyone should have received a flyer announcing submission and registration deadlines.
2. Trish Adler, our most able typist, has departed the ACES scene and is now supporting her husband, as he grinds his way through college at BYU. We will miss her, but look forward to Pat Adler picking up the slack. She is "cutting her teeth" on this Journal/Newsletter.
3. The cost of serving non-U.S. members is substantial. Bank charges on conventional foreign checks average \$25 per transaction, so we must restrict foreign members to **BANK DRAFTS** or **INTERNATIONAL MONEY ORDERS**. All foreign correspondence, publications must be sent via air mail. The postage on a copy of the conference proceedings can be as high as \$35.00. We must establish a policy on this at the 4th Annual Review.
4. The publication of this issue of the Journal/Newsletter was delayed for several reasons. One of the reasons is that some authors do not understand what "camera-ready" means. We sometimes receive as camera-ready figures, second-generation shabby xerox copies of what was a marginally acceptable figure in its original form. The editors must then request a clean copy (and even then they do not always get it) or re-do the figures themselves. Sloppy equations require re-typing the entire article, consuming valuable time and delaying publication. Please send **ORIGINAL** figures, even if they are paste-ups. We can do a much better job, faster from any original. If you hate to part with a one-and-only original, we will gladly return them to you if you request. Please do not fold your submissions when mailing them. Most laser-printer/xerox pages suffer from cracked and flaking carbon print and we end up with white streaks along the fold lines.

Announcing

The Fourth Annual Review of Progress in Applied Computational Electromagnetics

at the Naval Postgraduate School
Monterey, CA

March 22 - 24, 1988

Call for Participation

Sponsored by DOD/USAECOM, USAISESA, NOSC and DOE/LLNL
in cooperation with
The Applied Computational Electromagnetics Society (ACES)

The purpose of this Fourth Annual Review is to provide a forum for information exchange among practitioners of applied computational electromagnetics. Contributions by both users and developers of electromagnetic computer modeling codes are solicited, addressing topics pertaining to experience gained in practical applications. Research and development issues are of secondary interest.

The Review will highlight topics related to the design, selection, performance, and implementation of current and emerging electromagnetic modeling codes and techniques.

Suggested topics for presentation include (but are not limited to):

- *NEC, MiniNEC, GTD, Finite Difference, and other code applications and modifications.
- *The use of Graphical input/output in EM modeling.
- *Modeling enhancements and new modeling techniques.
- *Time and frequency domain results
- *Data presentation
- *Error checking
- *Validation of Codes
 - *Experimental
 - *Code comparison
 - *Analytic checks
 - *Solution convergence

*Applications

- *Antenna analysis
- *Internal coupling and shielding
- *Scattering
- *Design studies
- *Sources, network connections, transmission lines
- *Buried conductors and ground interface effects
- *Wire and surface models
- *Educational applications

*Computers

- *User adaptation to new computers and PCs.
- *Precision requirements
- *User interfacing
- *Workstations

Several special-interest sessions will be featured at this year's Review:

1. An EM Code User's panel discussion will be devoted to examples and applications of various codes and suggestions for needed enhancements.
2. A PC Applications Workshop and Poster session will operate each afternoon from 3-5 PM. Several PCs will be available for anyone to use for demonstrating their own codes, enhancements, etc.
3. A Software Validation panel will conduct a discussion of the relative importance of validation by analysis, code comparisons and measurements.

Abstract Deadline: 15 Feb 1988 (Late abstracts cannot be guaranteed inclusion in the program, but may be assigned to the Poster Session).

A camera-ready manuscript version of oral presentations must be provided to the conference committee before presentation. These will be included in the Proceedings of the Review. Presentation time must not exceed 20 minutes; it is preferable to allow some of this time for questions. (Abstract guidelines are included on the reverse side).

Registration fee: Prepaid \$150 (Deadline 5 Mar 1988)
Late registration \$165

Registration fee will provide the attendee with a compilation of abstracts, a one year membership in ACES, and a subscription to the ACES newsletter.

Send Conference remittance and abstracts to: Professor Richard W. Adler
Naval Postgraduate School
Code 62 AB
Monterey CA 93943
(408)-646-2352 (AUTOVON 878-2352)

Make checks payable to: The Applied Computational Electromagnetics Society.
Conference programs will be sent to attendees by 5 March 1988.

INSTRUCTIONS FOR PREPARATION OF ABSTRACTS*

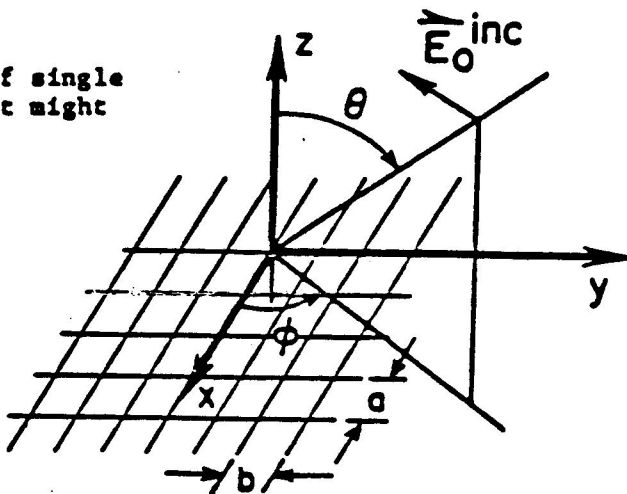
E.K. Miller
P.O. Box 5504, L-153
Lawrence Livermore National Laboratory
Livermore, CA 94550

The abstract should be in the same format as these instructions. Center the heading as indicated above. Capitalize the entire title. The heading and the text should be single-spaced between the heading and the first paragraph and between paragraphs. References should be included parenthetically in the text, for example (A.B. Smith, Radio Sci., 26, 348-392, 1978). To permit photographic reproduction, all material must lie within a rectangle of dimensions 13 by 22 cm.

If the address below the title is not adequate for mailing or if correspondence is to be sent to other than the first author, then please supply the full mailing address. Please submit the original typed abstract and three copies to the address given above.

Deadline for abstract is 15 Feb. Notification of acceptance or rejection will be mailed to the first author or other indicated author shortly thereafter. The advance program including information on accommodations will follow.

(Example of single figure that might be used)



Maximum lower boundary 22 cm below top edge of title.

* We gratefully acknowledge S.W. Maley of the University of Colorado for abstract format.

NOMINATIONS COMMITTEE REPORT

At the Fourth Annual Review of Progress in Applied Computational Electromagnetics, scheduled for 22-24 March 1988 in Monterey, California, we will be electing new officers and AdCom members-at-large. The positions open are President, Vice President, Secretary, Treasurer, and two "at-large" positions. If you would like to be a candidate for any of these positions -- or if you would like to nominate someone else for any position -- contact Janet McDonald, the chairperson of the Nominations Committee. Her address is:

USAISESA/ASBH-SET-P
Ft. Huachuca, AZ 85613-5300,

and her telephones are (602)538-7639/7680.

PUBLICATIONS COMMITTEE NEWS

Beginning in 1988, we shall publish at least one special issue per year, in addition to the two regular issues. These special issues will enable the ACES Journal and Newsletter to capitalize on certain promotional opportunities. At the same time, special issues are a vehicle by which the ACES Journal and Newsletter can play a more active role in support of technical activities.

Each special issue will feature papers on a single topic. Some of the special issues will also have special guest editors. We need your recommendations for suitable topics. Therefore, send your ideas to the Editor-in-Chief

David E. Stein
P.O. Box 530685
Grand Prairie, TX 75063-0685

or telephone (214)266-4309/4590 (days), (214)641-2404 (evenings). The first special issue will be published by mid-1988, and it is necessary to announce the topic at the Fourth Annual Review in March 1988. For this reason, please do not wait until March to send your recommendations; send them now. Furthermore, be specific regarding scope. A proposed topic which encompasses the near-totality of computational electromagnetics is of little value.

AVAILABLE SOFTWARE

Ted Roach

We now show 14 software programs in the library as indicated in the last volume of the newsletter. I have removed program disk #001 as this is practically the same as the Artech House version with only the dimension statements moved and few other changes. Purchasers are directed to Artech House for this program and will then receive some of the other fine program on that disk. I have at MICROCUBE, six of the remaining SOFTWARE LIBRARY programs, namely items 2, 3, 4, 5, 12, and 13. Disk number 013, Miscellaneous, could use some additions. We have no new short basic programs that are in from members that will go on it. I also have a few public domain items that are very handy but would need to get approval from their authors to include. One is LIST.COM that allows one to look through a file with scrolling backward and forward and includes neat features such as word-wrap for any word processor files, conversion of hex to ascii, search and other features. We are also looking at other programs in the library to determine if they should be deleted or kept.

Our efforts since the previous newsletter, have been to recompile some of the previous library programs using Quick-Basic 3. This has provided a good reduction of computer time for those computers that have a math coprocessor installed. We have also cleaned up the file handling on our frequency sweep version of Mininec2 (LIBRARY DISK #002). While most of us are moving to MININEC3 for use on the PC's, I find the sweep program so useful that we will leave it in the library until someone converts MININEC3 to do the same function. For the future, I'd like to also convert our frequency sweep output files to the GRAPS format so that display on the SMITH CHART can be automatic.

One thing that we have noted and need to check further on is the possibility that the Quick-Basic compiler without a coprocessor may be slower than the old BASCOM compiler. For the present we are continuing to work on expanding the array sizes of MININEC files to computers with 640k and 512k of users memory for both the MININEC2 and 3 programs. We note that QUICK-BASIC 4.0 is out and has some interesting new features. Of particular interest to MININEC users, it is supposed to be faster and handle larger arrays, than the previous version 3.0. Redimensioning should be more straight forward if we don't have to divide the larger arrays up into four quadrants. I don't have an upgrade yet. See the short review in PC MAG., 8 Dec. 87 issue, pg 33.

Old library numbers 008 (MININEC3), 009 (GRAPS), and 010 (IGUANA) are now available from Dick Adler. These programs are available in a package deal with documentation included.

The remaining program numbers 006 and 007 are still available from Jim Breakall. Number 011 is still obtained from Dr. Anders and new disk number 014 from Ray Leubers.

There exists a set of three programs for use on the PC that finds Gain, Field Strength, and Isolation for antennas above a ground plane. These were developed by R.G. Fitzgerald of N.B.S. Boulder (retired) and may be of interest to ACES members for data that has been confirmed experimentally over a long period of time. Equations for these programs were obtained from classic antenna articles by Norton, Friis, and others. We can probably get permission to include these in our library. Note: These programs are in FORTRAN and need 640k RAM and DOS 2.1 or later to run.

I see that we finally have a copyright release form for the software library (included back of the last newsletter). I will try to get releases for everything that we have in the library. Anyone who has provided material for the library, please fill out a copy of that form and send it to myself or to Dick Adler.

For your information, I note that in the last few issues of the IEEE Circuits and Devices Magazine, Dr. Miles Copeland is expressing interest in PC software for electrical engineering. This looks like it may develop into a very useful source of information for circuits and network analyses, much as ACES is a source for E/M information. I don't propose that ACES move too far afield from electromagnetics but most of our activities require many disciplines and we might recruit some members for ACES from this group, if we make them aware of our existence. Dr. Copeland is with the Dept. of Electronics at Carleton University in Ottawa, Ontario, Canada.

With the annual meeting coming up in March, 1988, we need to look at how our library can be most useful to our membership. I suspect that there may be other members of ACES who will be very interested in joining the software committee. We probably do not need to limit membership in the committee at this time. Please let me know of your specific area of interest and ability to support this group.

OTHER NOTES:

Library disk 012, the SIGDEMO network analysis demo disk has now been updated with many new features including EGA, joining of points on graphs, automatic optimization at single frequencies of S11, S21, etc. Inductors are still left off the demo version.

The EE PUBLIC DOMAIN LIBRARY which has been providing the public domain software listings from RF DESIGN, MICROWAVES, and other magazines is now up to 17 disks. A price of \$10 per disk saves you from having to type the listing in and gives some preliminary check of operation. Telephone (516)822-1697.

The PC-SIG public domain library is now probably over 800 disks and rapidly climbing. Some that I have received recently were lacking enough documentation to make them usable. However for the most part, these have been well checked out and include some useful programs. Telephone (408)730-9291.

The Proceedings of the 21st Conference of the Central States VHF Society held in July, 87 is now available from HAM RADIO MAGAZINE for \$10.00. This included 28 papers on antennas, amps, filters, VHF and microwave techniques, etc. Looks like a good buy from HAM RADIO, Greenville, NH 03048.

ACES LIBRARY - UPDATE

CURRENT INDEX OF ITEMS IN LIBRARY:

<u>Item#</u>	<u>Description</u>	<u>Computer</u>
001	DELETED	
002	MININEC2F frequency sweep	IBM-PC
003	ENHANCED MININEC2 double ARRAY size to 20 wires, etc.	IBM-PC
004	ENHANCED MININEC2	IBM-PC
005	THIN WIRE MININEC2	IBM-PC
006	NEC2	DEC VAX
007	NEC3	DEC VAX
008	NEEDS MININEC3, NEC-PC, IGUANA, GRAPS	IBM-PC/XT or AT
009	MININEC3/GRAPS	IBM-PC/XT or AT
010	DELETED	
011	NAC3 Dr. Anders MOM code for thin wire antennas, compiled for fully expanded PC up to 800 segments	IBM-PC
012	SIGDEMO Demo disk for Network Analysis, Nodal Analysis/Filter design. A fast, easy to use, moderately priced commercial program	IBM-PC
013	Misc BASIC programs RF Designers Toolbox	IBM-PC
014	AT-ESP Ray Luebbers' full PC implementation of the mainframe ESP Code including graphics using VDI drivers	IBM-PC/XT or AT

"THE NUMERICAL ELECTROMAGNETIC ENGINEERING DESIGN SYSTEM"

NEEDS 1.0

(AVAILABLE only to ACES MEMBERS)

An integrated, menu driven PC software package

combining: MININEC3.11

NEC2-PC (with SOMNEC)

IGUANA 4.1

GRAPS

MININEC3.11

The latest version of MININEC, both regular and co-processor versions.

NEC2-PC

A 300 segment PC version (co-processor required) with useful enhancements.

IGUANA 4.1

The Integrated Graphics Utility for Automated NEC Analysis partially automates the data entry process for NEC2 and MININEC3. The most painless way to learn the input data setup for NEC.

GRAPS

A simple rectangular, polar and Smith Chart plotting package, designed for use in IGUANA.

NEEDS also provides additional convenient tools for data input/output processing with NEC and MININEC.

DOCUMENTATION

User Manuals for all four programs are supplied as part of the NEEDS package.

SOFTWARE

Ten 5 1/4" 360k floppy diskettes supplied.

CONFIGURATION

**Required: IBM PC-XT/640K RAM
CGA graphics
Math Co-Processor (for NEC2-PC)**

**Optional: Graphics compatible dot-matrix printer
(Ex: Epson or HP ThinkJet)
HPGL - compatible pen plotter
Microsoft Mouse (bus version)
Parallel and 2 serial ports
Graph-Bar Sonic Digitizer**

**Cost: \$ 100 to ACES members only. (Foreign members add \$25.)
Make checks payable to The Applied Computational Electromagnetics Society.**

**Order from: Dr. Richard W. Adler
Code 62AB
Naval Postgraduate School
Monterey, CA 93943**

NEEDS contains software from the original #008, #009 and #010 software libraries.

NEEDS becomes #008.

MININEC3 and GRAPS are available to ACES members who do not need nor want IGUANA. The 2 program package is #009 and is \$35 which includes three 5 1/4" floppies with 2 manuals.(Foreign members add \$10.)

TWO NEW MININEC3 "SERVICE PROGRAMS"

Robert T. Hart

DRAW

INTRODUCTION

DRAW is a program written for use on an IBM-PC, and is used in conjunction with MININEC3. An antenna can be analyzed on MININEC3, and pattern data stored on a disc. The DRAW program then uses that data to draw the antenna pattern on the CRT display, and can be copied on a conventional line printer.

An example using the DRAW program is shown in Figure 1. The resolution is limited by the CRT, and a pen plotter will give much higher resolution. However, a pen plotter is not always available and the patterns plotted by the DRAW program are to provide operator convenience.

USAGE

This particular program is limited to applications of the MININEC3 program to plot far-field patterns. A modified DRAW program with appropriate scaling could be used for near-field patterns. No modifications to MININEC3 are required.

PROCEDURE

During the usage of MININEC3, after an antenna configuration has been established and the choice is made to compute far-field patterns, MININEC3 asks for calculation in dBI or volts per meter. Choose d for dBI.

In response to the next prompt, select the pattern angles as follows: for an elevation pattern plot, the zenith angle should be entered as -90,1,180. This zenith angle entry causes the pattern to be plotted from -90 to 90 degrees in steps of 1 degree. For free space patterns, changing 180 to 360 will allow the full pattern plot. The next entry is for azimuth angle and should be entered as X,0,1. X corresponds to the desired azimuth angle for which the particular pattern is to be run.

For an azimuth pattern plot, enter X,0,1, where X is the desired angle for which the azimuth pattern is to be run. Select the azimuth angle as 0,1,360 for a full azimuth plot, or change 0 and 360 for only the desired portion of the azimuth plot in one degree increments.

The next choice on MININEC3 is file pattern (Y/N). Select Y. MININEC3 then asks for a pattern name. For a zenith plot give it the name A:ELPLOT, and for an azimuth plot give it the name A:AZPLOT.

Both the zenith and azimuth plots may be stored on a single disc in the A:drive of the IBM-PC. (Note A: drive must be used to be compatible with the DRAW program). For additional plots, use additional discs. If data has been previously recorded on a disc, it will be erased and the new data stored. For a single antenna it may be desirable to store several patterns, for example several zenith plots at various azimuth angles, before terminating MININEC3. Each disc should be temporarily labeled for future use.

To use the DRAW program, call up BASICA and load the DRAW program. When RUN is executed, the operator has the choice of either an azimuth or elevation plot. Elevation terminology is used rather than zenith, since the plot is labeled in degrees relative to the horizon. (Zenith angle +/-90 degrees).

After selecting elevation or azimuth, the operator is then prompted to select vertical, horizontal, or combined polarization. Since all three are stored on the disc, separate plots can be made in any sequence desired by the operator. At this time it is essential that the data disc be in drive A:.

After the pattern is drawn on the CRT, it may be copied on a conventional line printer such as Epson FX-85 by using the print screen command. However, to copy the screen on a printer, the command "GRAPHICS" from DOS must have been used prior to selecting BASICA. The computer on which the DRAW program was developed included a Hercules Graphics Card.

BASICA Program

The BASICA program "DRAW" is listed on the following page.

R.T. Hart
Senior Principal Engineer
Harris Corporation
PO Box 334
Melbourne, FL 32902

```

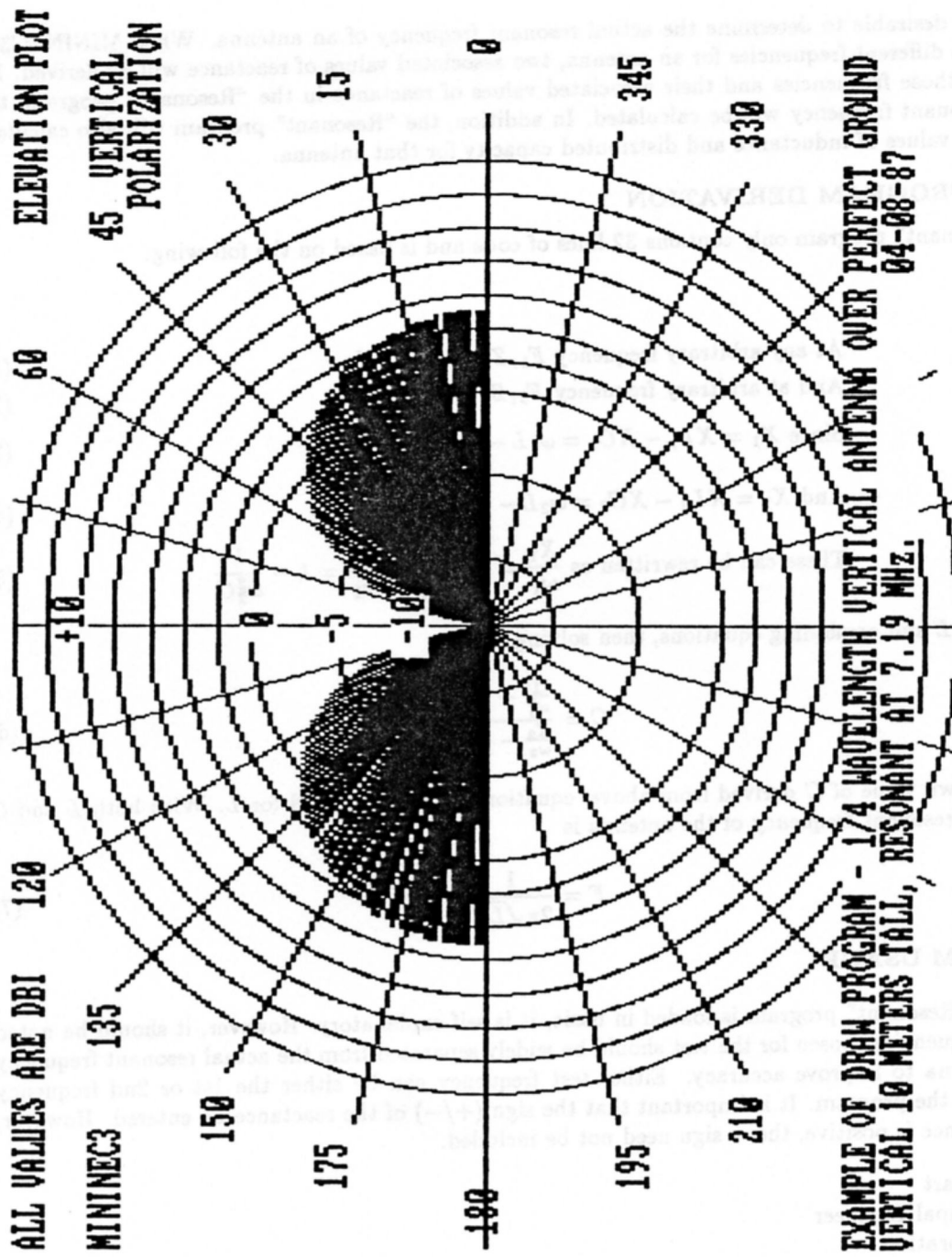
10 REM ***** DRAW IS A BASICA PROGRAM TO BE USED WITH MININEC3 ***
20 CLS :REM USE AN IBM PC WITH A HERCULES GRAPHICS CARD
30 REM THIS PROGRAM WAS DEVELOPED BY R.T. HART W5QJR
40 KEY OFF:PI=3.14159
50 LOCATE 25,1
60 PRINT "TO ESCAPE USE CTRL-BREAK
70 LOCATE 15,12
80 PRINT" DO YOU WANT AN AZIMUTH OR ELEVATION PLOT ? INPUT A OR E ";
90 A$=INPUT$(1)
100 CLS:LOCATE 10,10
110 PRINT " SELECT EITHER VERTICAL, HORIZONTAL, OR A COMBINED PLOT "
120 PRINT:PRINT
130 PRINT " FOR THE HORIZONTAL POLARIZATION COMPONENT SPECIFY - ----- H"
140 PRINT
150 PRINT " FOR THE VERTICAL POLARIZATION COMPONENT SPECIFY -----V"
160 PRINT
170 PRINT " IF YOU WANT TO COMBINE VERTICAL AND HORIZONTAL SPECIFY ---C"
180 HVC$=INPUT$(1)
190 CLS:SCREEN 2: REM FOLLOWING STEPS DRAW THE PLOT FORMAT
200 IF A$="A" THEN PRINT "ALL VALUES ARE DBI
AZIMUTH PLOT
ELEVATION PLO
VERTICAL
HORIZONTAL
COMBINED
POLARIZATION"
POLARIZATION"
POLARIZATION"

210 IF A$="E" THEN PRINT "ALL VALUES ARE DBI
T"
220 IF HVC$="V" THEN PRINT "MININEC3
POLARIZATION"
230 IF HVC$="H" THEN PRINT "MININEC3
POLARIZATION"
240 IF HVC$="C" THEN PRINT "MININEC3
POLARIZATION"

250 FOR D=0 TO 360 STEP 15
260 AB$="TA=D;NU110"
270 DRAW "X"+VARPTR$(AB$)
280 NEXT D
290 CIRCLE (320,100),240
300 CIRCLE (320,100),223
310 CIRCLE (320,100),206
320 CIRCLE (320,100),189
330 CIRCLE (320,100),171
340 CIRCLE (320,100),154
350 CIRCLE (320,100),137
360 CIRCLE (320,100),120
370 CIRCLE (320,100),77
380 CIRCLE (320,100),34
390 LOCATE 7,40:PRINT " 0 "
400 LOCATE 2,40:PRINT "+10"
410 LOCATE 11,39:PRINT "-10"
420 LOCATE 9,39:PRINT "-5"
430 LOCATE 13,78:PRINT "0"
440 LOCATE 9,75:PRINT "15"
450 LOCATE 6,72:PRINT "30"
460 LOCATE 3,66:PRINT "45"
470 LOCATE 1,57:PRINT "60"
480 LOCATE 1,23:PRINT "120"
490 LOCATE 3,14:PRINT "135"
500 LOCATE 6,8:PRINT "150"
510 LOCATE 9,5:PRINT "175"
520 LOCATE 13,2:PRINT "180"
530 LOCATE 17,5:PRINT "195"
540 LOCATE 20,8:PRINT "210"
550 LOCATE 23,14:PRINT "225"
560 LOCATE 23,66:PRINT "315"
570 LOCATE 20,72:PRINT "330"
580 LOCATE 17,75:PRINT "345"
590 IF A$="A" THEN 840:REM FOLLOWING STEPS PLOT THE ELEVATION DATA
600 CLOSE #1
610 FILE$="A:ELPLOT.OUT"
620 OPEN FILE$ FOR APPEND AS 1
630 PRINT #1,500;"",500;"",500;"",500;"",500
640 CLOSE #1
650 OPEN FILE$ FOR INPUT AS #1
660 INPUT #1, Q2,Q1,P1,P2,P3
670 IF Q1=500 THEN 1090
680 IF Q2=500 THEN 1090
690 IF P1=500 THEN 1090
700 IF P2=500 THEN 1090
710 IF P3=500 THEN 1090

```

```
720 IF HVC$="H" THEN Y=Q1
730 IF HVC$="V" THEN Y=Q2
740 IF HVC$="C" THEN Y=P1
750 IF Y<-14 THEN Y=-14
760 X=50+50/14*Y
770 IF P2<0 THEN B=ABS(P2)
780 IF P2=0 THEN B=0
790 IF P2>0 THEN B=0-P2
800 DRAW "BM320,100"
810 AC$="TA=B;U=X;"
820 DRAW "X"+VARPTR$(AC$)
830 GOTO 660
840 CLOSE #1:REM STEPS 76 TO 99 PLOT THE AZIMUTH DATA
850 FILE$="A:AZPLOT.OUT"
860 OPEN FILE$ FOR APPEND AS 1
870 PRINT #1,500;" ";500;" ";500;" ";500;" ";500
880 CLOSE #1
890 OPEN FILE$ FOR INPUT AS #1
900 INPUT #1, Q2,Q1,P1,P2,P3
910 IF Q1=500 THEN 1090
920 IF Q2=500 THEN 1090
930 IF P1=500 THEN 1090
940 IF P2=500 THEN 1090
950 IF P3=500 THEN 1090
960 IF HVC$="H" THEN Y=Q1
970 IF HVC$="V" THEN Y=Q2
980 IF HVC$="C" THEN Y=P1
990 IF Y<-14 THEN Y=-14
1000 X=50+50/14*Y
1010 B=P3+270
1020 IF B<360 THEN 1040
1030 B=P3-90
1040 DRAW "BM320,100"
1050 AC$="TA=B;U=X;"
1060 DRAW "X"+VARPTR$(AC$)
1070 GOTO 900
1080 REM STEPS 101-104 OVERWRITE THE VALUES FOR DBI AFTER PLOTTING
1090 LOCATE 7,40:PRINT " 0 "
1100 LOCATE 2,40:PRINT "+10"
1110 LOCATE 11,39:PRINT "-10"
1120 LOCATE 9,39:PRINT "-5 "
1130 LOCATE 23,1
1140 PRINT " DEFINE THIS DRAWING - USE MAXIMUM OF 2 LINES - COPY BEFORE HITTING RETURN "
1150 REM FOR LINE PRINTER - COPY BY USING PRINT SCREEN WITH GRAPHICS
1160 LOCATE 23,1
1170 INPUT Z$
1180 CLS
1190 GOTO 20
```



INTRODUCTION

It is often desirable to determine the actual resonant frequency of an antenna. When MININEC3 is run at two different frequencies for an antenna, two associated values of reactance will be derived. By inputting those frequencies and their associated values of reactance in the "Resonant" program, the actual resonant frequency will be calculated. In addition, the "Resonant" program will also calculate the actual values of inductance and distributed capacity for that antenna.

BASIC PROGRAM DERIVATION

The "Resonant" program only contains 32 lines of code and is based on the following:

$$\text{At any arbitrary frequency } F_1, Z_1 = R_1 + jX_1 \quad (1)$$

$$\text{And at arbitrary frequency } F_2, Z_2 = R_2 + jX_2 \quad (2)$$

$$\text{Since } X_1 = XL_1 - XC_1 = \omega_1 L - \frac{1}{\omega_1 C} \quad (3)$$

$$\text{And } X_2 = XL_2 - XC_2 = \omega_2 L - \frac{1}{\omega_2 C} \quad (4)$$

$$\text{These can be rewritten as } \frac{X_1}{\omega_1} = L - \frac{1}{\omega_1^2 C}, \frac{X_2}{\omega_2} = L - \frac{1}{\omega_2^2 C} \quad (5)$$

Solving for L and combining equations, then solving for C ,

$$C = \frac{\frac{1}{\omega_1^2} - \frac{1}{\omega_2^2}}{\frac{X_2}{\omega_2} - \frac{X_1}{\omega_1}} \quad (6)$$

With a known value of C derived from above, equation (5) can be solved for L . With both L and C known, the resonant frequency of the antenna is

$$F = \frac{1}{2\pi\sqrt{LC}} \quad (7)$$

PROGRAM USAGE

When the "Resonant" program is loaded in basic, it is self explanatory. However, it should be noted that the frequencies chosen for the test should be widely separated from the actual resonant frequency of the antenna to improve accuracy. Either test frequency can be either the 1st or 2nd frequency entered into the program. It is important that the sign (+/-) of the reactance be entered. However, if the reactance is positive, the + sign need not be included.

Robert T. Hart
 Senior Principal Engineer
 Harris Corporation
 PO Box 334
 Melbourne, Florida 32902


```

10 CLS
20 LOCATE 2,33
30 PRINT "RESONANT"
40 LOCATE 5,1
50 PRINT " THIS PROGRAM ALLOWS DETERMINATION OF THE RESONATE FREQUENCY,THE INDUCTANCE,AND THE DISTRIB
UTED CAPACITY OF AN ANTENNA. INPUT DATA NEEDED IS THE REACTANCE VALUE OF THE ANTENNA AT TWO FREQUENCIES
FROM MININEC3."
60 LOCATE 9,1
70 PRINT " INPUT 1st TEST FREQUENCY (MHz)";
80 INPUT F1
90 PRINT " INPUT VALUE OF REACTANCE AT 1st TEST FREQUENCY (USE PROPER SIGN)";
100 INPUT X1
110 PRINT " INPUT 2nd TEST FREQUENCY (MHz)";
120 INPUT F2
130 PRINT " INPUT VALUE OF REACTANCE AT 2nd TEST FREQUENCY (USE PROPER SIGN)";
140 INPUT X2
150 W1=F1*1000000!*2*3.1416
160 W2=F2*1000000!*2*3.1416
170 C=(1/W1^2-1/W2^2)/(X2/W2-X1/W1)
180 CC=FIX(C*1E+12)
190 L=X1/W1+1/(W1^2*C)
200 LL=(FIX(L*1E+09))/1000
210 FR=1/(2*3.1416*((L*C)^.5))
220 FF=(FIX(FR*.0001))/100
230 PRINT:PRINT
240 PRINT " TEST FREQUENCY 1 WAS";F1;"MHz WITH X=";X1;"OHMS"
250 PRINT " TEST FREQUENCY 2 WAS";F2;"MHz WITH X=";X2;"OHMS"
260 PRINT " ACTUAL VALUE OF INDUCTANCE IS";LL;"MICROHENRYS"
270 PRINT " VALUE OF DISTRIBUTED CAPACITY IS";CC;"pfd"
280 PRINT " SELF RESONANT FREQUENCY OF THE ANTENNA IS";FF;"MHz"
290 LOCATE 22,30
300 PRINT "END OF PROGRAM"
310 END
320 REM RESONANT PROGRAM WRITTEN BY TED HART, HARRIS CORPORATION

```

RESONANT

THIS PROGRAM ALLOWS DETERMINATION OF THE RESONATE FREQUENCY,THE INDUCTANCE, AND THE DISTRIBUTED CAPACITY OF AN ANTENNA. INPUT DATA NEEDED IS THE REACTANCE VALUE OF THE ANTENNA AT TWO FREQUENCIES FROM MININEC3.

```

INPUT 1st TEST FREQUENCY (MHz)? 7
INPUT VALUE OF REACTANCE AT 1st TEST FREQUENCY (USE PROPER SIGN)? -19.69284
INPUT 2nd TEST FREQUENCY (MHz)? 10
INPUT VALUE OF REACTANCE AT 2nd TEST FREQUENCY (USE PROPER SIGN)? 246.6903

```

```

TEST FREQUENCY 1 WAS 7 MHz WITH X=-19.69284 OHMS
TEST FREQUENCY 2 WAS 10 MHz WITH X= 246.6903 OHMS
ACTUAL VALUE OF INDUCTANCE IS 8.128 MICROHENRYS
VALUE OF DISTRIBUTED CAPACITY IS 60 pfd
SELF RESONANT FREQUENCY OF THE ANTENNA IS 7.19 MHz

```

END OF PROGRAM

by

J. K. Breakall
Lawrence Livermore National Laboratory
Livermore, CA

Ted Roach, in a letter to members of the ACES Software Exchange Committee, asked if someone could review and evaluate the programs on a disk he received, written by R. G. FitzGerrell at NBS, Boulder some time ago. While on a trip to visit with Dick Adler at the Naval Postgraduate School in Monterey, Dick provided me the use of his fine PC equipment to look through the disk and run some of the programs. There are two programs I found of interest and decided to compare them with MININEC and NEC. They have apparently been updated and converted to FORTRAN 77 on the PC, from versions that had previously resided on the mainframe. I will not go into detail describing each of these and just present my findings since there is a readme file with plenty of description and references on these codes.

The first program is called GAIN77 and it computes the impedance and gain of either horizontal or vertical dipoles in free space and over perfect and imperfect ground. It also will compute results for a monopole over perfect ground. The dipole or monopole can either have a constant radius or be tapered from the feed point to the tip. I tried the following cases and show the MININEC results for each. I should mention that GAIN77 uses the sinusoidal current distribution assumption while MININEC performs a full boundary value solution using the Method of Moments. I believe that GAIN77 must use the Fresnel reflection coefficient method for ground effects with some modification to the impedance results. MININEC models the antenna as if it were over perfect ground for impedance and then calculates radiation with the Fresnel reflection coefficient method. Therefore both should do poorly when the antennas are close to ground. NEC of course, with its Sommerfeld approach could handle the close ground situation with no problem.

I modeled a horizontal dipole in free space with a length of .5 wavelengths and radii of .001 and .00001 wavelengths with both codes. Then I modeled the thinner dipole over perfect ground at the heights of .05 and .5 wavelengths, since results were worse for the thicker antenna in free space, as expected, because of the sinusoidal assumption. The same dipole was then modeled over lossy ground, dielectric constant of 15 and conductivity of .01 Siemens/meter at the same heights. A vertical .5 wavelength dipole at a height of .3 wavelengths is modeled next over the same lossy ground. An example of tapering was tried on a .5 wavelength dipole in free space with the radius varying from .0005 at the center to .00025 wavelengths at the tips.

The results follow:

Configuration	GAIN77		MININEC3	
	Impedance	Gain	Impedance	Gain
.5 Lambda Dipole Free Space a=.001	75.7+j57.6	2.0	79.9+j38.8	2.1
a=.00001	74.5+j43.8	2.1	75.7+j45.4	2.1
.5 Lambda Horizontal Dipole Perfect Gnd a=.00001 Ht=.05	7.1+j36.3	8.1 at 90 deg el	5.9+j38.8	9.0 at 90 deg el
Ht=.5	70.5+j26.1	8.3 at 30 deg el	70.6+j27.5	8.4 at 30 deg el
.5 Lambda Horizontal Dipole Epsilon=15 Conduct=.01 Lossy Gnd Ht=.05	34.7+j39.8	1.4 at 90 deg el	5.9+j38.8	9.2 at 90 deg el
Ht=.5	72.0+j33.4	7.2 at 30 deg el	70.6+j27.5	7.3 at 30 deg el
.5 Lambda Vert Dipole Epsilon=15 Conduct=.01 Ht=.3 Lossy Gnd	83.1+j41.4	1.2 at 20 deg el	107.5+j44.7	.9 at 20 deg el
.5 Lambda Tapered Dipole a=.0005 to .00025 Free Space a=.0005 constant	75.3+j48.6		72.5+j1.2	
	75.4+j52.5		78.7+j40.0	

HEIGHTS AND RADII IN WAVELENGTHS

As can be seen from the results, the agreement is good for the thin dipole in free space, within about an Ohm for both the real and imaginary parts of the impedance and the gain is within a tenth of a dB. Over perfect ground at the lowest height the results again are in good agreement in impedance within about 2 Ohms and a dB in gain. The .5 wavelength height results are very close. Over lossy earth the MININEC results for impedance will of course be the same as over perfect ground since there is no interaction of the lossy ground on the impedance matrix taken into account. The gain for MININEC at the lower height looks too high, which one could expect from the Fresnel method breaking down at such low heights. One would have to run NEC with the Sommerfeld method to see how close the GAIN77 answers are at this height. They look reasonable.

At the .5 Lambda height the results agree within 5 Ohms in Impedance and a tenth of a dB in gain. This indicates that the effect of the ground on impedance, whether lossy or perfect, is minimal at the .5 wavelength height. There is only about a dB reduction of gain over this type of ground also for horizontal polarization at this height. For the vertical dipole at .3 wavelengths height the real part of the impedance is about 20 Ohms different from the MININEC perfect ground case. The gain for both codes are in excellent agreement.

The tapered dipole in free space was modeled in MININEC using a 2 section stepped radius change with the thicker section in the center of the dipole. The real part of the impedance is in agreement, but the imaginary part is quite different. A dipole of constant radius is also shown for comparison. The topic of tapering is discussed in more detail in another paper in this same issue of the Journal/Newsletter by R. Adler and myself.

The other code looked at is called PROSE77 and calculates field strength including the near and surface fields of either a horizontal or a vertical dipole versus distance (E vs d) over perfect or lossy ground. I modeled a vertical .5 wavelength dipole at 1 MHz (150 meters long) at a height of 90 meters over perfect and lossy ground and compared results with NEC3. I used a radius of .001 meters and looked at the field at distances of 1 to 5 Km. One thing I discovered with PROSE77 is that the radiated power is not printed out so it is not possible to compute absolute field strength for some input power which would be most useful. If one looks into this in the references the normalizations used will probably appear and make sense. I simply normalized the NEC3 results to the first distance of 1 Km.

The results follow:

Configuration	Distance (m)	Total E-field in (mVolts/M)	
		PROSE	NEC3
.5 Lambda Vert Dipole Ht=90m, 1MHz Perfect Gnd			
Field pt Ht=10m	1000	11.6	11.6
	2000	5.8	5.9
	3000	3.9	3.9
	4000	2.9	3.0
	5000	2.3	2.4
		Z=89.2+j40.8	Z=92.8+j40.2

Same Antenna over Lossy Gnd Epsilon=15 Conduct=.01			
	1000	10.6	10.6
	2000	5.1	5.2
	3000	3.3	3.5
	4000	2.4	2.6
	5000	1.9	2.1
		Z=87.2+j39.9	Z=85.5+j21.0

As can be seen from the results the field drop-offs agree very well. To really make this PROSE77 code more useful, however, one would like to be able to determine absolute field strengths as well for some fixed input power. This code is still much faster and easier than using NEC3 if one simply wants to see relative field drop-off for a certain ground and polarization of an antenna at a specific height.

In closing, I hope this short review and evaluation of these codes has been informative and helpful and I would recommend that they be included in the Software Library.

EM Modeling Notes*

Gerald Burke
Lawrence Livermore National Laboratory
Livermore, CA 94550

"EM Modeling Notes" was missing from the last ACES Newsletter due to lack of time for writing, but the previous issue contained a discussion of recent work to improve accuracy of the antenna code NEC in VLF applications. Further progress in this area is described here with results showing the improvements as well as how bad the present code can be for small loops. This column also includes a comparison of NEC results for a horizontal wire over ground with the eccentrically insulated transmission line model of R. W. P. King [1]. NEC results are in excellent agreement with King's which have been validated by measurements. While there are certainly situations involving complex antennas over ground that may trip up NEC, this confirmation for a horizontal wire adds some additional reassurance.

An expanded report of the VLF modifications described in the last column has now been written [2], and the resulting code NEC3VLF is working well in checkout. It has not yet become the standard version of NEC-3 for distribution, but the modifications will be included in the next update. Progress has now been made in fixing the loop problems demonstrated in the last column by implementing loop basis and weighting functions. The need for loop bases and weights has been noted previously [3] for a Galerkin method-of-moments code similar to MININEC. These changes were more messy to implement than the previous ones in NEC3VLF due to the problems of locating small loops within a complex wire structure and the interaction of the changes with other code functions such as solutions for symmetric structures and grounds. A code with the option for loop bases and weights is now operational, and while more work is needed before it is bug free for arbitrary models, we can demonstrate the benefits and the severity of the problems in the present code.

Implementation of Loop Basis and Weighting Functions

The difficulty in modeling loops is easily seen when the electric field of a wire is written as

$$\vec{E}(\vec{r}) = \frac{-j}{4\pi\omega\epsilon} \left[\nabla \int_{\ell} \frac{e^{-jkR}}{R} \frac{\partial I(s')}{\partial s'} ds' + k^2 \int_{\ell} \frac{e^{-jkR}}{R} \hat{s}' I(s') ds' \right]. \quad (1)$$

As frequency is reduced the field of the spline basis function, as used in NEC, is dominated by the first term in Eq. (1) which comes from the gradient of the scalar potential. The second term decreases as ω^2 relative to the first. However, the sum of equal basis functions around a loop is a constant current with zero derivative, so that the first term in (1) vanishes. Thus the sum of matrix columns representing the spline basis functions around

* Work performed under the auspices of the U. S. Department of Energy by the Lawrence Livermore National Laboratory under Contract W-7405-Eng-48.

the loop is much less than the individual columns resulting in an ill-conditioned matrix. With unlimited precision the basis functions used in NEC could handle arbitrarily small loops. In single precision, however, accuracy is quickly lost as frequency is reduced.

The problem is still worse when a loop is excited by coupling to a source such as a dipole that produces a large scalar potential. The loop current is then determined by the line integral around the loop of the field of the dipole. At low frequency the dipole field is dominated by the gradient term in Eq. (1) which must vanish in the line integral around the closed loop. Hence the sum of matrix rows representing loop segments is much less than the individual rows, indicating an ill-conditioned matrix. This problem in NEC is worse than the degeneracy of the basis function fields since the integral of \vec{E} around the loop is sampled in a relatively crude form as the sum of the fields at the centers of segments. Hence, use of double precision does not help the solution for a loop coupled to a dipole, and large, incorrect loop currents can result. This problem may occur whenever a wire end with large charge density is near a small loop.

The basis function problem can be fixed by replacing one of the spline basis functions on each loop with a constant function around the loop. At low frequencies the loop basis function is then dominant in the solution with the remaining spline functions accounting for small variations in the current. This change was easily implemented in NEC3VLF since a constant current on each segment is a component of the normal spline basis functions. The fields due to point charges on the segment ends were dropped in NEC3VLF, so the field of the constant current involves only the vector potential as is needed for the loop.

Loop basis functions can also be used on electrically large loops since replacing one spline basis function with a constant loop function does not change the space spanned by the basis. The constant function is exactly equal to an equal amplitude sum of the spline functions. However, care is needed when using loop basis functions on joined loops which have two or more segments in common since discarding more than one spline function on the shared segments will result in a singular matrix.

Use of a loop basis function in NEC is sufficient to obtain accurate results for a loop containing a voltage source. When the excitation is from an external source, such as a dipole, a loop weighting function is also needed to accurately sample the field inducing current in the loop. In implementing the loop weighting function the gradient of the scalar potential is dropped from the field evaluation since it must vanish when integrated around a closed loop. With an accuracy and effort compatible with the point matching normally used in NEC, the line integral of \vec{E} around the loop is then approximated as the sum of the vector potentials at the centers of segments. The equation for a loop weighting function is then

$$j\omega \sum_{j=1}^N \alpha_j \sum_i \hat{s}_i \cdot \vec{A}_j(\vec{r}_i) = \sum_i \hat{s}_i \cdot \vec{E}^I(\vec{r}_i)$$

where α_j is the unknown amplitude of basis function j and the summation on i covers all segments in the loop. \vec{A}_j is the vector potential due to basis function j , including spline and loop functions, and \vec{E}^I represents a source field due to an incident wave or voltage

sources in the loop.

The loop-weighted equation replaces one of the point-matched equations, typically for the same segment on which the spline basis function was removed for the loop basis function. The loop-weighted equation, on which we have assumed an exact integral of the gradient of the scalar potential, cannot be constructed from a sum of the normal delta function weighted equations. Hence, unlike loop basis functions, use of a loop weighting function will change the results for either small or large loops. On small loops the change should be the elimination of errors in the old code. On larger loops some asymmetry may be introduced into the current on an otherwise symmetric loop, but such effects should be within the bounds of convergence of the solution.

A tricky problem in implementing loop basis and weighting functions is that of locating all loops in a complex wire structure. A preliminary code was developed for this task, although further work is needed. For each segment in a structure the code attempts to trace a loop of connected segments. At each junction it chooses the segment that is most nearly directed back toward the starting point. If a free end is encountered it backs up to the last multiple-wire junction and tries another path, however, at present it gives up after the second attempt. If a loop that it has found has already been found from a different starting segment it discards it without checking whether another loop could be traced from the present starting segment. Also, it does not presently find loops that are closed by connection to a ground plane and may not avoid situations that lead to a singular matrix. Clearly this is a tricky problem. Maybe we can borrow something from some other code (circuits?). Another approach would be to let the user specify the loops for loop bases and weights. This could most easily be done in an interactive graphics system such as IGUANA's Model Builder.

In the new code, the check for loops and the use of loop basis and weighting functions is activated by entering a non-zero value as the first real number on the GE card in the NEC input data. The value entered sets the upper limit on the perimeter of loops that will be found.

Results for Small Loops

The coding for loop basis and weighting functions was added to the NEC3VLF code described in [2]. All NEC3VLF results shown here were computed in 32-bit single precision, while NEC-3 results are from the double precision version (NEC-3D) unless otherwise stated. Validation of results for small loops is more difficult than for open wires since the double precision NEC-3, which was used as a standard for dipoles, may give the same wrong results as single precision for loops. The most useful checks on the solution for loops were found to be convergence as the number of segments is increased, the average gain as a check of radiated power versus input power and correction of obviously wrong results for decreasing frequency.

The first structure considered was a loop antenna excited by a voltage source. In this case the VLF limitation is due to the degeneracy of the fields of the spline basis functions

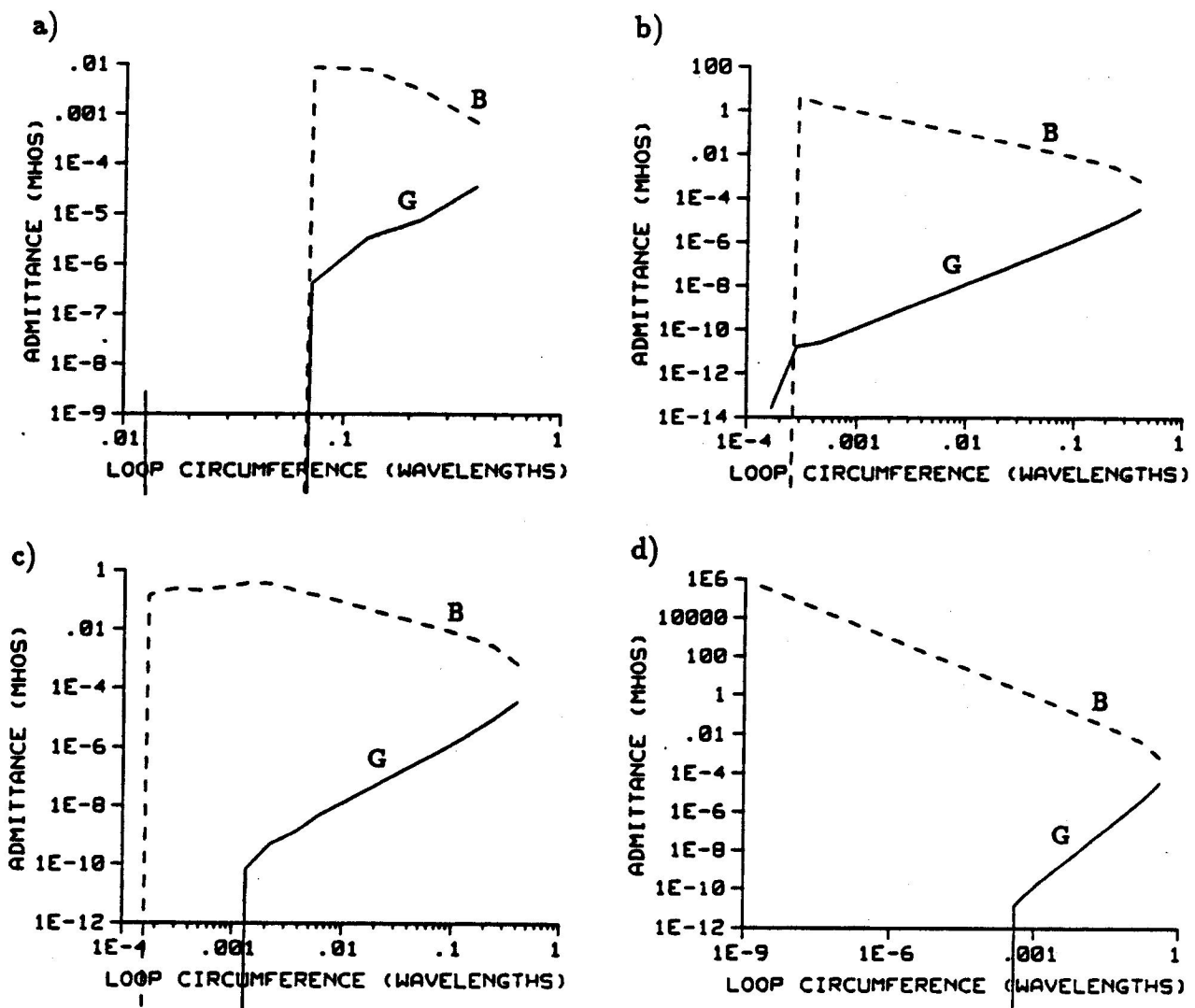


Fig. 1. Input admittance of a loop antenna computed by a) NEC-3 in single precision, b) NEC-3 in double precision, c) NEC3VLF and d) NEC3VLF with loop basis and weighting functions. The loop was modeled with 22 segments and the ratio of wire radius to loop radius was $4.2(10^{-2})$. Solution failure is shown by deviation from the low frequency asymptotic behavior

rather than the field sampling. Use of double precision in NEC-3 does reduce the low frequency limit in this case at the expense of increased computation time and storage. As shown in Fig. 1, NEC3VLF with loop basis and weighting functions gives the correct behavior for input conductance to about the same limiting frequency as double precision NEC-3. The new code appears to have no limitation for computation of input susceptance. Hence after the solution for conductance fails the correct value can be determined by integrating the far-field power on an otherwise lossless antenna. The reason for failure of the conductance at a circumference of about $4(10^{-4})\lambda$ has not been isolated, but may be unavoidable given the difference in magnitude from the susceptance.

A square loop excited by a driven dipole was modeled to test convergence on a fixed structure. For a loop with perimeter of 0.4λ the results in Fig. 2, from NEC3VLF with loop basis and weighting functions, are reasonable for one segment per side and converge

rapidly. Results from double precision NEC-3 in Fig. 3 show a large error for one segment per side but are reasonably well converged with ten to twenty segments per side. When the frequency is reduced so that the loop perimeter is 0.04λ the NEC3VLF results in Fig. 4 show the same convergence as at the higher frequency while the NEC-3 results in Fig. 5 have not converged with twenty segments per side. The dipole was modeled with three segments in all of these cases.

The incorrect loop currents have little effect on the dipole current until they become very large. Even the large loop current with one segment per side in Fig. 5 produced only a 14 percent perturbation in the input resistance and negligible change in the susceptance of the dipole. The average gain for this case was 11, however. Hence this is an unusual case where the integral of radiated power, although a stationary function of current, is overwhelmed by the gross errors in current and is less accurate than the computed input power.

In the NEC3VLF results of Figs. 2 and 4 the match point on the left-hand segment on the lower side of each loop has been replaced by the loop weighting function. This introduces some asymmetry into the current which should be symmetric about d/λ of 0.05 and 0.25 in Fig. 2. The asymmetry is most apparent for 2 segments per side and decreases with convergence as the number of segments is increased.

The next structure modeled was a loop connected to a stub antenna as shown in Fig. 6. The NEC-3 result in Fig. 6a shows an incorrect loop current which grows as f^{-2} relative to the stub current as frequency is reduced. NEC3VLF with loop basis and weighting functions maintains the current distribution shown in Fig. 6b with the current decreasing linearly with frequency. The results for input impedance and average gain are shown in Table 1.

Table 1. Input impedance and average gain of the stub antenna on a loop in Fig. 6 computed by NEC-3 in double precision and NEC3VLF with loop basis and weight functions. C is the circumference of the loop.

C/ λ	NEC-3D			Loop Basis and Wt. Functions		
	R (ohms)	X (ohms)	\bar{G}	R (ohms)	X (ohms)	\bar{G}
6.26(10 ⁻¹)	2.22(10 ¹)	-6.30(10 ²)	0.90	2.13(10 ¹)	-6.58(10 ²)	0.88
6.26(10 ⁻²)	1.19(10 ⁻¹)	-8.65(10 ³)	1.14	1.15(10 ⁻¹)	-8.89(10 ³)	0.88
6.26(10 ⁻³)	1.18(10 ⁻³)	-8.67(10 ⁴)	24.9	1.14(10 ⁻³)	-8.91(10 ⁴)	0.88
6.26(10 ⁻⁴)	1.18(10 ⁻⁵)	-8.67(10 ⁵)	2400.	1.14(10 ⁻⁵)	-8.91(10 ⁵)	0.88
6.26(10 ⁻⁵)	-6.25(10 ⁻⁶)	-8.70(10 ⁶)	-0.5	1.14(10 ⁻⁷)	-8.91(10 ⁶)	0.88

Finally, a stub antenna was modeled on a wire grid fin similar to the probe on some aircraft tails. As shown in Fig. 7, the NEC-3 result had an incorrect clockwise circulation of current on the grid while NEC3VLF with loop basis and weighting functions produced a uniform flow of current toward the stub. As frequency is reduced the circulating current from NEC-3 grows as f^{-2} relative to the stub current while the NEC3VLF result remains stable.

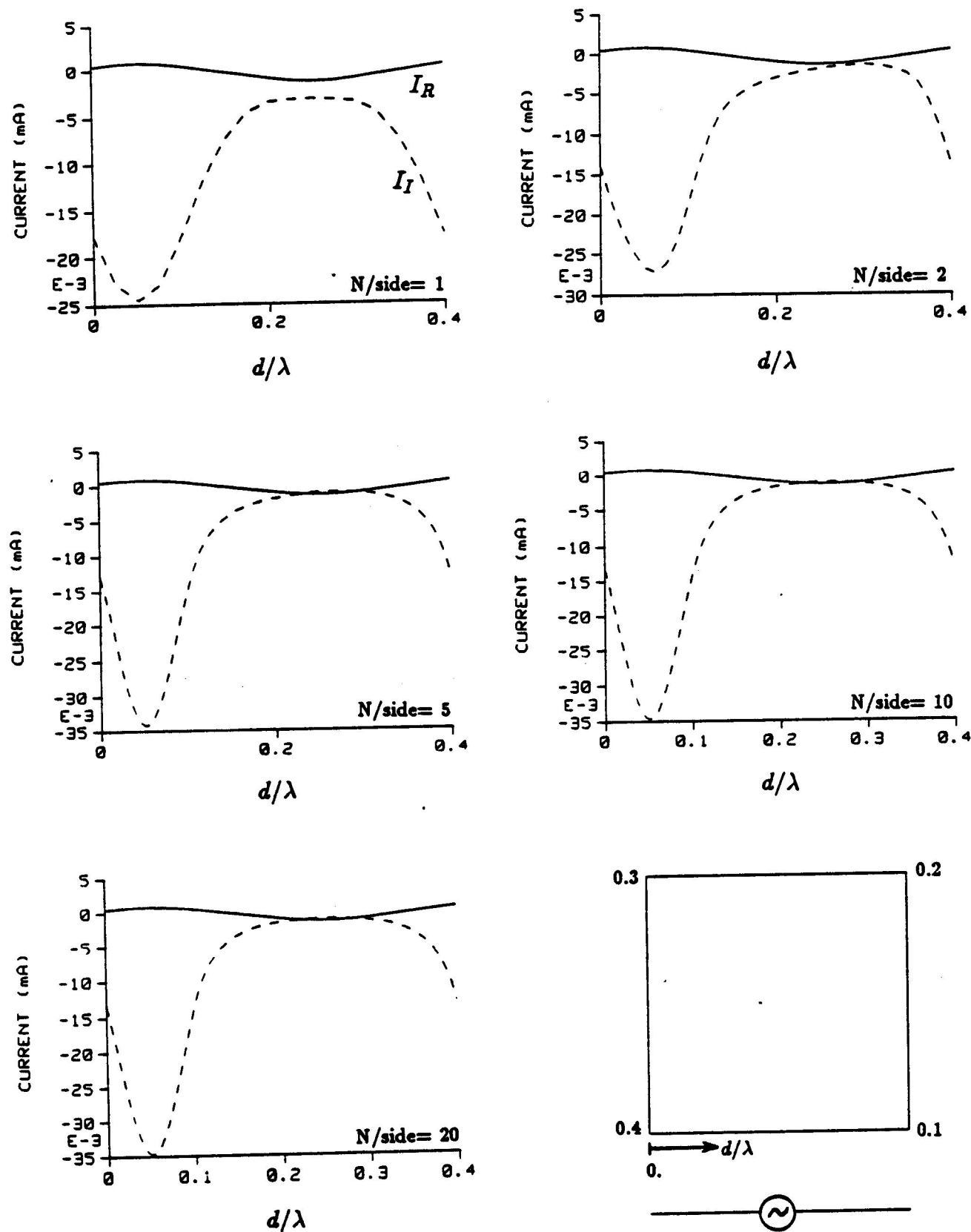


Fig. 2. Real and imaginary parts of current on a square loop excited by coupling to a dipole as computed by NEC3VLF with loop basis and weight functions. Convergence is shown as the number of segments per side of the loop is varied from 1 to 20. The loop circumference is 0.4λ and the wire radius is $10^{-4}\lambda$. The source current was approximately $4.0(10^{-4}) + j4.2(10^{-1})$ mA in each case.

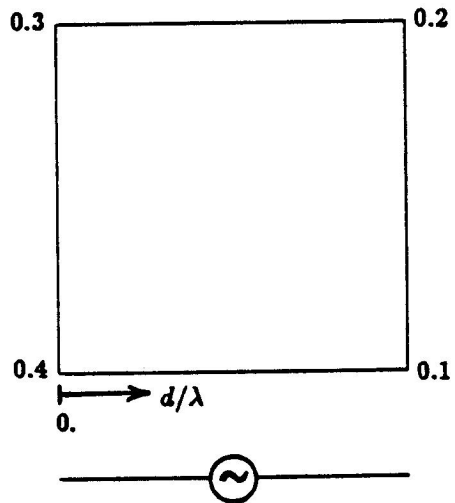
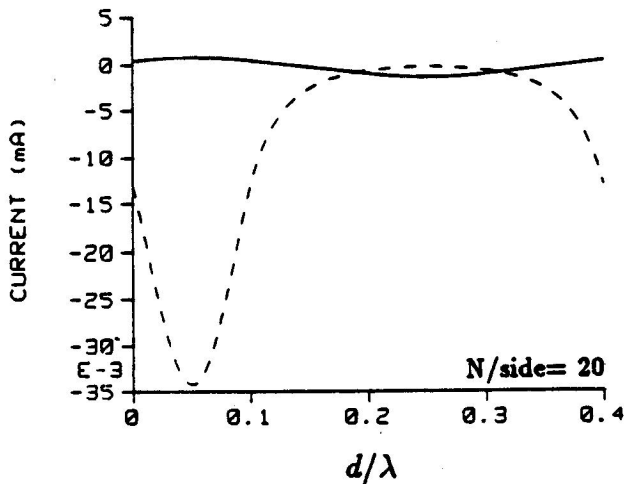
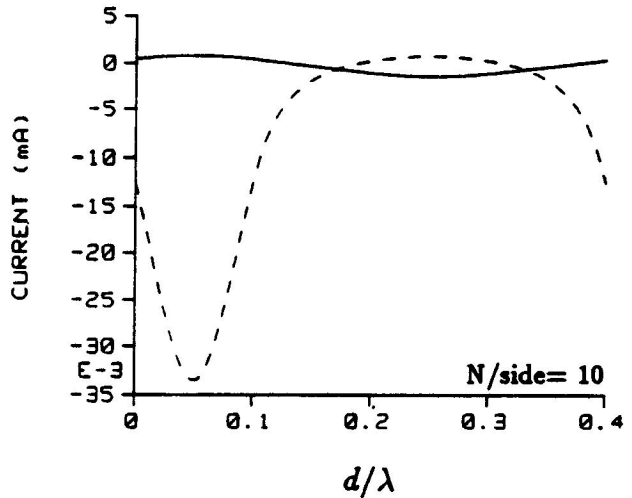
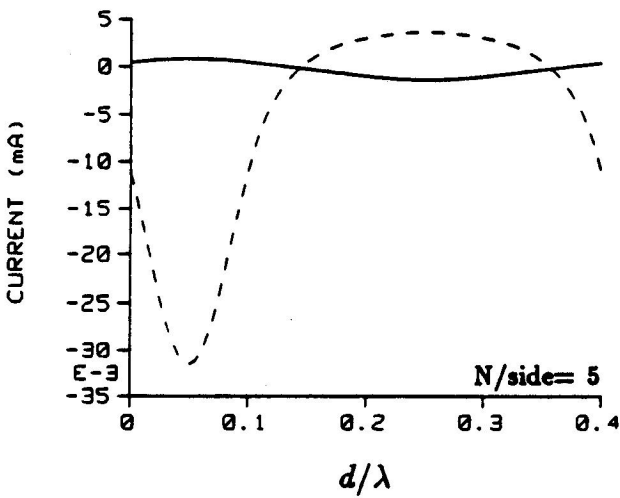
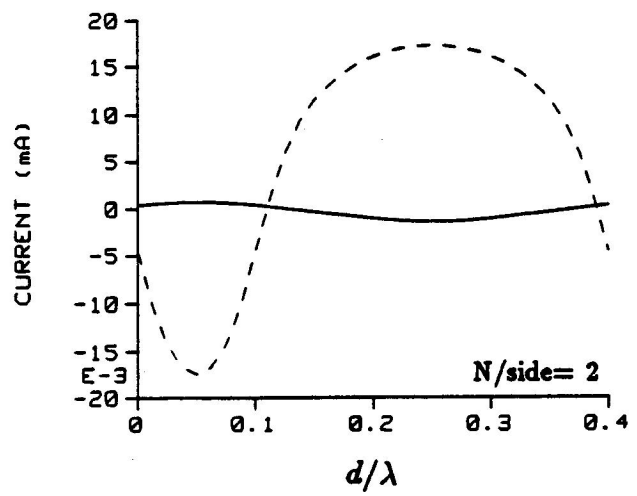
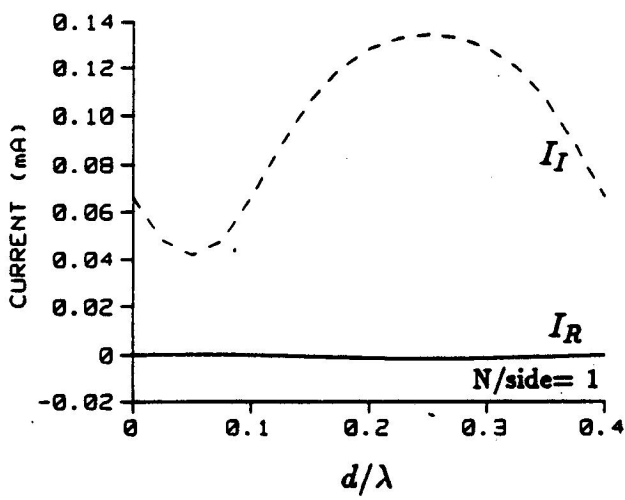


Fig. 3. Real and imaginary parts of current on a square loop excited by coupling to a dipole as computed by NEC-3 in double precision. Convergence is shown as the number of segments per side of the loop is varied from 1 to 20. The loop circumference is 0.4λ and the wire radius is $10^{-4}\lambda$. The source current was approximately $4.0(10^{-4}) + j4.2(10^{-1})$ mA in each case.

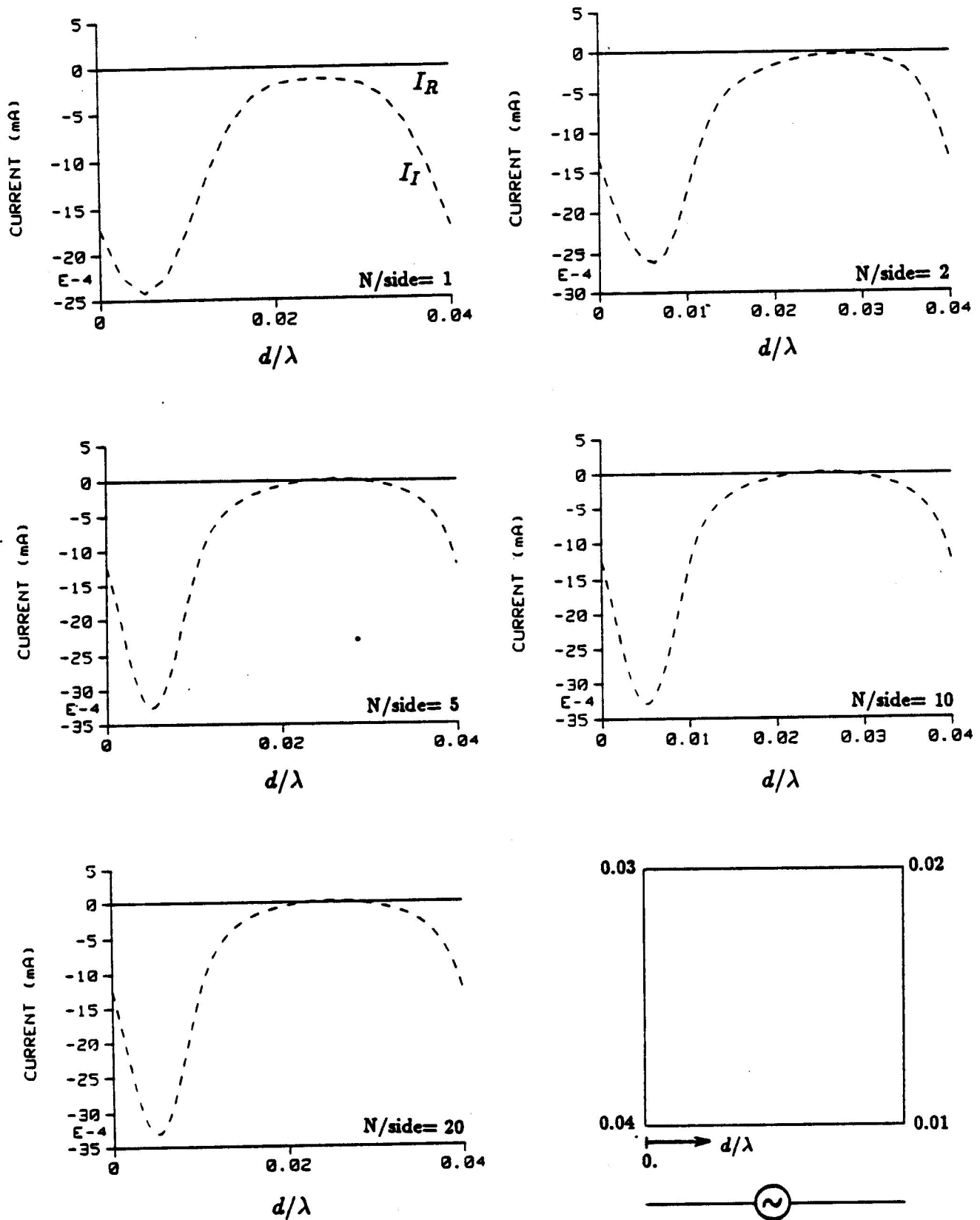


Fig. 4. Real and imaginary parts of current on a square loop excited by coupling to a dipole as computed by NEC3VLF with loop basis and weight functions. Convergence is shown as the number of segments per side of the loop is varied from 1 to 20. The loop circumference is 0.04λ and the wire radius is $10^{-8}\lambda$. The source current was approximately $3.6(10^{-8}) + j4.0(10^{-2})$ mA in each case.

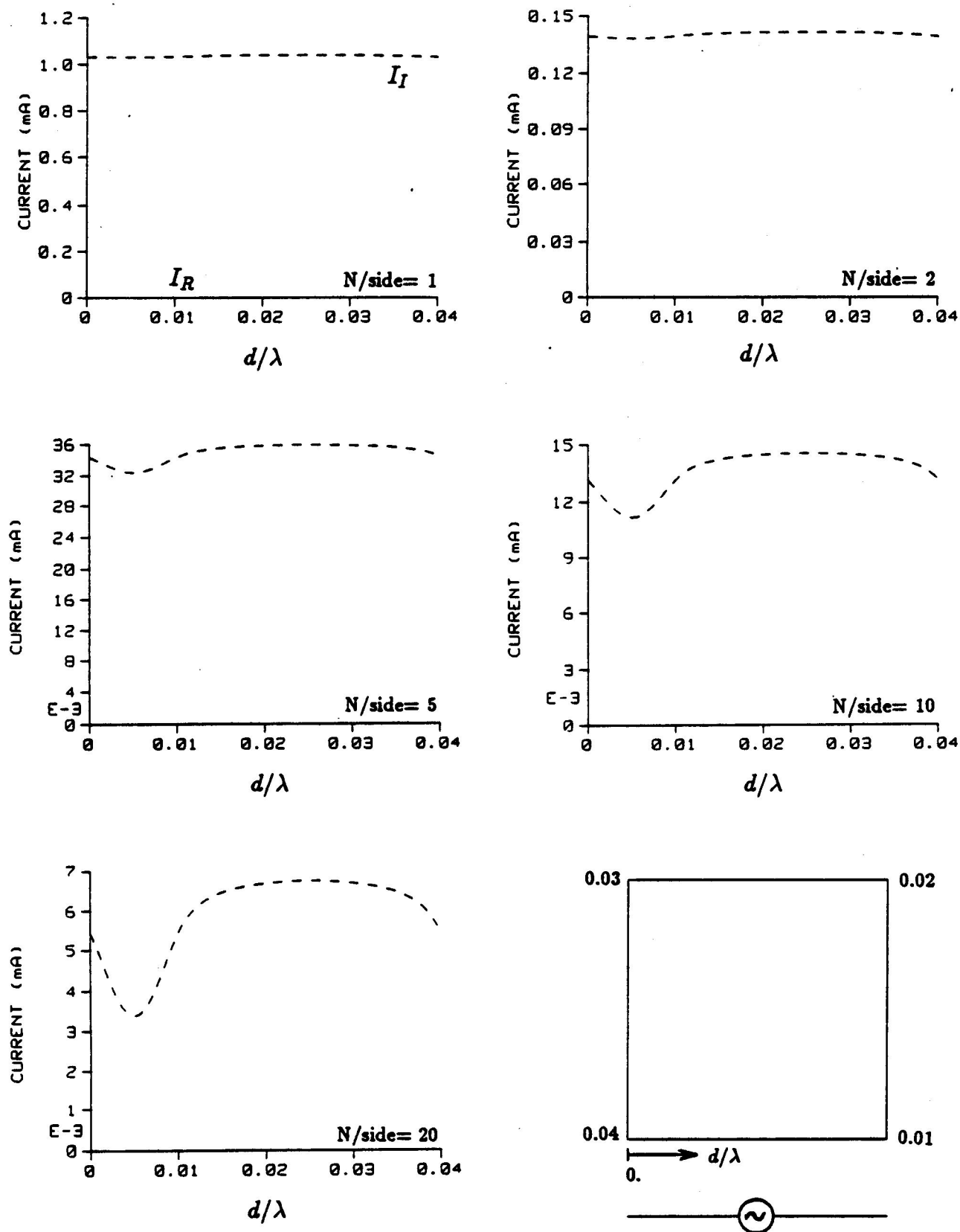


Fig. 5. Real and imaginary parts of current on a square loop excited by coupling to a dipole as computed by NEC-3 in double precision. Convergence is shown as the number of segments per side of the loop is varied from 1 to 20. The loop circumference is 0.04λ and the wire radius is $10^{-5}\lambda$. The source current was approximately $3.6(10^{-8}) + j4.0(10^{-2})$ mA in each case.

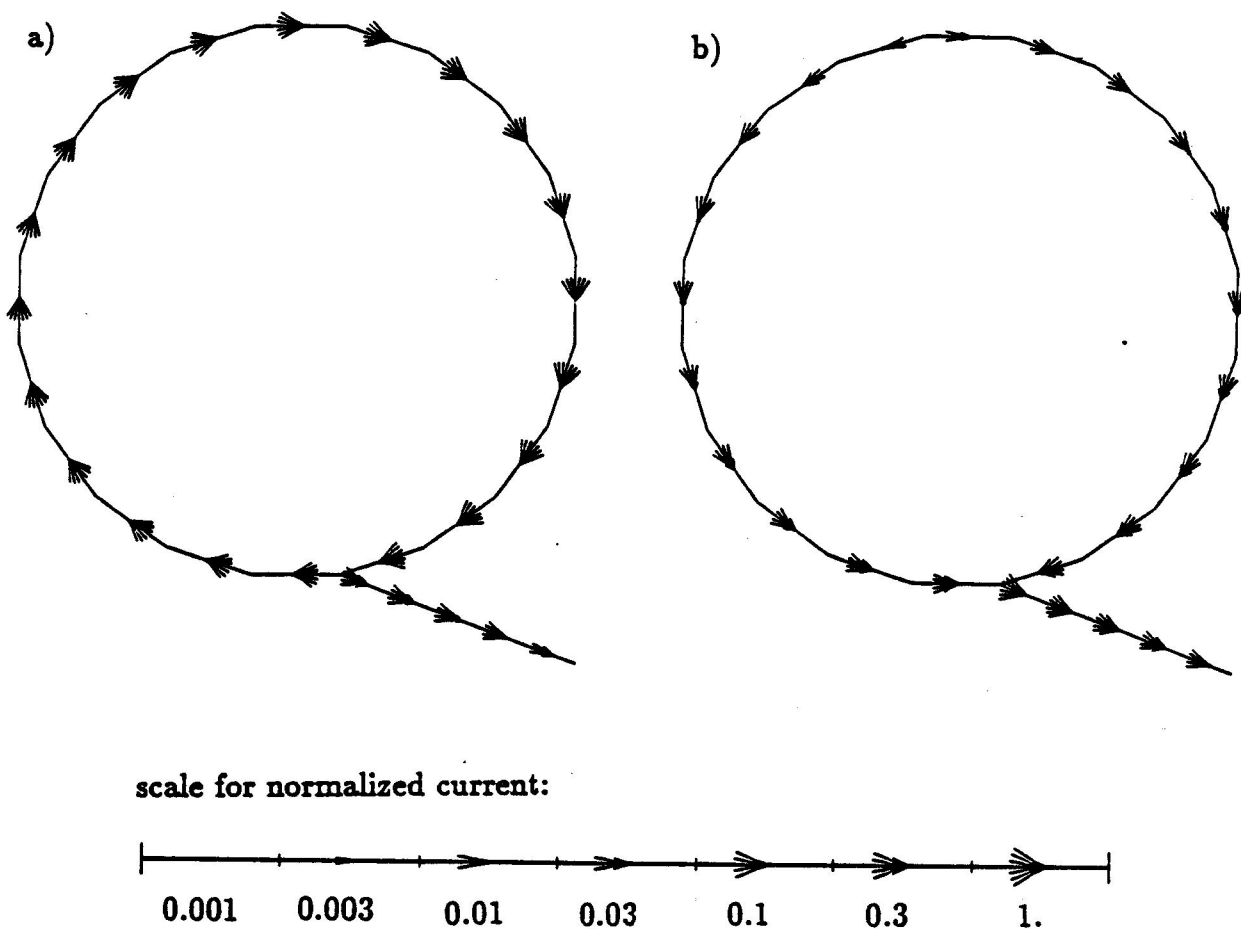


Fig. 6. Imaginary part of current on a loop with connected stub antenna. The loop circumference is 0.063λ and wire radius is $10^{-5}\lambda$. The source is one volt at the base of the stub, and the current is normalized by I_{max} ; a) NEC-3 result with incorrect loop current, $I_{max} = 0.41$ mA; b) NEC3VLF result with $I_{max} = 0.11$ mA.

The input impedance and average gain for this structure modeled with loop basis and weighting functions is shown in Table 2. The NEC3VLF result showed some sensitivity to the order of segments in the grid, which determines the segments on which the match points and spline basis functions will be replaced. The difference of the average gains from the correct value of 1.0 was found to be due to extraneous input power at small, but not negligible, voltages across the segments on which match points were dropped. These errors are within acceptable bounds for most applications, particularly for case 2 in which the segments were entered sequentially by wires rather than by cells. The input impedance and average gain obtained with NEC-3 in single and double precision are shown in Table 3. The last two frequencies resulted in division by zero in NEC-3S.

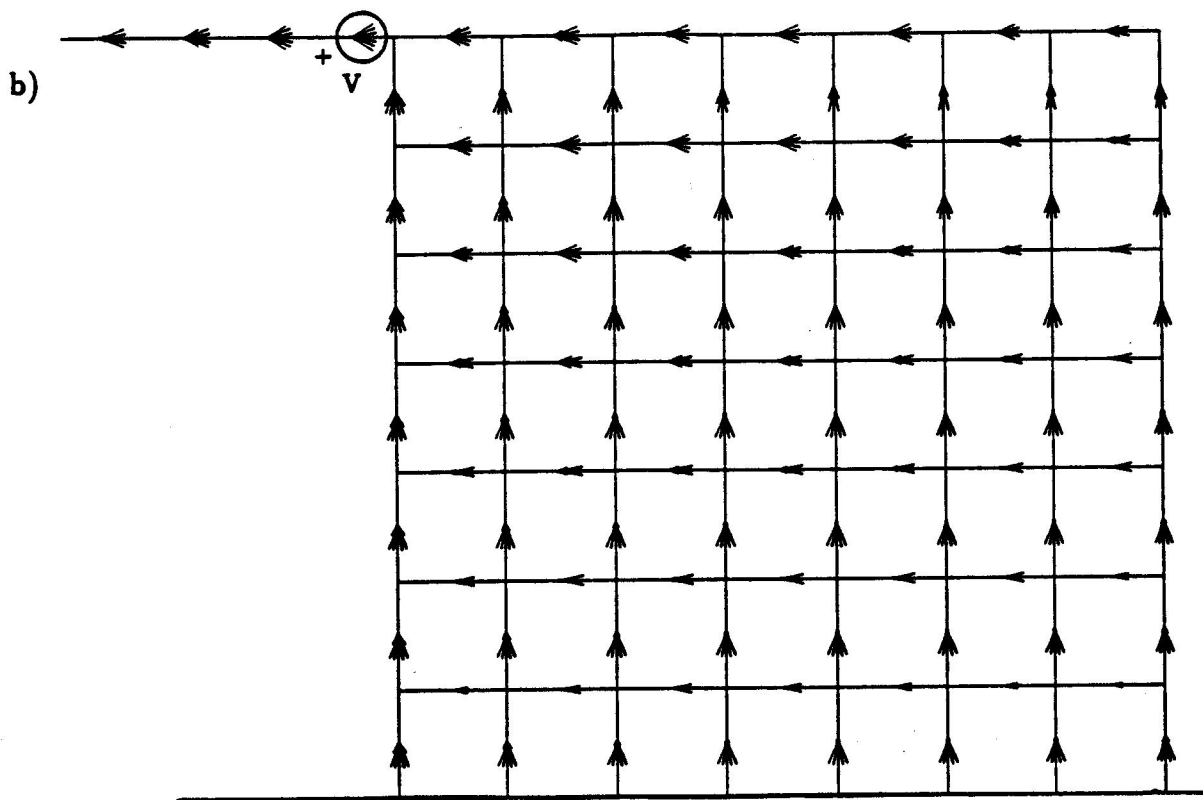
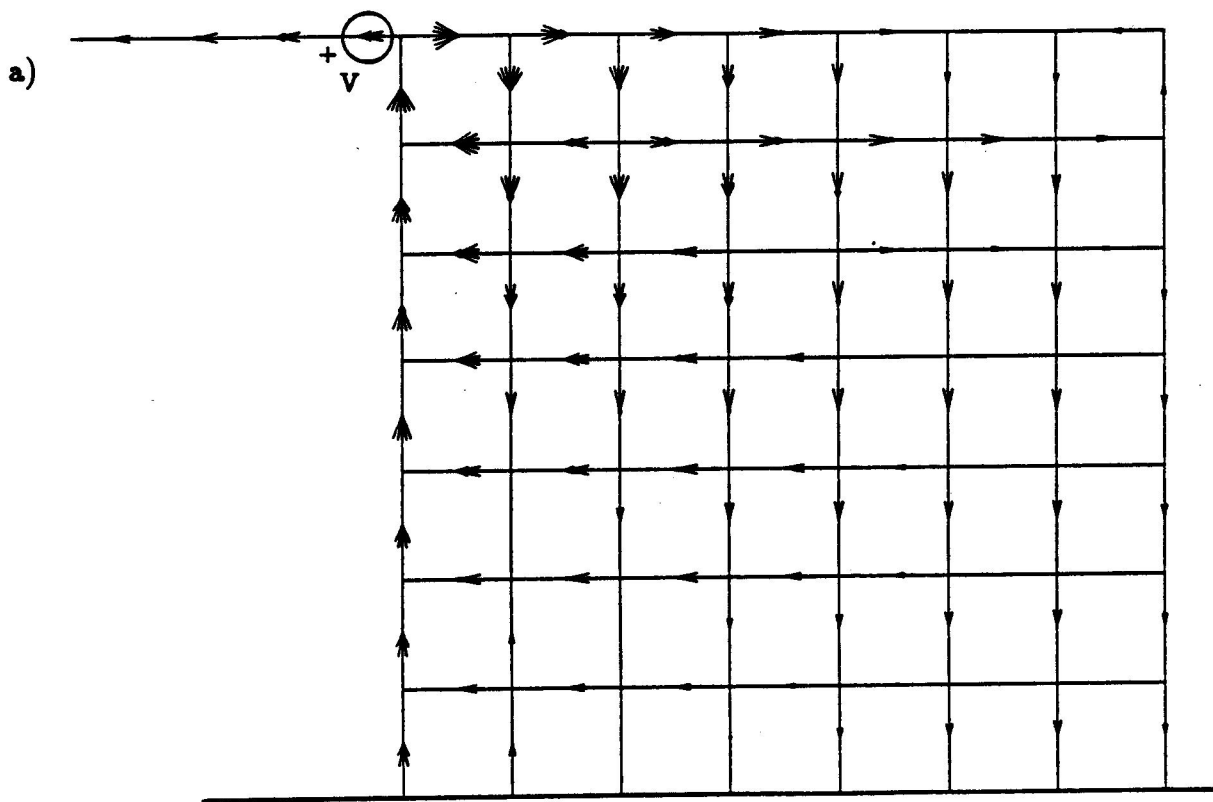


Fig. 7. Imaginary part of current on a wire grid fin with stub antenna. The fin is 0.014λ high and is on a ground plane. The source is one volt at the base of the stub and current is normalized by I_{mas} ; a) NEC-3D result with incorrect grid current, $I_{mas} = 2.62$ mA; b) NEC3VLF result with $I_{mas} = 0.10$ mA.

Table 2. Input impedance and average gain of the wire grid with stub antenna as computed by NEC3VLF with loop basis and weight functions for segment length Δ . Results are shown for two orderings of the segments.

Δ/λ	Case 1			Case 2		
	R (ohms)	X (ohms)	\bar{G}	R (ohms)	X (ohms)	\bar{G}
$2 \cdot (10^{-2})$	$4.90(10^1)$	$-8.11(10^2)$	0.77	$5.91(10^1)$	$-8.00(10^2)$	0.93
$2 \cdot (10^{-3})$	$1.39(10^{-1})$	$-9.77(10^3)$	0.77	$1.65(10^{-1})$	$-9.80(10^3)$	0.92
$2 \cdot (10^{-4})$	$1.37(10^{-3})$	$-9.78(10^4)$	0.77	$1.63(10^{-3})$	$-9.81(10^4)$	0.91
$2 \cdot (10^{-5})$	$1.37(10^{-5})$	$-9.78(10^5)$	0.77	$1.63(10^{-5})$	$-9.81(10^5)$	0.91
$2 \cdot (10^{-6})$	$1.37(10^{-7})$	$-9.78(10^6)$	0.77	$1.63(10^{-7})$	$-9.81(10^6)$	0.91

Table 3. Input impedance and average gain of the wire grid with stub antenna as computed by NEC-3 in single precision (NEC-3S) and double precision (NEC-3D).

Δ/λ	NEC-3S			NEC-3D		
	R (ohms)	X (ohms)	\bar{G}	R (ohms)	X (ohms)	\bar{G}
$2 \cdot (10^{-2})$	60.98	$-7.82(10^2)$	1.01	60.98	$-7.82(10^2)$	1.14
$2 \cdot (10^{-3})$	0.60	$-9.38(10^3)$	0.30	$1.78(10^{-1})$	$-9.66(10^3)$	1.19
$2 \cdot (10^{-4})$	-7.55	$-8.74(10^4)$	-0.0001	$1.76(10^{-3})$	$-9.67(10^4)$	5.66
$2 \cdot (10^{-5})$	***	***	***	$1.75(10^{-5})$	$-9.67(10^5)$	484.
$2 \cdot (10^{-6})$	***	***	***	$9.81(10^{-5})$	$-9.04(10^6)$	0.08

The severity of the errors with the standard NEC solution would seem to make use of the new treatment for loops essential. However, the implementation of this treatment is not as straightforward as were the VLF enhancements for dipoles. The NEC3VLF code with loop basis and weighting functions is now operational but needs more work to be able to handle arbitrary structures including symmetry, ground planes and out-of-core solutions. The present NEC-2 and NEC-3 can be very inaccurate for a loop antenna near the ground. The problems are related to those discussed above but are made worse by the limited accuracy of the interpolation tables for Sommerfeld integrals. It is not known how much loop basis and weighting functions would help in this case but it appears well worth trying. The code modifications and results described above are discussed in more detail in [4]

The Horizontal Wire Over Ground

We now shift topics to validation of results for antennas over ground. With the Sommerfeld integral model for ground, NEC-3 can model arbitrary wire structures in air near an interface, buried in the ground or penetrating from air into the ground. A horizontal wire can be modeled to within about $10^{-6}\lambda_0$ of the interface, or closer with some adjustment of the numerical integration code. Validation of such results is difficult due to lack of accurate measurements for known ground parameters.

One case for which measurements and analytical results are available is for the propagation factor on a horizontal wire near an interface. This problem can be solved from a modal approach leading to a nonlinear equation involving an infinite integral over wave number to be solved for the propagation factor [5]. When the wire is in air with wave number k_2 over a ground with wave number k_4 and $k_4 \gg k_2$ a closed form result for the propagation factor on the wire has been derived by King et al. [1,6] by considering a coaxial transmission line with lossy outer conductor and eccentrically located inner conductor as the outer conductor radius goes to infinity. The result for the propagation factor $k_L = \beta_L - j\alpha_L$ is

$$k_L = k_2 \left\{ 1 + \frac{2}{\ln(2d/a)} \left[\frac{1}{(2k_4d)^2} - \frac{K_1(2k_4d)}{2k_4d} - j\pi \frac{I_1(2k_4d)}{4k_4d} + j \left(\frac{2k_4d}{3} + \frac{(2k_4d)^3}{45} + \frac{(2k_4d)^5}{1575} + \dots \right) \right] \right\}^{1/2} \quad (2)$$

where a is the wire radius and d is the height of the wire above the ground. This equation is written for time dependence $e^{j\omega t}$ and is the conjugate of that given in [6]. K_1 and I_1 are modified Bessel functions of order 1. Specialized forms of this expression, given in an appendix of [6], are needed for accurate evaluation in the limits of large or small d . The propagation factor from this formula has been compared with measurements for a wire over water with good agreement [7].

To determine the propagation factor on a wire with NEC, a wire several wavelengths long was modeled with a voltage source near one end and the other end loaded to minimize the standing wave. The attenuation constant α_L was then determined from linear regression on the log of magnitude of the current while β_L was found from the phase shift divided by distance.

The values for α_L and β_L determined from NEC are compared with those from Eq. (2) in Fig. 8 for a ground with $\tilde{\epsilon} = 10 - j1000$ and for wire radii of $10^{-8}\lambda_0$, $10^{-6}\lambda_0$ and $10^{-4}\lambda_0$. This complex permittivity would correspond to a reasonably good ground ($\sigma = 0.01$ S/m) at about 200 kHz. The agreement is seen to be very good for this case. NEC was also run to determine the resonant length of a dipole versus height and was in good agreement with King's equation. Similar good accuracy would be expected from NEC for lower ground conductivity, although Eq. (2) would lose accuracy in this case.

With these results the modeling of a long wire antenna such as a Beverage with NEC-3 seems pretty safe. The feed and termination points with ground stakes were validated by an independent numerical treatment developed by Johnson [8]. Of course a real antenna may have more than a simple ground stake or counterpoise where it meets the ground and then things get complicated.

Acknowledgment

The work on modeling loops at VLF was funded by the Naval Ocean Systems Center, San Diego, CA. through J. Logan and S. T. Li.

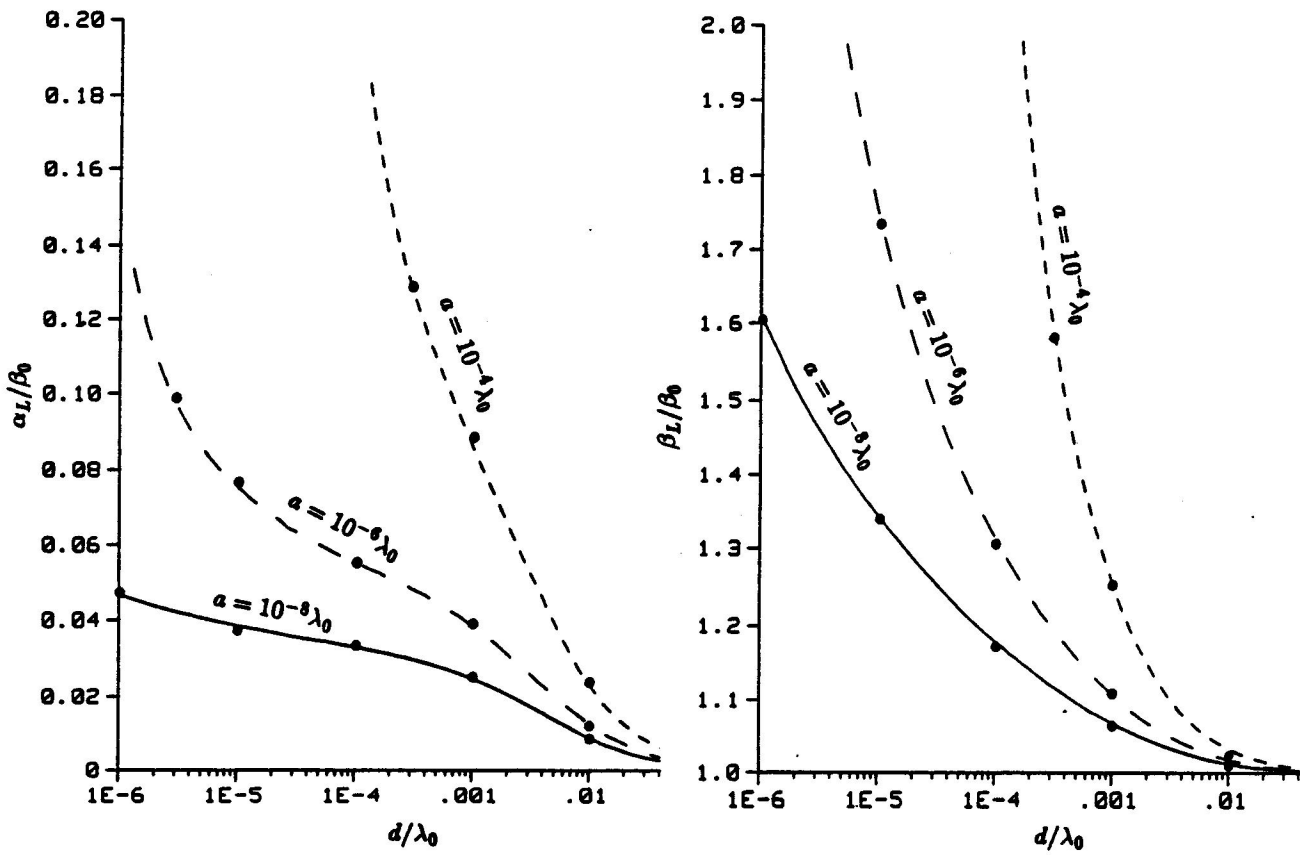


Fig. 8. Propagation factor $k_L = \beta_L - j\alpha_L$ on a horizontal wire with radius a at height d over ground. NEC results are shown by points and results of Eq. (2) by lines.

REFERENCES

- [1] R. W. P. King and G. S. Smith, *Antennas in Matter*, M. I. T. Press, Cambridge MA, 1981.
- [2] G. J. Burke, *Enhancements and Limitations of the Code NEC for Modeling Electrically Small Antennas*, Lawrence Livermore National Laboratory, Rept. UCID-20970, Jan. 1987.
- [3] D. R. Wilton, University of Houston, private communication.
- [4] G. J. Burke, *Treatment of Small Wire Loops in the Method of Moments Code NEC*, Lawrence Livermore National Laboratory, Rept. UCID-21196, October 1987.
- [5] J. R. Wait, "Electromagnetic wave propagation along a buried insulated wire," *Canadian Journal of Physics*, vol. 50, 1972.
- [6] R. W. P. King, T. T. Wu and L. C. Shen, "The horizontal wire antenna over a conducting or dielectric half space: current and admittance," *Radio Science*, vol. 9, No. 7, pp. 701-709, July 1974.
- [7] R. M. Sorbello, R. W. P. King, K. M. Lee, L. C. Shen, and T. T. Wu, "The horizontal-wire antenna over a dissipative half-space: generalized formula and measurements," *IEEE Trans. Antennas and Propagation*, vol. AP-25, no. 6, November 1977.
- [8] W. A. Johnson, "Analysis of a vertical, tubular cylinder which penetrates an air-dielectric interface and which is excited by an azimuthally symmetric source," *Radio Science*, vol. 18, no. 6, pp. 1273-1281, Nov.-Dec. 1983.

COMPARATIVE PERFORMANCE OF MININEC FOR VARIOUS COMPUTERS AND LANGUAGES

C. C. Smith
Kaman Sciences Corporation
P. O. Box 7463
Colorado Springs, CO 80933

It is a truism in computer science that the best benchmark of performance is the very task that you intend to use the computer for. General purpose benchmarks tend to give artificial results that do not reflect performance in a specific task. This user note is intended to provide readers with a simple benchmark of MININEC3 performance for a few computers and languages.

Even with such a restricted field of performance as MININEC3, variations in results occur with different test cases. This no doubt is due to differing efficiencies in such tasks as computation and RAM access. The two test cases shown here show such variations.

Both test cases are performed at 3.0 MHz. The first is a single wire in free space with 40 segments. End one is at (0,0,0) and end two is at (0,0,47.5). The radius is 0.001. Pulse 20 is driven with one volt at zero phase. The expected result is $Z = 66.4 - j47.1$ at the drive point. The time to fill the matrix and the time to factor it are noted.

The second test case has three wires over perfect ground. Wire one has 12 pulses, end one at (-10,-1,2) and end two at (-.5,0,10). Wire two has 12 pulses, end one at (10,1,2) and end two at (.5,1,10). Wire three has one pulse, end one at (-.5,0,10) and end two at (.5,0,10) so that it joins to end two of both wires one and two. (MININEC3 actually places 11 non-zero pulses on wires one and two, and two pulses on wire three). Pulse 24 is driven with one volt and zero phase. The expected impedance is $Z = 2.03 - j925.5$ at the drive point.

The results are given in the tables below. The computers tested were an IBM XT (with added memory), an AT&T 6300, a Toshiba 1100+, and an Atari 520ST. BASCOM compiled BASIC (CB) was tested on the IBM, the AT&T and the Toshiba. In addition, on the AT&T, a Mark Williams C (MWC) version, a Turbo Pascal 8087 (TP-8087) version and a standard Turbo Pascal (TP) version were tested. On the Atari, the language was Logical Design Works compiled BASIC (LDW) (with the trace feature on to facilitate further debugging.

Times were noted by using the timer inherent to the language. Only rough timing was done externally to eliminate totally spurious results due to code errors from being reported.

Test Case 1

Computer	/ Code	Fill	Factor
IBM XT	/ CB	0:18	1:01
AT&T 6300	/ CB	0:08	0:30
AT&T 6300	/ MWC-8087	0:03	0:08
AT&T 6300	/ TP -8087	0:05	0:20
AT&T 6300	/ TP	0:14	1:01
Toshiba 1100+	/ CB	0:09	0:32
Atari 520 ST	/ LDW	0:14	0:26

Test Case 2

Computer	/ Code	Fill	Factor
IBM XT	/ CB	5:03	0:16
AT&T 6300	/ CB	2:26	0:08
AT&T 6300	/ MWC-8087	*	*
AT&T 6300	/ TP -8087	1:25	0:04
AT&T 6300	/ TP	7:30	0:14
Toshiba 1100+	/ CB	2:39	0:08
Atari 520 ST	/ LDW	*	*

Note: a * denotes that a substantial error occurred in computing Z so that time results are considered invalid.

These results are informative but not conclusive. A benchmark with loads and radiation patterns should also be devised, since these are time consuming additions to the code that undoubtedly receive much use.

**A COMPARISON OF NEC AND MININEC ON
THE STEPPED RADIUS PROBLEM**

by

J. K. Breakall
Lawrence Livermore National Laboratory
Livermore, CA

and

R. W. Adler
Naval Postgraduate School
Monterey, CA

Dick Adler and I both were asked to model antennas using tapered wires or actually stepped radii in sections along a wire. I was trying to model a large Yagi where I had some measurements of the pattern and impedance and Dick was tasked to provide results on a large Log-Periodic (LP) antenna using tapered elements. We both thought this should be a fairly easy task and simply put in the geometry of the elements with the appropriate radii in each section. Well, to our amazement and surprise we stumbled onto something which we feel is quite serious and of concern to further modeling when stepped radii are involved. We will try to be as brief as possible on this finding since this section is just supposed to be an area to report problems and results and not to be a full blown arena for additional papers. Here we go!!

The antenna which we chose to describe and which serves as an example for the problem is as follows: A dipole is modeled in free space which includes 3 sections, the middle section being .25 wavelengths in length and of radius .00025 lambda and then 2 end sections of each .125 wavelengths in length and of radius .000125 lambda. Therefore, there is a step in radius of a factor of 2 at .125 lambda from the center of the dipole where the feedpoint will be located. The total length of the dipole is .5 lambda. We first modeled this antenna with NEC using symmetry and kept increasing the number of segments in each section to see if some convergence could be obtained in an impedance versus frequency sweep around resonance. We varied segmentation from 2 to 50 segments per section until we seemed to have achieved convergence. The results are shown in Figures 1a and 1b for the real and imaginary parts of the input impedance respectively. As can be seen the real part seems to be quite insensitive to the number of segments and converges very quickly. However, the imaginary part is very sensitive and it took about 40 segments per section before convergence was obtained. When we tried to use the results of this convergence study in the modeling of the Yagi using a lot of segments per section, the patterns and impedance appeared very suspicious and incorrect. We spoke to Bill Myers at TASC and John Denny at Bell Labs and they also informed us of similar findings when they modeled Yagis in the past. We tried to model the Yagi with MININEC, a formidable task since the total number of segments is limited on our version on the PC. We seemed to be getting very good agreement with the measured information we had when this was tried. Was MININEC working better and giving more accurate results than NEC? We decided to investigate this question further.

We modeled our dipole mentioned above with NECGS using rotational symmetry in a wire cage equivalent of the actual problem with wires across the annulus formed by the stepped transition region in radii. The geometry is shown in a blown-up view in Figures 2 and 3. We used the equal area rule which states that the total unwrapped area of each of our 6 wire cage wires would equal the same surface area of the actual antenna. This is discussed in an excellent paper by A. C. Ludwig in the IEEE Transactions on Antennas and Propagation, September, 1987. The results are shown for all three models, MININEC3, NECGS, and NEC3 in Figures 4 and 5. As can be seen, the real part of the impedance is in agreement with NECGS and NEC3 and in general agreement with MININEC3, considering the magnitude of the impedance. For the imaginary part MININEC3 and NECGS are closer in agreement than NEC3, especially at the higher frequencies. To appreciate the differences more clearly, we have plotted the imaginary part behavior on the same scale as the real part in Figure 6. NEC3 is clearly not agreeing with NECGS or MININEC3 and one can see the more sensitive nature of the imaginary part of the impedance. The Yagi is very sensitive to the imaginary part of the impedance when forming the proper current ratios and phasings required to generate a clean pattern with low sidelobes. Slight changes in these current ratios and phasings will have dramatic effect on the sidelobes. The gain, of course, is not as sensitive. To show why the apparently converged result in NEC3 is really incorrect we have plotted the impedance variation with 50 segments per section in Figures 7, 8, and 9. Again the real part is in agreement with NECGS, as expected, from the quick convergence mentioned above. The imaginary part of the impedance is substantially different, however, which explains the abnormal behavior in the Yagi and LP results.

Well, what should one do to come up with a solution to this problem? We have found that one can use MININEC3 to model a tapered element correctly and then plot the impedance versus frequency, as has been done here. Then one can select an equivalent radius for the element which can be just the average of the radii for all sections of stepped changes. In the case of the dipole described here, the average or equivalent radius would be $(.00025 + .000125)/2$ or $.0001875$ lambda. Then one simply adjusts the length of this equivalent constant radius element to have the same resonance as that of the fully tapered element, as found using MININEC3. One will then find that the impedance versus frequency behavior will be the same for either the exact tapered element and the equivalent radius element.

We have found that another problem exists in MININEC3, if the radius of the wires are greater than about $.001$ wavelengths. It was discovered that there is a difference between NEC and MININEC when used to verify experimental Yagi measurements performed at the NBS and described in a previous paper in the ACES newsletter by Breakall (Vol 1 No 2, p58). We have since found that the problem only occurs when the wire radius is greater than the above mentioned criterion. The radius used in the NBS Yagis was $.004$ lambda which exceeds the criterion. It causes a frequency shift to appear between NEC and MININEC. When the radius is less than $.001$ lambda, NEC and MININEC seem to track very well on Yagis and impedance sweeps on dipoles. This problem has been relayed to Jim Logan and company at NOSC and he said they have some ideas on the problem and will report any changes or fixes. Jerry Burke has been given the results for the stepped radius problem in NEC and will also be looking at possible reasons and fixes.

In summary, we have identified a problem for tapered dipole/monopole elements. NEC cannot correctly predict input impedance for tapered conductors (especially the reactive part which seriously affects Yagi gain and resonance and also Log-Periodic Array frequency response). MININEC can be trusted to correctly predict tapered dipoles, but only for thin ones where the radius is less than $.0005 \lambda$. For these thin elements, we use MININEC to find an equivalent length constant-radius element. This equivalent element is then used in NEC for arrays, etc. For elements thicker than MININEC can handle, it is possible to build a circular cage of thin conductors, but it would be very resource-consuming to have to do it with NEC. (NECGS is much faster for rotationally symmetric structures but is not universally available since it is a derivative of NEC3, which is branded as "military critical technology"). An interesting note: we found no theoretical treatment available for tapered dipoles and very little measured impedance data. We had to take our clues from tapered Yagi antenna designs.

Well, that's about all for this time. We feel we are going to be in this column more than we would like, based on these and other findings which we will report on later. We hope that you will also tell us your findings. We are sure there must be an ample number out there; enough to keep this Pandora's Box overflowing. Most can be solved with simple explanations and fixes. If nobody reports them, we will never know and you might be allowing somebody to go down the same darkened path. Let's hear from you all.

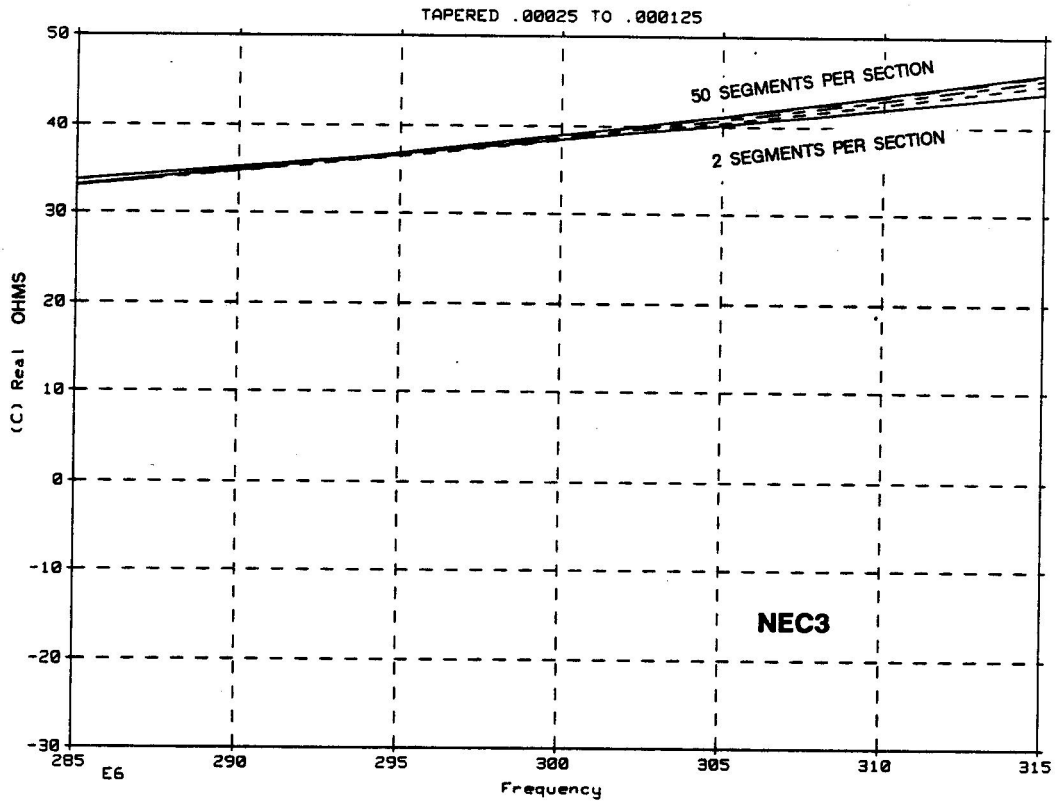


Figure 1a: IMPEDANCE VS. FREQUENCY FOR TAPERED DIPOLE 2 TO 50 SEGMENTS PER SECTION

sig

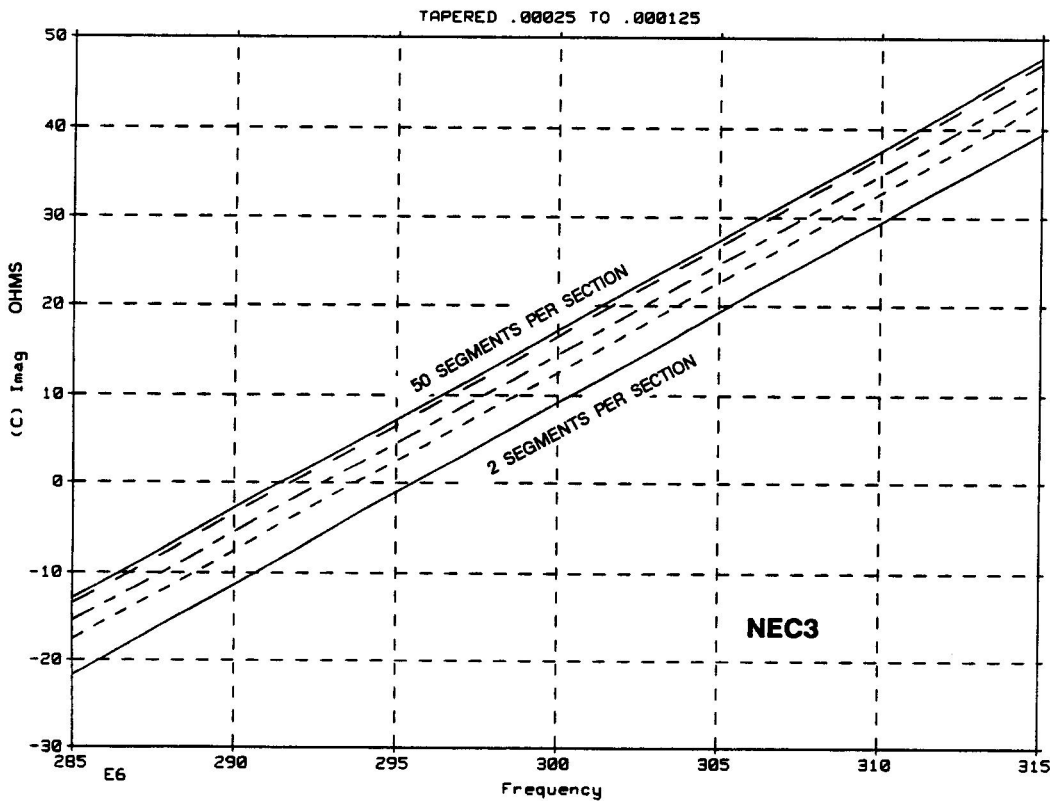


Figure 1b: IMPEDANCE VS. FREQUENCY FOR TAPERED DIPOLE 2 TO 50 SEGMENTS PER SECTION

sig

TAPERED DIPOLE USING CYLINDRICAL WIRE CAGE

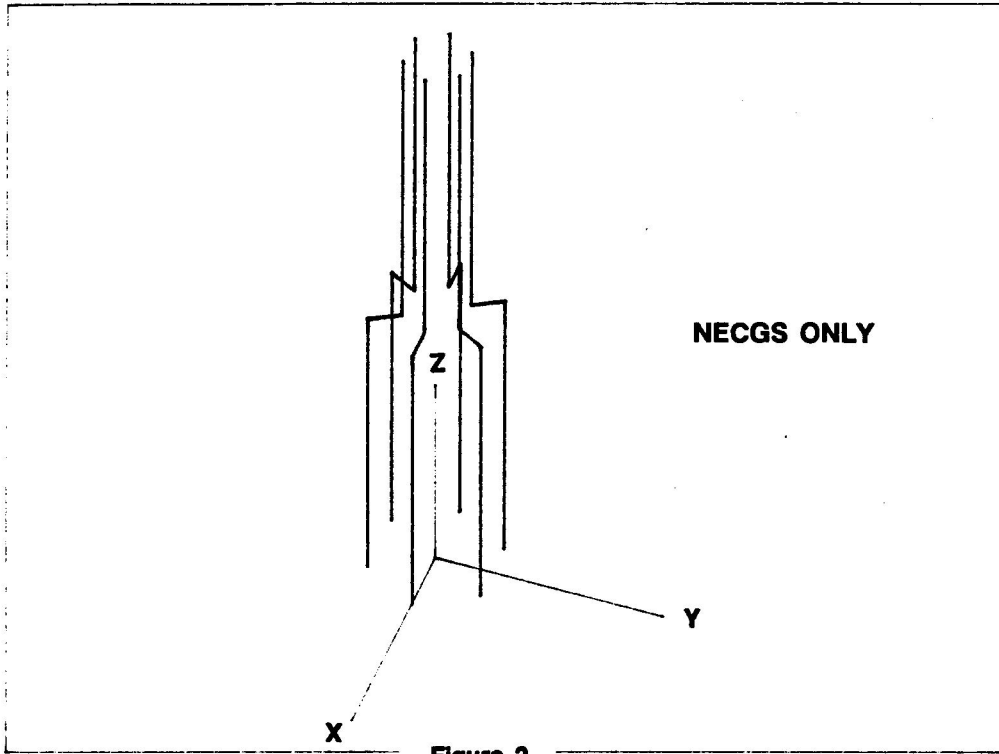


Figure 2

TAPERED DIPOLE USING CYLINDRICAL WIRE CAGE

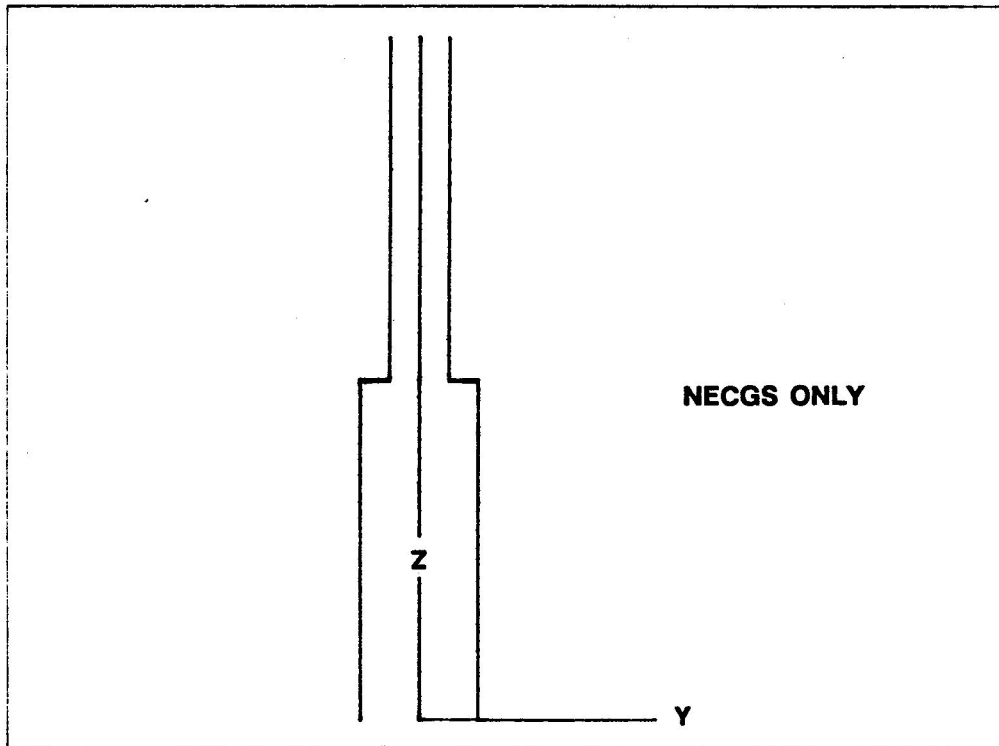


Figure 3

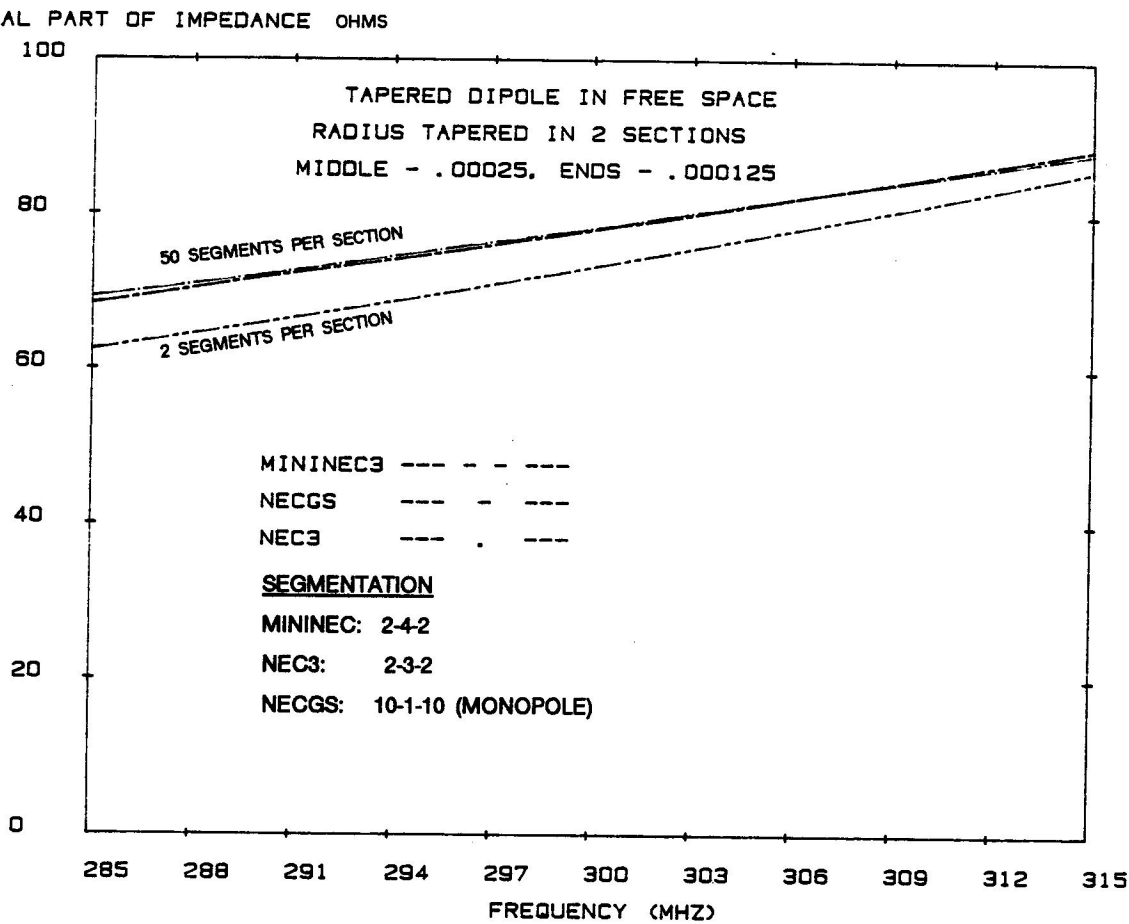


Figure 4

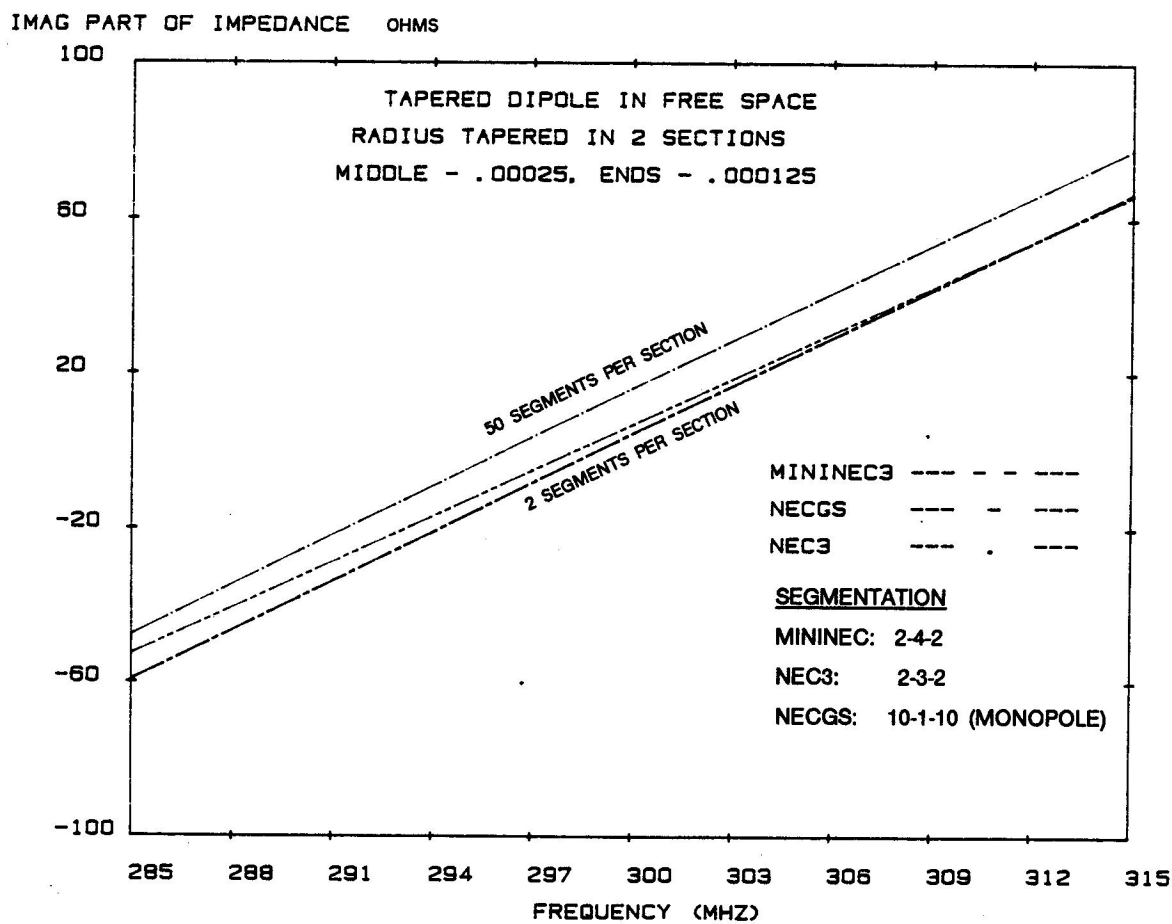


Figure 5

IMAG PART OF IMPEDANCE OHMS

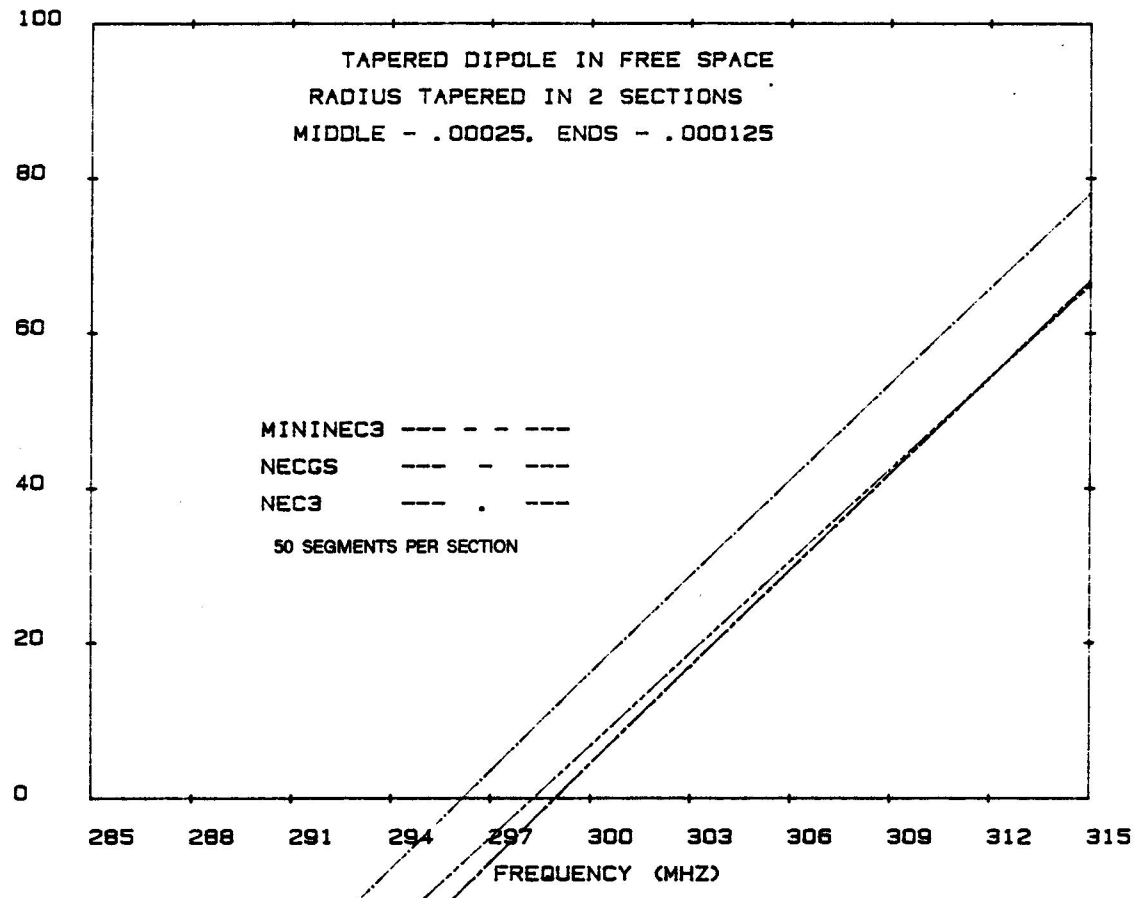


Figure 6

REAL PART OF IMPEDANCE OHMS

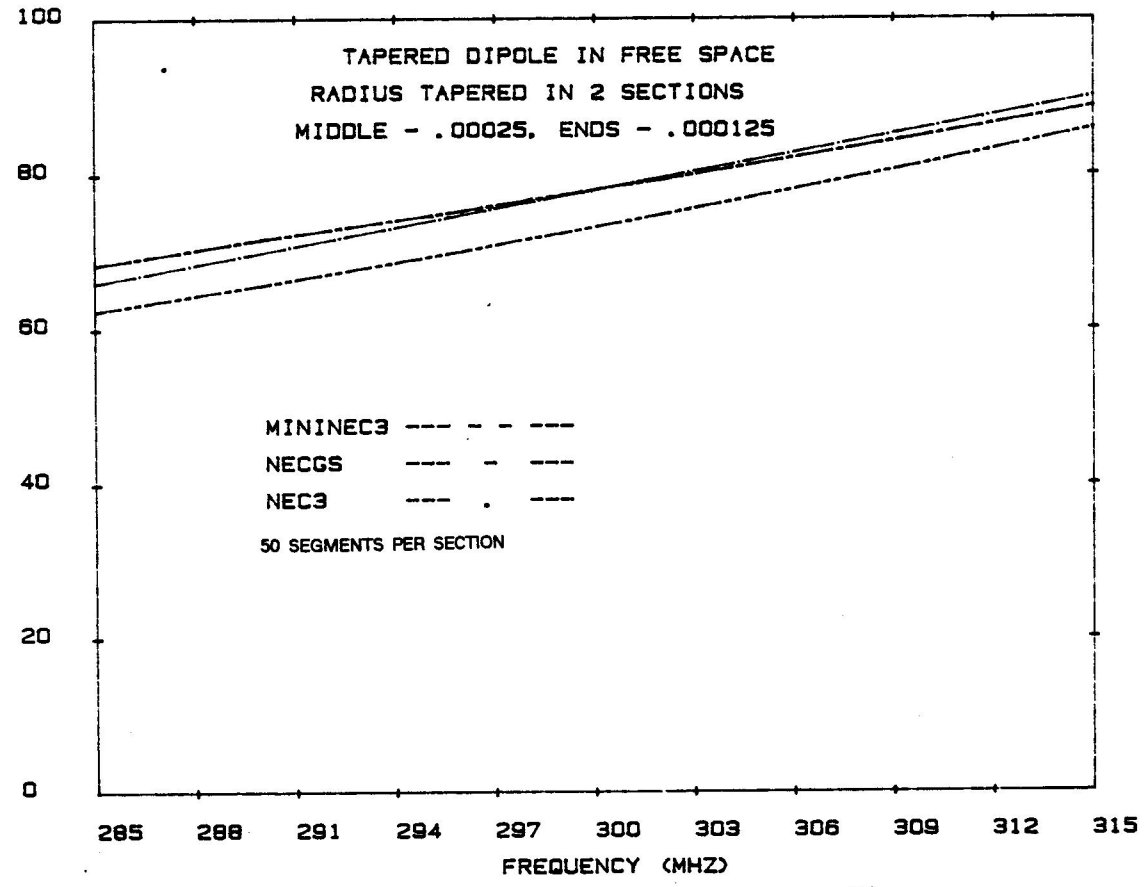


Figure 7

IMAG PART OF IMPEDANCE OHMS

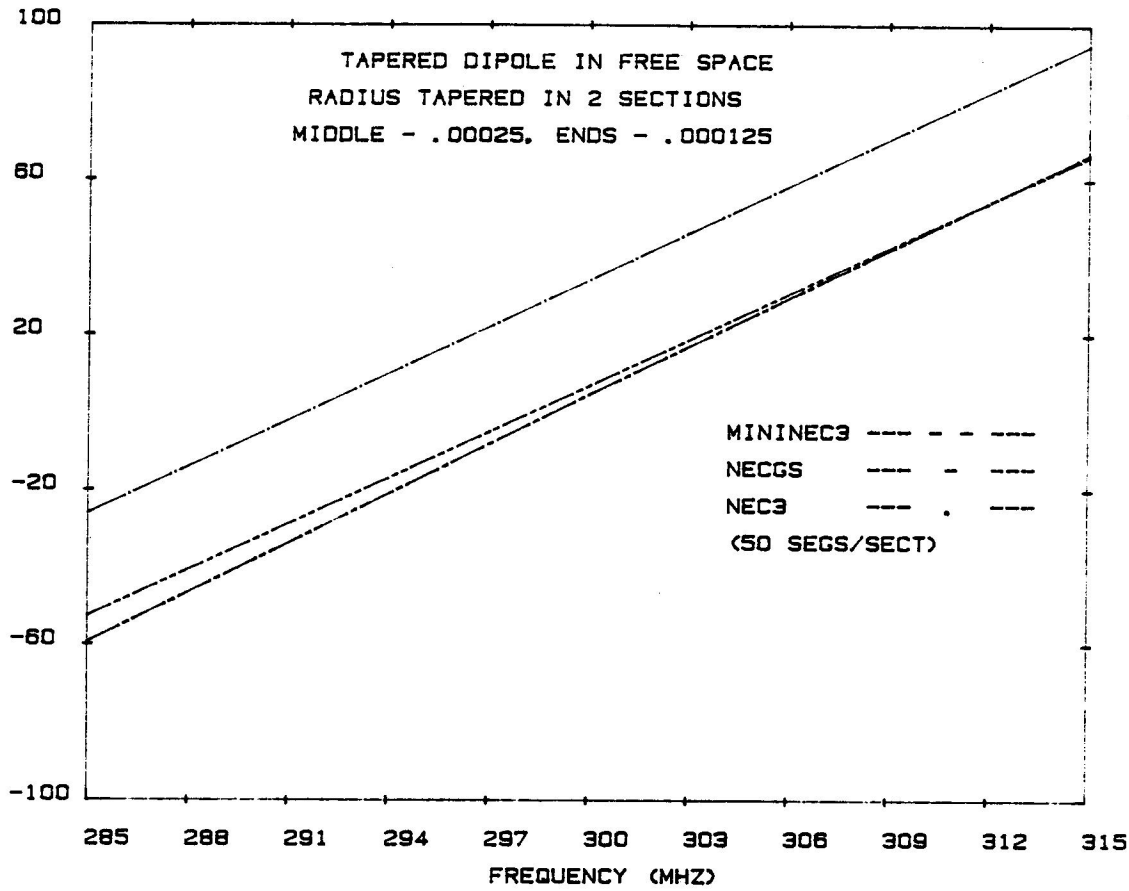


Figure 8

MAG PART OF IMPEDANCE OHMS

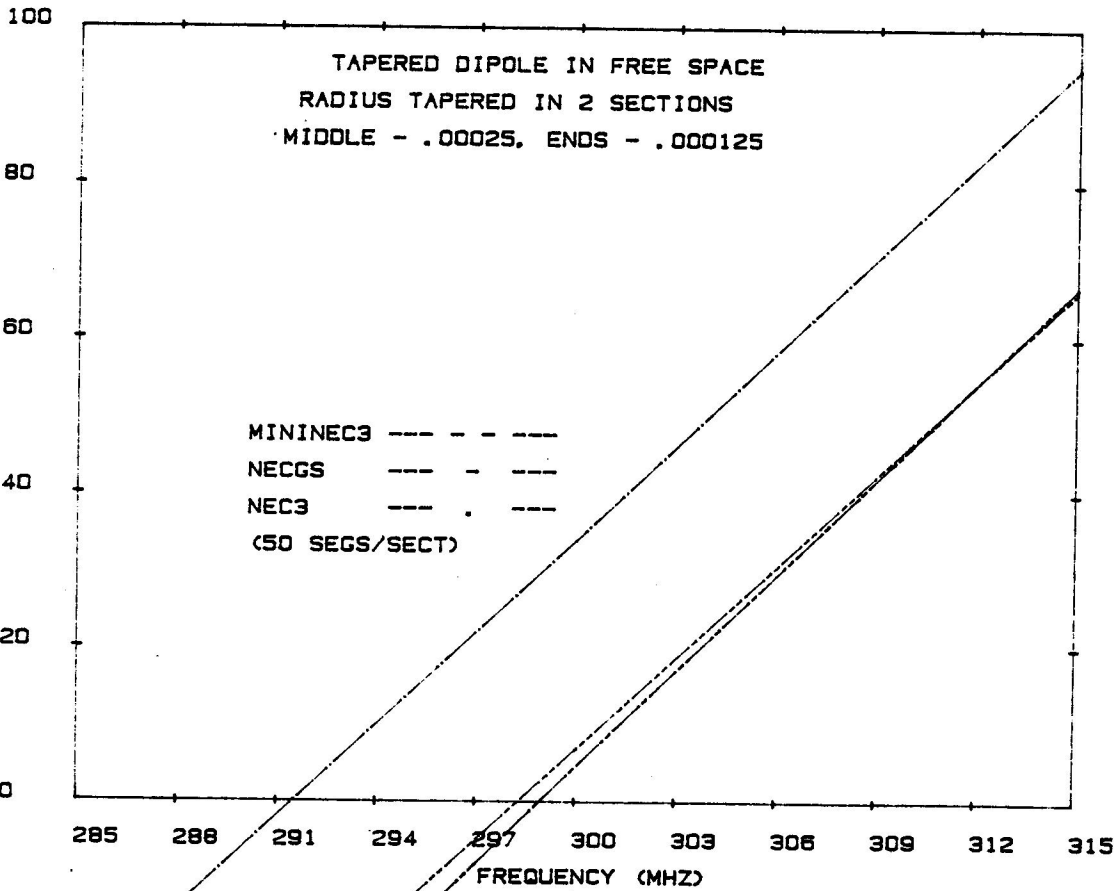


Figure 9

BACKSCATTERING FROM A CUBE

A.C. LUDWIG

General Research Corporation

P.O. Box 6770, Santa Barbara, CA 93160

ABSTRACT

Three analytical techniques--the method of moments, geometrical theory of diffraction, and physical optics (without fringe current correction)--are applied to the case of backscattering from a cube. Results are compared to experimental data. It is relatively easy to compute specular scattering with good accuracy; it is much more difficult to obtain good accuracy for corner incidence, which is emphasized here precisely because it provides a more rigorous test of an analytical technique. As expected, the method of moments provides good results when the segmentation is on the order of 0.1 wavelengths, and in some cases up to 0.26 wavelengths. Single-diffraction geometrical theory of diffraction predicts peak scattering within a few dB for a cube dimension of 0.1-3 wavelengths, which is the full range of experimental data, but is not accurate between peaks. Physical optics predicts peak scattering within a few dB for a cube dimension of 1-3 wavelengths, and is also not accurate between peaks.

A cube is a useful benchmark case for the class of scattering bodies consisting of flat faces. In this paper, monostatic backscattering is computed using the geometrical theory of diffraction (GTD) and physical optics (PO), which are nominally high frequency techniques, and the method of moments (MOM), which is nominally a low frequency technique. Experimental results are compared to the computed data.

This paper is not intended to be the final word on this subject; on the contrary, it has the modest goal of presenting a comparison of results obtained using a simple-minded application of currently available tools. GTD analysis was restricted to single-diffraction terms, physical optics was not corrected for fringe currents, and the NEC MOM code was used as is, without any real attempt to probe into reasons why results are good or bad. Bistatic scattering was not addressed. Any of these improvements would greatly increase the difficulty of the analysis. In summary, the goal of this paper is to address two questions: (1) how accurately can backscattering from a cube be calculated using a quick and dirty application of available techniques; and (2) what are the limitations of the techniques for a given size, incidence angle, etc.?

GTD and PO generally agree near specular reflections in directions normal to any of the faces of the body. Therefore, to discriminate between the techniques, the direction $\theta = 45^\circ$, $\phi = 45^\circ$ for the geometry of Fig. 1.1, which is about as far as possible from specular, is emphasized. For this angle, data were obtained for wavelengths λ such that the cube dimension a/λ ranges from 0.1 to 1.8 using MOM, and 0.1 to 10.0 for GTD and PO. However, as discussed below, no technique is accurate over the full computed range. Experimental data was obtained for the a/λ range of 0.1 to 3.0.

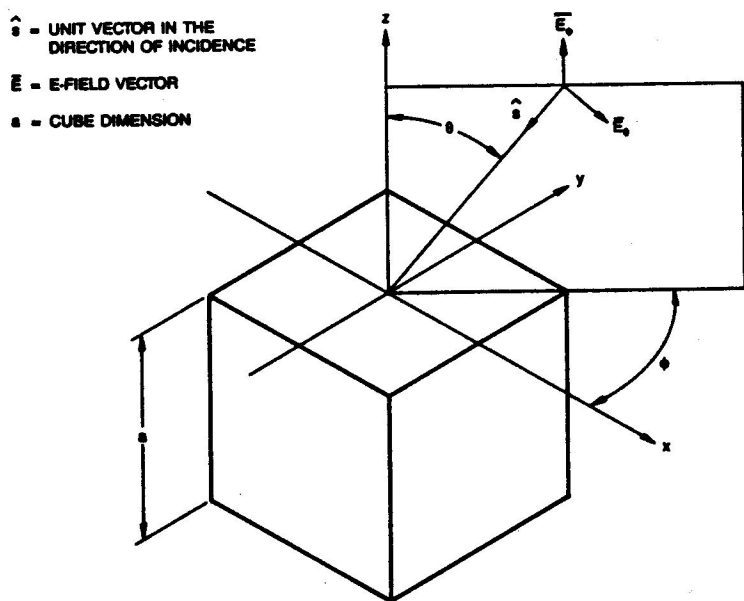


Figure 1.1. Global coordinate system.

The Livermore Numerical Electromagnetics Code [1] (NEC) was used for the method of moments calculations. This code includes both a patch model based on the magnetic field equation, and a wire grid model based on the electric field equation. For the patch model, each cube face was divided into 25 square patches of equal size, giving a total of 150 patches. For the wire model, the division was basically the same, but with the edges of each patch replaced by a wire, giving a total of 300 wires. The wire diameter was $0.0318a$, to satisfy the "same surface area" criterion [2].

According to the NEC User's Manual [1], this patch subdivision should be good for a/λ up to 1.0, and the wire subdivision should be good for a/λ up to 0.5. As shown in Fig. 2.1, in fact the patch and

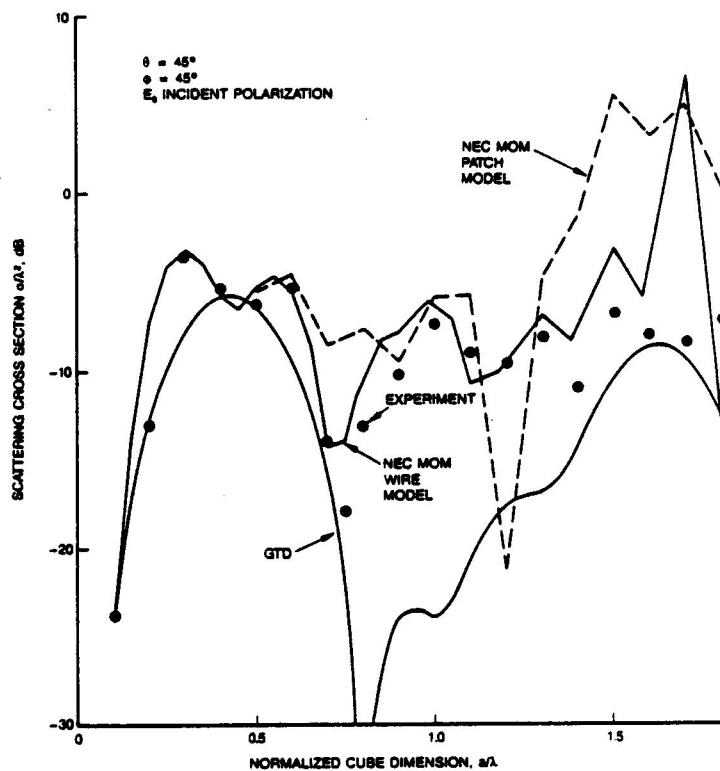


Figure 2.1. Cube monostatic backscattering versus a/λ .

wire grid results agree well up to $a/\lambda = 0.5$, but the experimental results agree better with the wire model results for $a/\lambda > 0.5$. (Also shown in the figure are GTD results which are discussed in the following section.) The experimental and analytical results shown in Fig. 2.1 have not been scaled in magnitude, and the agreement in absolute terms is excellent. For $a/\lambda > 1.0$, the MOM results diverge badly, which is not surprising. Of course, a finer patch subdivision could increase the range of accuracy, but the 300 by 300 matrix for the cases run here is close to the practical limits of the VAX 785 used to obtain the solution. Symmetry was not used to reduce the number of variables, and this would be a good way to extend the region of validity. Internal resonances are also a potential problem for $a/\lambda \geq 0.5$, and shorting these out would be another useful improvement.

In summary, the patch MOM results agree with the experimental results only up to $a/\lambda = 0.5$, which corresponds to a 0.1λ by 0.1λ patch size. Somewhat surprisingly, the wire model results agree reasonably well up to $a/\lambda = 1.3$, which corresponds to a wire grid segment length of 0.26λ . For larger values of a/λ , the wire grid and patch model MOM results diverge from each other and from the experimental results.

The GTD computation was based on corner diffraction coefficients similar to those used by Sikta et al. [3]. The actual coefficients used were developed by Marhefka [4]. Only single diffraction terms were considered. It is well known that multiple diffraction is important for cube dimensions on the order of 1λ , so these results are certainly not representative of good GTD practice for small values of a/λ . However, the complexity of GTD analysis rises sharply when multiple diffraction is included, so these results do show what can be obtained with a relatively simple GTD analysis. For the case considered here, the diffracted field from each contribution is given by

$$E_{||}^d = -D_s E_{||}^i \frac{e^{-jks}}{s} \quad (3.1)$$

$$E_{\perp}^d = -D_h E_{\perp}^i \frac{e^{-jks}}{s}$$

where superscripts d and i denote diffracted and incident fields, respectively; subscripts $||$ and \perp denote parallel and perpendicular field components, respectively

s is the two-way path length from the illumination source to the corner¹

$$k = 2\pi/\lambda$$

D_s and D_h are the "soft" and "hard" diffraction coefficients

$\bar{E}_{||}$ and \bar{E}_{\perp} are parallel and perpendicular to the plane of incidence, defined with respect to a local coordinate system for each edge,

¹The distance s is calculated using a "far-field" approximation so the source is implicitly assumed to be at an infinite distance from the cube.

as illustrated in Fig. 3.1. The unit vector \hat{s} is in the direction of incidence; \hat{s} , $\bar{E}_{||}$ and \bar{E}_{\perp} are mutually orthogonal. Also shown in Fig. 3.1 are the local incidence angles β_0 and ϕ_0 . The unit vector \hat{s} is the same in both global and local coordinates (Figs. 1.1 and 3.1), but the field components and incidence angles in global and local coordinates are in general completely different. The explicit form for the diffraction coefficients are

$$D_{\hat{n}} = \bar{j} \frac{\tan \beta_0}{8n\pi k} \left\{ \left| F \left[\frac{1}{2\pi \cos^2 \beta_0} \right] \right| 2 \cot \frac{\pi}{2n} \right. \\ \left. + \left| F \left[\frac{\cos^2 \phi_0}{2\pi \cos^2 \beta_0} \right] \right| \left(\cot \frac{\pi - 2\phi_0}{2n} + \cot \frac{\pi + 2\phi_0}{2n} \right) \right\} \quad (3.2)$$

where β_0 and ϕ_0 are as defined in Fig. 3.1
 n is the wedge angle parameter; the internal wedge angle is $(2 - n)\pi$, so $n = 3/2$ for a cube, $n = 2$ for a flat plate

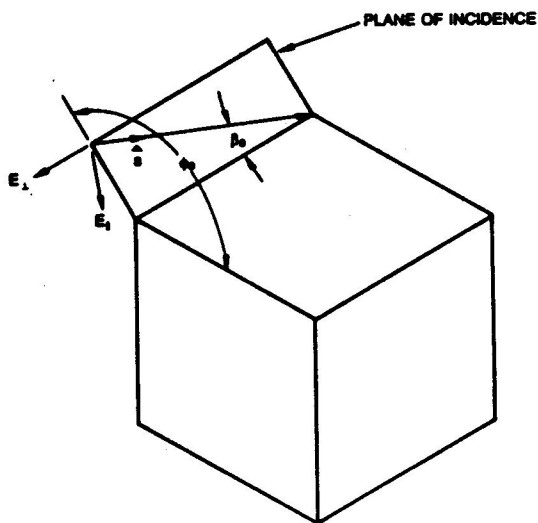


Figure 3.1. Local edge coordinate system.

and F is defined by

$$F[\mathbf{x}] \equiv 2j|\sqrt{\mathbf{x}}|e^{j\mathbf{x}} \int_{|\sqrt{\mathbf{x}}|}^{\infty} e^{-j\tau^2} d\tau \quad (3.3)$$

Each of the three edges forming a corner will make a contribution to the scattered field, if it is illuminated by the incident field. If the global incident angles are restricted to the quadrant

$$0 < \theta < \pi/2 \quad (3.4)$$

$$0 < \phi < \pi/2$$

then there will be 18 edge contributions, as illustrated in Fig. 3.2.

A computer program was written to evaluate the resultant of any subset of these contributions. For example, by selecting contributions

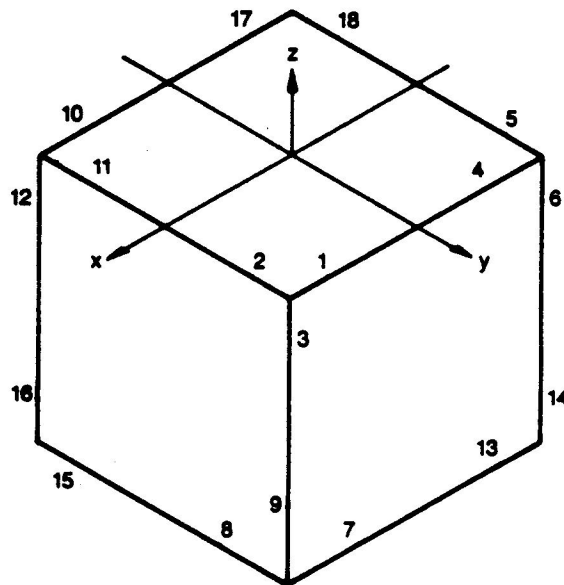


Figure 3.2. Eighteen edge contributions to the scattered field.

1, 3, 4, 6, 7, 9, 13, and 14, the scattering of just one face is obtained (see Fig. 3.2), and if the parameter n is set equal to 2, the result is the scattering of a square flat plate.² This was the case considered by Sikta et al. [3], and was used as the first test case; the new results agree well with Sikta et al., as shown in Fig. 3.3. For the

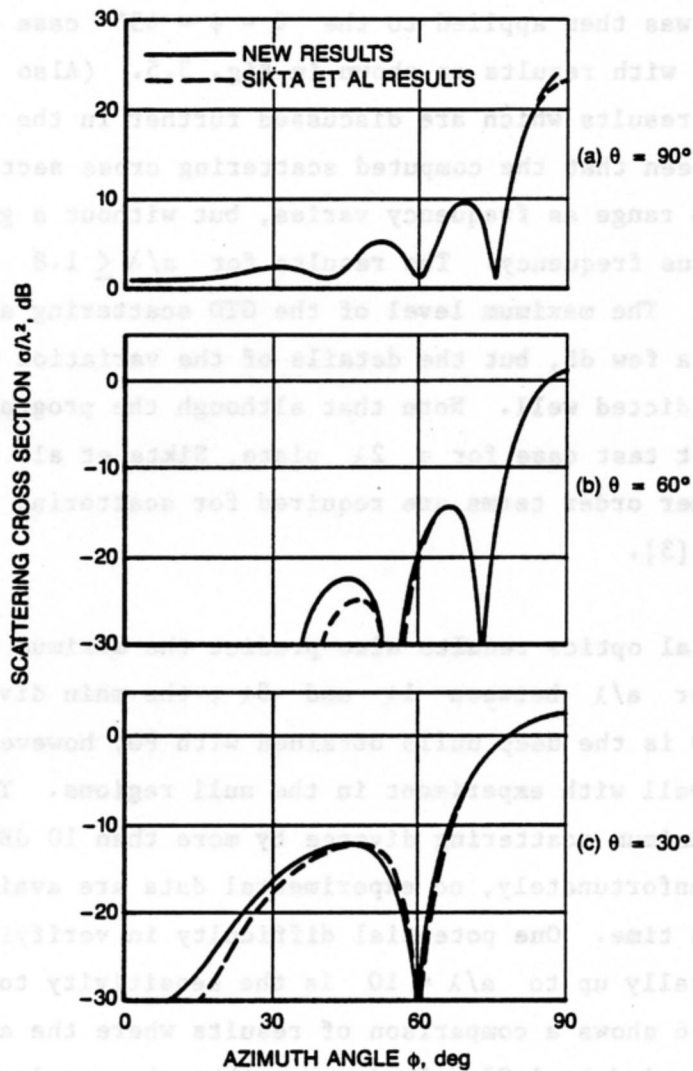


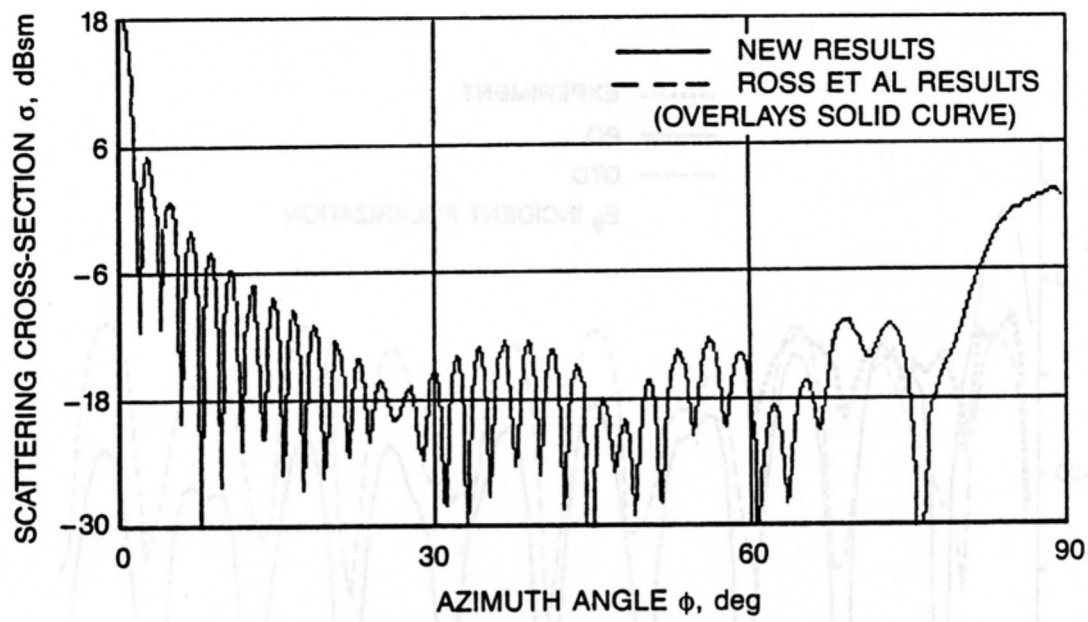
Figure 3.3. First test case: scattering from a 2λ by 2λ square flat plate.

²It is necessary to be careful that ϕ_0 is calculated correctly when n values other than 1.5 are used.

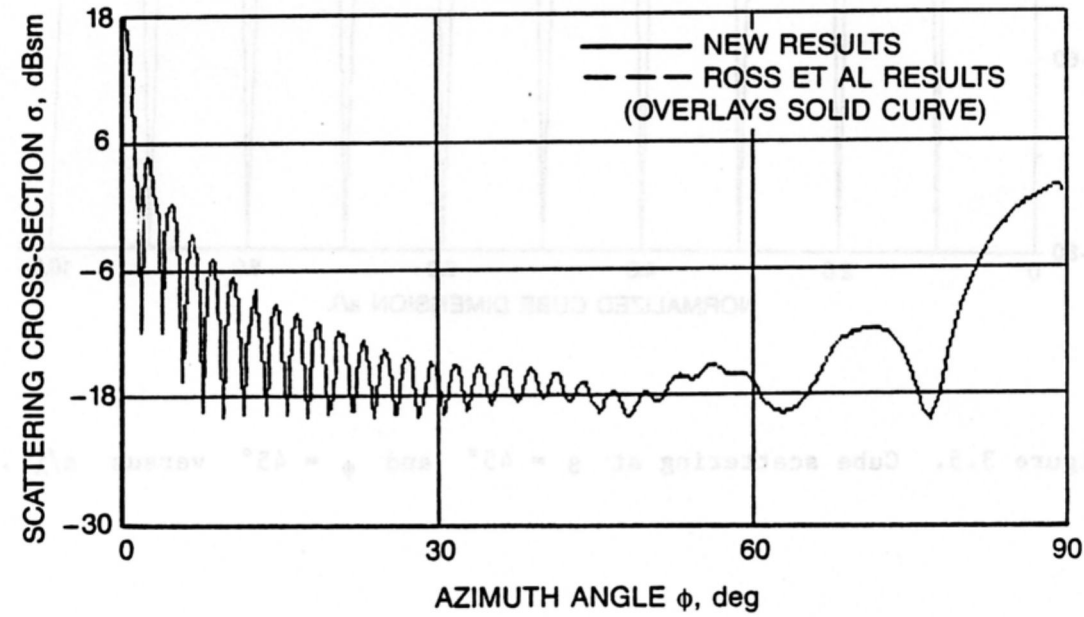
second test case, the cube was modified to match a rectangular block evaluated by Ross et al., and reproduced by Kell and Ross [5]. The block dimensions are 14.763λ , 17.716λ , and 2.226λ in the x , y , and z directions, respectively. In this case, the new results are indistinguishable from Ross et al., as shown in Fig. 3.4.

The program was then applied to the $\theta = \phi = 45^\circ$ case of particular interest here, with results as shown in Fig. 3.5. (Also shown in the figure are PO results which are discussed further in the following section.) It is seen that the computed scattering cross section varies over about a 30 dB range as frequency varies, but without a general systematic trend versus frequency. The results for $a/\lambda \leq 1.8$ are replicated in Fig. 2.1. The maximum level of the GTD scattering agrees with experiment within a few dB, but the details of the variation with frequency are not predicted well. Note that although the program agreed well with the first test case for a 2λ plate, Sikta et al. comment that "...many higher order terms are required for scattering outside the principal planes" [3].

The physical optics results also predict the maximum level within a few dB for a/λ between 1λ and 3λ ; the main divergence between PO and GTD is the deep nulls obtained with PO; however, neither GTD nor PO agree well with experiment in the null regions. The PO and GTD results for maximum scattering diverge by more than 10 dB for larger values of a/λ ; unfortunately, no experimental data are available in this range at this time. One potential difficulty in verifying the results experimentally up to $a/\lambda = 10$ is the sensitivity to alignment errors. Figure 3.6 shows a comparison of results where the azimuth and polar angles are varied by 1.0° . It is seen that the results vary by



(a) E_ϕ polarization



(b) E_θ polarization

Figure 3.4. Second test case: rectangular block.

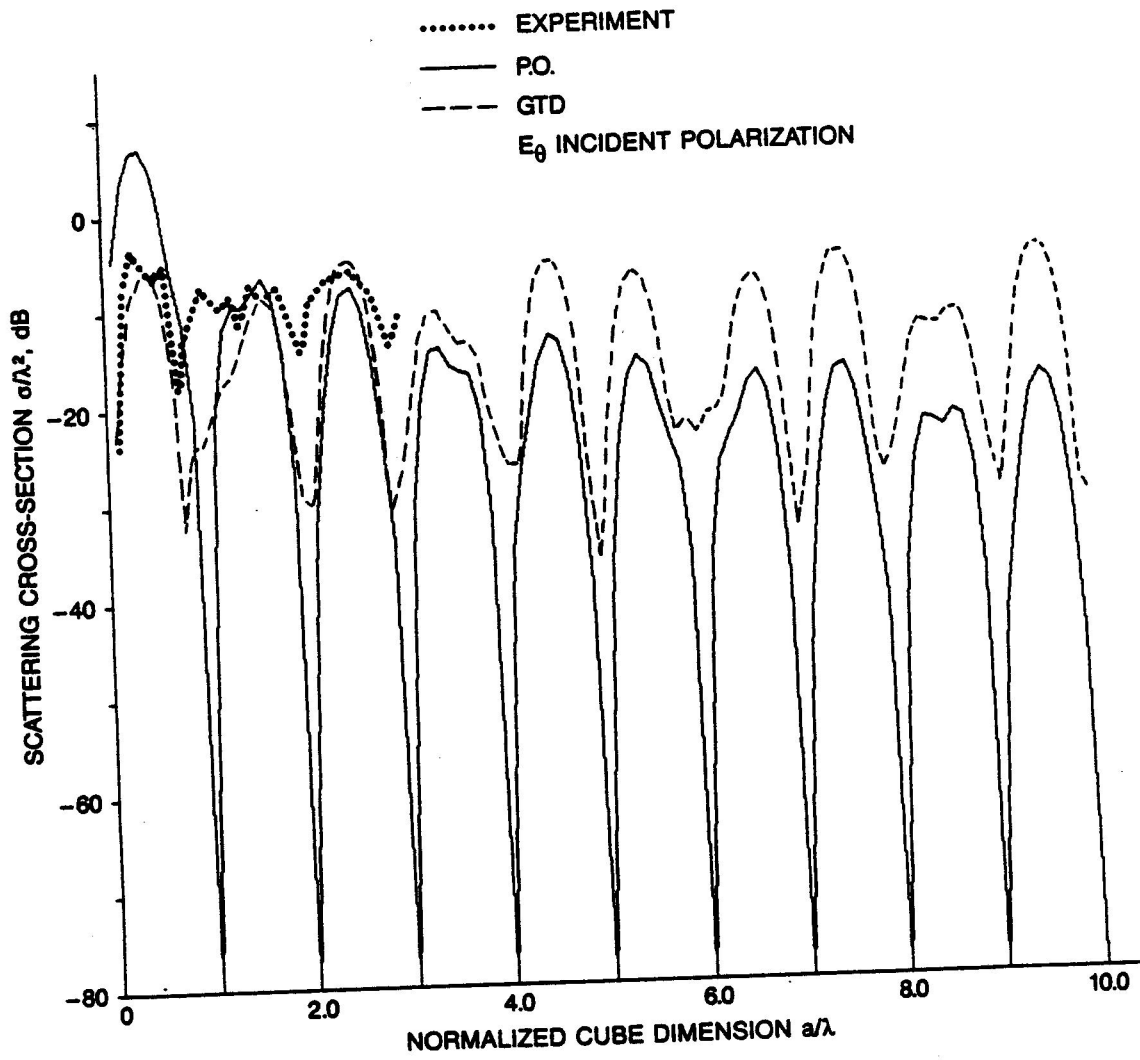
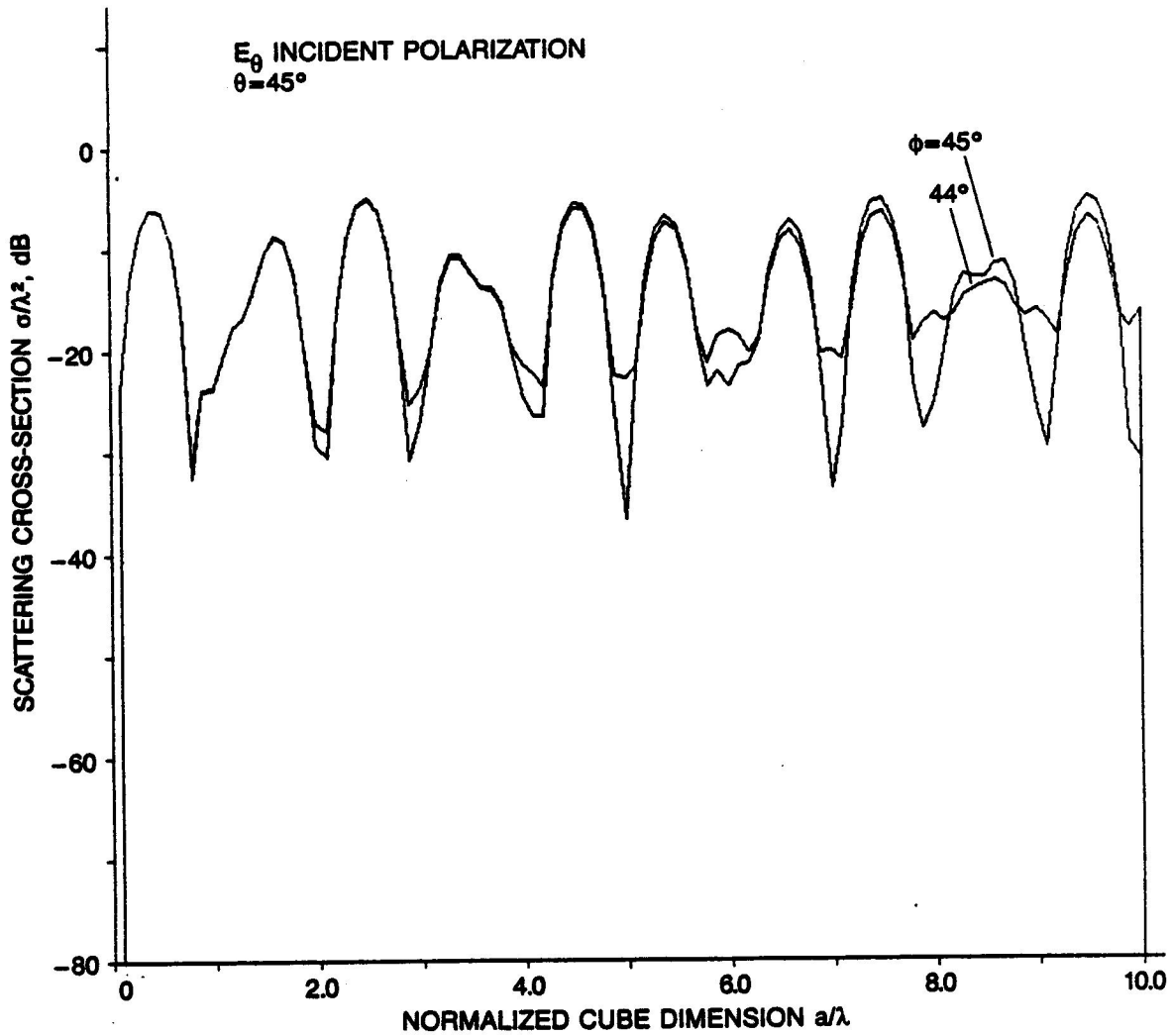


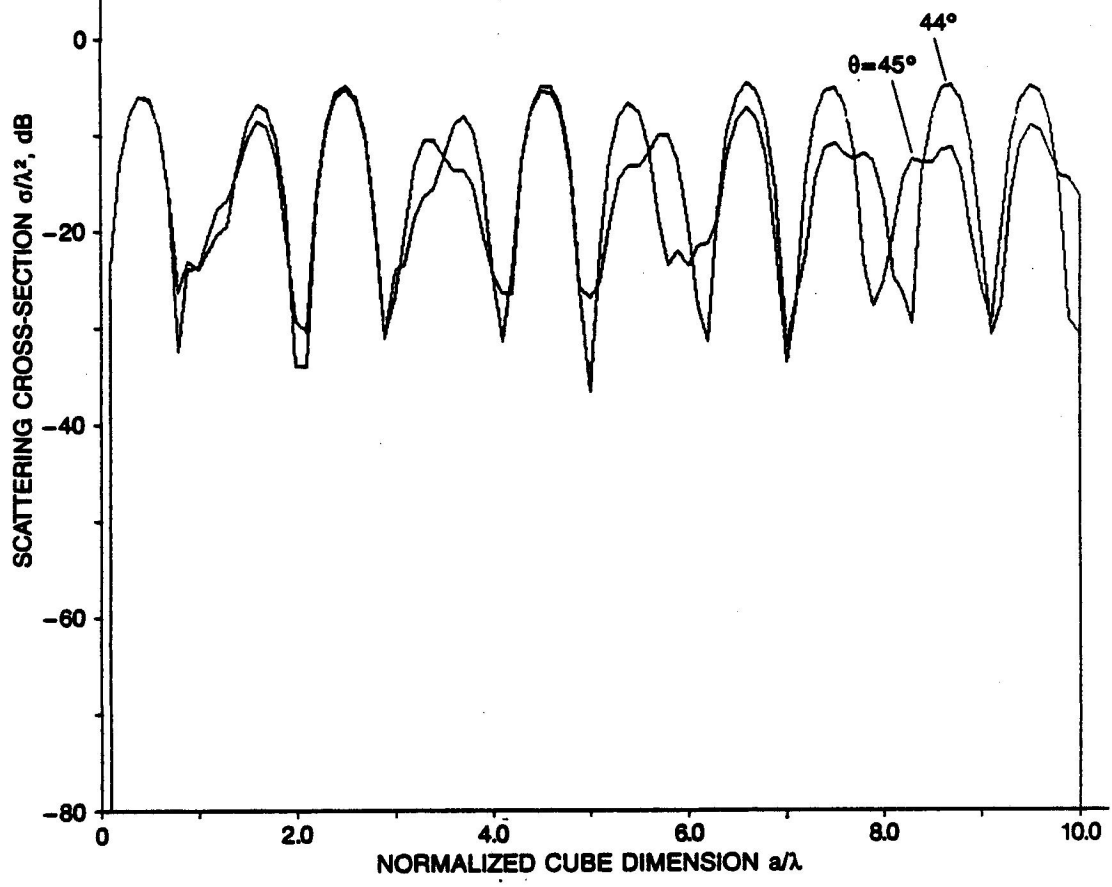
Figure 3.5. Cube scattering at $\theta = 45^\circ$ and $\phi = 45^\circ$ versus a/λ



(a) Sensitivity to azimuth angle

Figure 3.6. Sensitivity of scattering results to angle errors.

E_θ INCIDENT POLARIZATION
 $\phi = 45^\circ$



(b) Sensitivity to polar angle

Fig. 3.6 (Cont.)

several dB. Therefore, very careful angular alignment is required for a good verification.

As noted previously, the analytic and experimental results are not scaled and agree quite well in absolute terms. The analytic results are for monostatic backscattering; the experimental results were actually taken with a separate transmit and receive antenna with a 5-degree bistatic angle between them. This small bistatic angle probably accounts for some of the difference between experimental and calculated values at the larger values of a/λ . It would be useful to calculate the results for this bistatic angle to see how significant this is, or obtain true monostatic data, but this is left undone for this study.

The physical optics method is based on the approximation that on illuminated surfaces the currents \bar{J} are given by

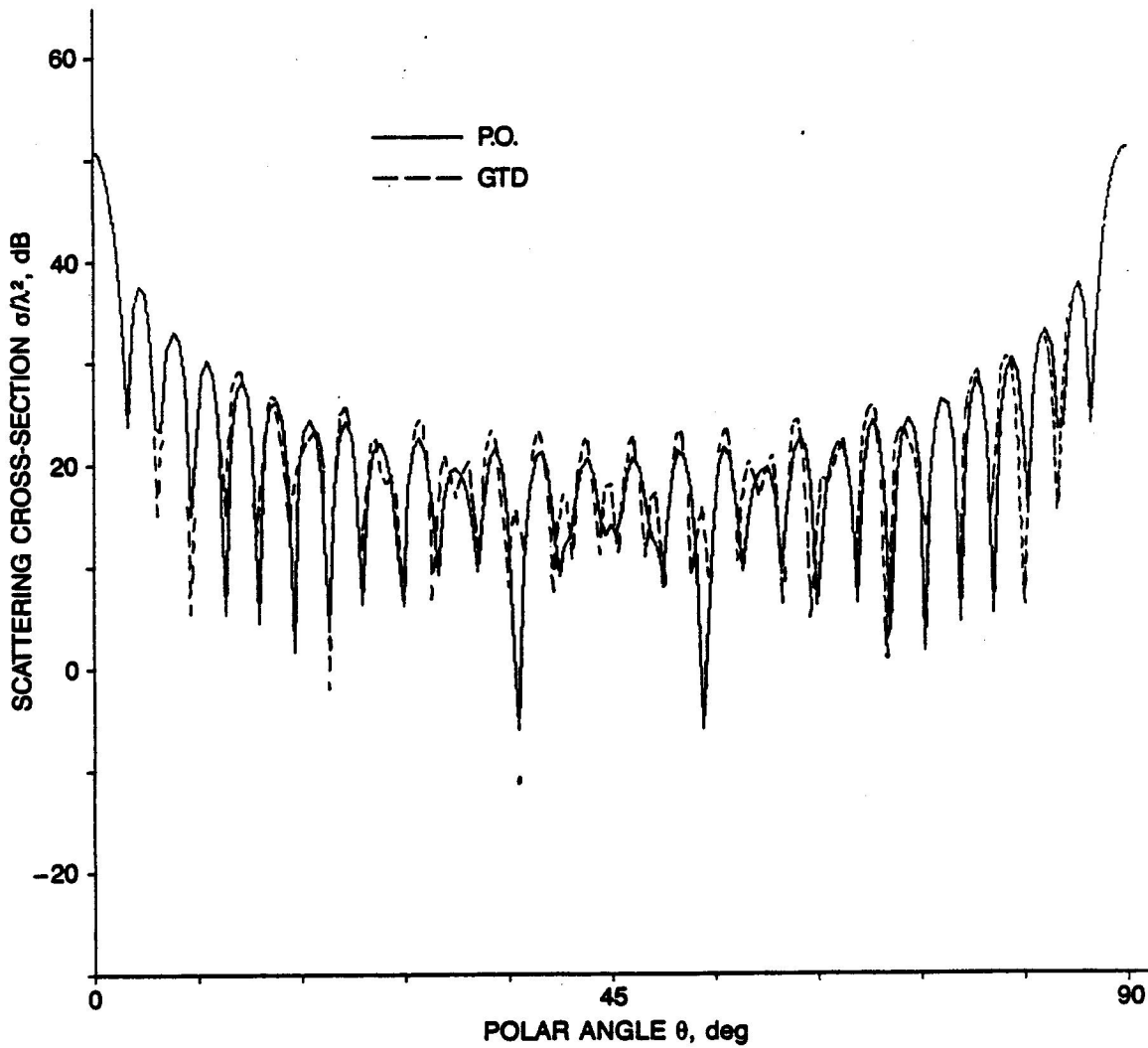
$$\bar{J} = 2\hat{n} \times \bar{H}_i \quad (4.1)$$

where \bar{H}_i is the incident magnetic field. On shadowed surfaces, the currents are zero. The scattered field is then obtained by integrating the current contributions over the surface using standard equations [6]. It is well known that physical optics gives a poor approximation for the currents near edges and/or shadow boundaries; however, in spite of this, the bottom line results for the scattered fields are often a good approximation. It is generally accepted that GTD is more accurate than PO for this class of problems.³ However, at the very least, PO provides an excellent check on GTD insofar as confirming the general character of the results, as shown below.

The scattering cross-section was calculated for a cube 10λ on a side for both a principal plane $\phi = 0^\circ$, and for $\phi = 45^\circ$; θ was varied over a $0^\circ - 90^\circ$ range. The PO results are compared with GTD results in Fig. 4.1. For this case, the physical optics results are identical for E_θ or E_ϕ incident polarization. The GTD results are not identical, but the comparison between PO and GTD is very similar for both polarizations; the E_θ polarization results are shown in Fig. 4.1. It is seen that the general features of the patterns agree quite well. However, in directions near nulls or near $\theta = 90^\circ$ for the $\phi = 45^\circ$ pattern, the results deviate by more than 20 dB.

The PO results at $\theta = 45^\circ$ and $\phi = 45^\circ$ versus a/λ have been shown previously in Fig. 3.5. Again, the general features agree well

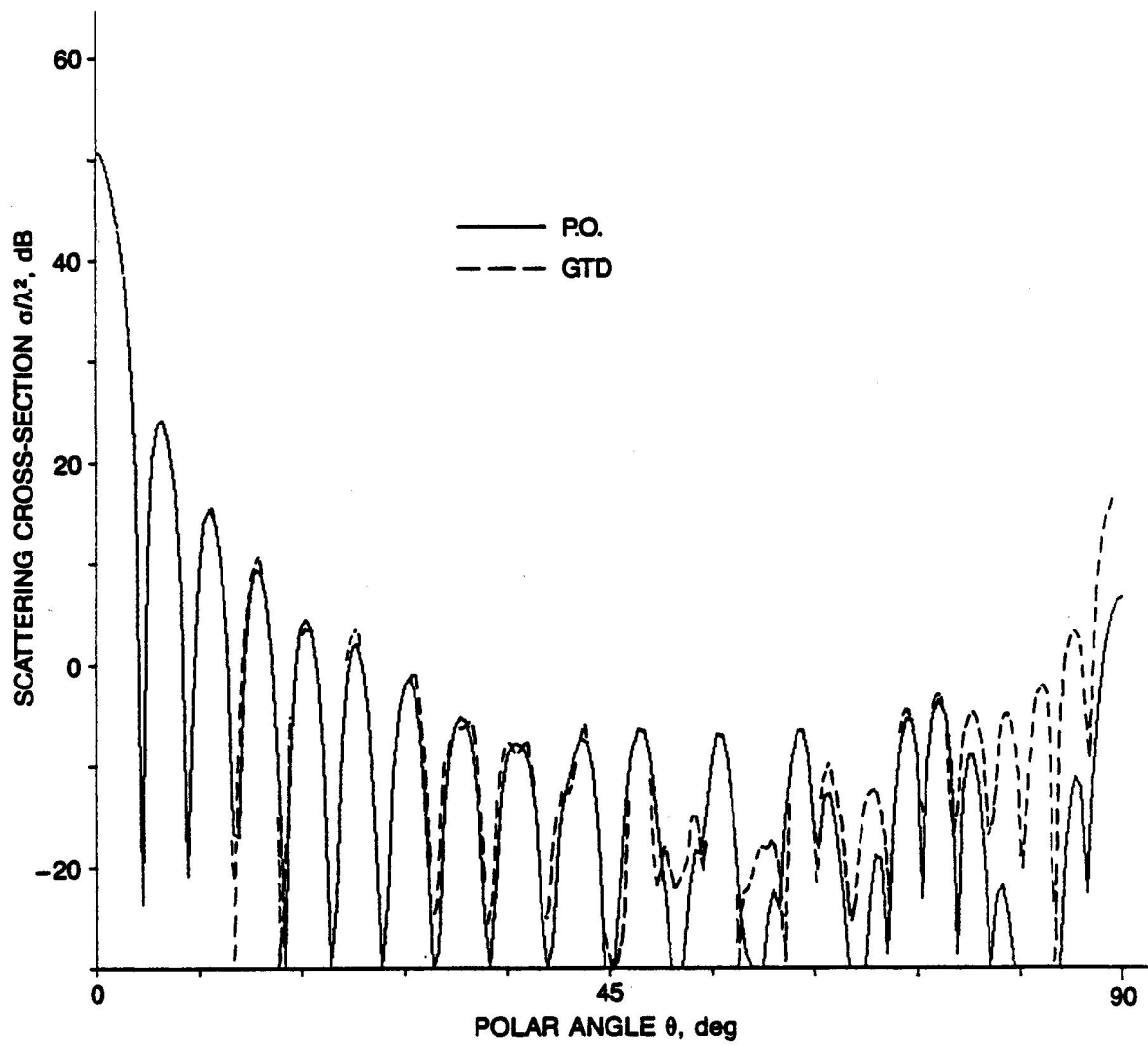
³If PO is corrected for fringe currents using the Physical Theory of Diffraction (PTD), the accuracy may be comparable or superior to GTD—each technique has its advocates.



(a) $\phi = 0^\circ$

Figure 4.1. PO and GTD results for a 10λ cube.

with GTD, but large deviations in level are evident. As mentioned above, it is generally believed that the GTD results are more accurate than PO.



(b) $\phi = 45^\circ$

Fig. 4.1 (Cont.)

The method of moments results are generally reliable only for segment lengths of 0.1λ or less, but the wire grid model provided good results up to a 0.26λ segment length. Single-diffraction GTD generally predicts the maximum values of backscattering versus frequency within a few dB over the entire range of experimental values--up to $a/\lambda = 3$ --but does not accurately model behavior between maxima.

Physical optics results are surprisingly accurate for most scattering directions, and even for the $\theta = \phi = 45^\circ$ direction are fairly accurate for $1 < a/\lambda < 3$; PO results diverge by roughly 10 dB from GTD results outside this range for the $\theta = \phi = 45^\circ$ direction.

Experimental results for the larger values of a/λ would be valuable, but special care must be taken to assure good angular alignment.

A cube is as basic and elementary a shape as a sphere; scattering from a sphere can be calculated so accurately and reliably that calculated values are used as a standard to calibrate experiments; in contrast, no technique considered here is really satisfactory for calculating scattering from a cube. This appears to be a problem worthy of further attention.

ACKNOWLEDGEMENT

The author is indebted to Dr. Gail Flesher of General Research Corporation for the experimental results, which greatly enhance the value of the results presented in this paper.

REFERENCES

1. G.J. Burke and A.J. Poggio, "Numerical Electromagnetics Code (NEC)--Method of Moments," NOSC Technical Document 116, Naval Ocean Systems Center, San Diego, California, January 1981.
2. A.C. Ludwig, "Wire Grid Modeling of Surfaces," IEEE Trans. on Antennas and Propagation (to be published Sept 1987).
3. F.A. Sikta et al., "First-Order Equivalent Current and Corner Diffraction Scattering From Flat Plate Structures," IEEE Trans. on Antennas and Propagation, AP-37, No. 4, July 1983, pp. 584-589.
4. R. Marhefka, private communication, May 1986.
5. R.E. Kell and R.A. Ross, "Radar Cross Section of Targets," Chapter 27 of The Radar Handbook, M. Skolnik (Ed.), McGraw-Hill, 1970.
6. W.V.T. Rusch and P.P. Potter, Analysis of Reflector Antennas, Academic Press, New York, 1970.

**A NUMERICAL EXAMPLE OF
A 2-D SCATTERING PROBLEM USING
A SUBGRID***

**John C. Kasher
Department of Physics
University of Nebraska at Omaha
Omaha, NE 68182
and
D-Division
Lawrence Livermore National Laboratory
Livermore, CA 94550**

and

**Kane S. Yee
23350 Tyonita Road
Los Altos Hills, CA 94022
and
D-Division
Lawrence Livermore National Laboratory
Livermore, CA 94550**

ABSTRACT

In this paper we present a detailed application of a subgridding scheme for the finite difference time domain (FDTD) numerical solution to Maxwell's equations. The subgridding scheme will be necessary for greater detail and for localized calculations when other methods for the subcell modifications of the regular FDTD are not applicable. We have made comparative calculations, as a function of mesh size, of the reflection coefficient and shunt capacitance associated with two infinite parallel plates with a finite discontinuity in plate separation.

*This work was performed under the auspices of the U. S. Department of Energy by Lawrence Livermore National Laboratory under contract No. W-7405-Eng-48.

1. Statement of the Problem

Shown in Figure 1 is a cross-section of infinite parallel plane conductors. The heights of the two sections are such that only the TEM wave will propagate for a chosen frequency. The plates should be considered to extend to infinity in the x and z directions, even though the boundaries for our calculations are at $X_L = 2\lambda$ to the left of the discontinuity, and $X_R = 11\lambda$ to the right. We will show that our calculational algorithm that uses grids of different sizes in different regions can give meaningful results. These results will be compared to calculations using a uniform coarse grid and a uniform fine grid throughout.

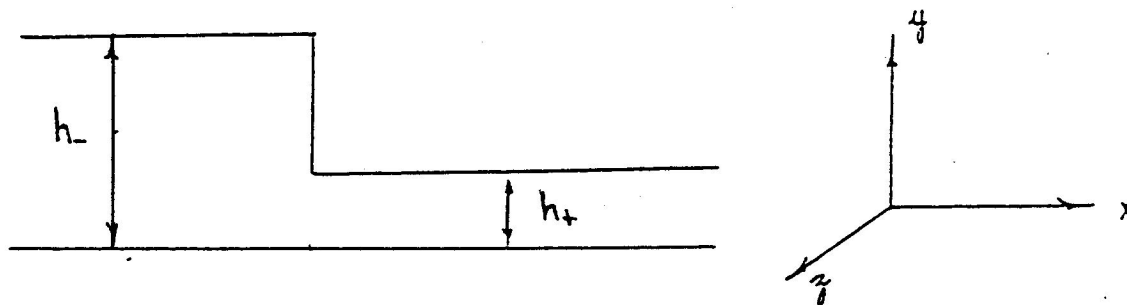


Fig. 1. The cross-section of infinite parallel plane conductors.

Our calculational tool, as sketched in Fig. 2, is the finite difference time domain algorithm¹ with various grid sizes and time steps in various regions.²

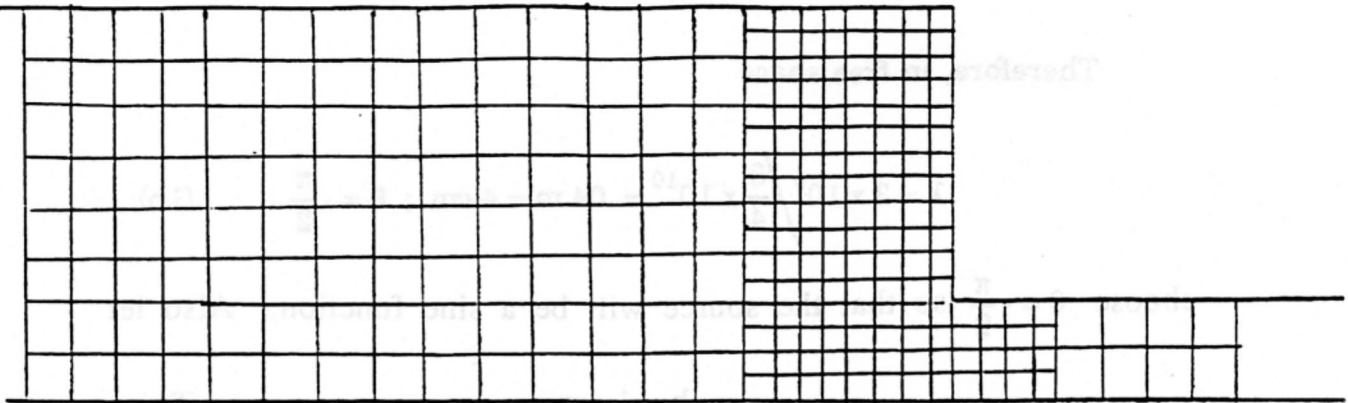


Fig. 2. A possible zoning for the FDTD calculation.

When a sinusoidal TEM wave traveling from the left encounters a step discontinuity, higher order TM modes will be generated in order to satisfy the boundary conditions. The frequency and the heights will be so chosen that only the TEM mode will propagate. Regions of various spatial and time divisions are shown in Fig. 3.

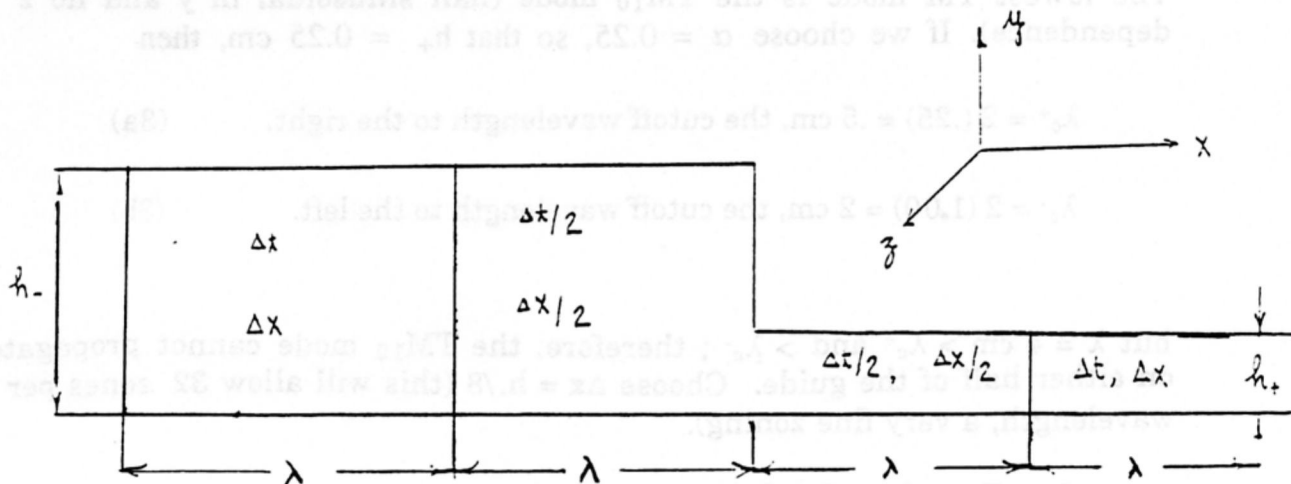


Fig. 3. Regions of different spatial and time subdivisions.

2. Input Information

We chose a sinusoidal wave with $\vec{E}^i = \hat{y} E^i$; $\vec{H}^i = \hat{z} H^i$. E^i and H^i do not depend on z .

$$E^i(x,t) = \text{Re} \{ A e^{j\omega t} e^{j\theta} e^{-jkx} \} ; \text{ where } k = \omega \sqrt{\mu\epsilon} \quad (1)$$

$$f = \frac{3}{4} \times 10^{10} \text{ Hertz} \quad (1a)$$

Therefore, in free space

$$\lambda = 3 \times 10^8 / \frac{3}{4} \times 10^{10} = .04 \text{ m} = 4 \text{ cm} ; \theta = -\frac{\pi}{2} \quad (1b)$$

choose $\theta = -\frac{\pi}{2}$ so that the source will be a sine function. Also let

$$h = 1 \text{ cm}, \quad (2a)$$

$$h_+ = \alpha h, \text{ where } 0 \leq \alpha \leq 1. \quad (2b)$$

It is physically plausible that the boundary conditions (namely, the vanishing of the tangential components of the electric field on the conducting planes) can be satisfied with TM modes and the TEM mode. The lowest TM mode is the TM_{10} mode (half sinusoidal in y and no z dependence). If we choose $\alpha = 0.25$, so that $h_+ = 0.25 \text{ cm}$, then

$$\lambda_{c^+} = 2 (.25) = .5 \text{ cm}, \text{ the cutoff wavelength to the right.} \quad (3a)$$

$$\lambda_{c^-} = 2 (1.00) = 2 \text{ cm}, \text{ the cutoff wavelength to the left.} \quad (3b)$$

but $\lambda = 4 \text{ cm} > \lambda_{c^+}$ and $> \lambda_{c^-}$; therefore, the TM_{10} mode cannot propagate on either half of the guide. Choose $\Delta x = h./8$ (this will allow 32 zones per wavelength, a very fine zoning).

3. Boundary Condition on the Left

Far away to the left of the discontinuity, we have

$$\vec{E}(x,t) = \hat{y} (E^i(x,t) + E^r(x,t)) \quad (4)$$

where $E^r(x,t)$ is a reflected TEM wave. If x_L is the left boundary,

$$\begin{aligned} E^r(x_L, t+\Delta t) &= E^r(x_L+ct+c\Delta t) \\ &= E^r((x_L+c\Delta t) + ct) \\ &= E^r(x_L+c\Delta t, t) \end{aligned}$$

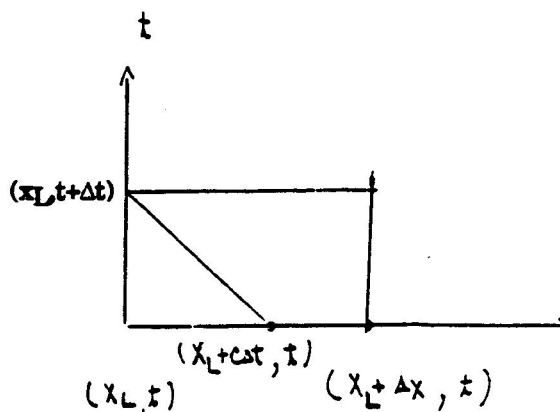


Fig. 4. Interpolation to get $E^r(x_L, t+\Delta t)$.

The value of E^r at $(x_L+c\Delta t, t)$ will be obtained by interpolation.

Thus,

$$E^r(x_L, t+\Delta t) = \frac{\Delta x - c \Delta t}{\Delta x} E^r(x_L, t) + \frac{c \Delta t}{\Delta x} E^r(x_L+\Delta x, t) \quad (4a)$$

It is to be observed that $c\Delta t \leq \Delta x$ is due to stability considerations. We also note that $E^i(x_L, t+\Delta t) = E^i(x_L-c(t+\Delta t))$ and this is given.

$$\begin{aligned} E(x_L, t+\Delta t) &= E^i(x_L, t+\Delta t) + E^r(x_L, t+\Delta t) \quad (5) \\ &= E^i(x_L, t+\Delta t) + \frac{\Delta x - c\Delta t}{\Delta x} (E(x_L, t) - E^i(x_L, t)) \\ &\quad + \frac{c \Delta t}{\Delta x} (E(x_L+\Delta x, t) - E^i(x_L+\Delta x, t)) \end{aligned}$$

$$\begin{aligned} E^i(x, t) &= \text{Re} \left\{ \exp(j\omega t + jkx_L - jkx - j\frac{\pi}{2}) \right\} \\ &= \sin(\omega t + kx_L - kx) \quad \text{if } \omega t + kx_L - kx > 0 \\ E^i(x, t) &= 0 \quad \text{if } \omega t + kx_L - kx < 0. \end{aligned}$$

Or

$$E^i(x_L, t) = \begin{cases} \sin \omega t, & \text{if } t \geq 0; \\ 0 & \text{if } t < 0. \end{cases}$$

$$E^i(x_L + \Delta x, t) = \begin{cases} \sin(\omega t - k \Delta x), & \text{if } \omega t - k \Delta x \geq 0; \\ 0, & \text{if } \omega t - k \Delta x < 0. \end{cases} \quad (5a)$$

$$\omega = 2\pi f = \frac{3\pi}{2} \times 10^{10}; k = \omega/3 \times 10^8. \quad (5b)$$

4. Boundary Condition on the Right

Far away to the right of the discontinuity, we have only a transmitted wave traveling to the right. If we let x_R be the right boundary, we have

$$\begin{aligned} E(x_R, t + \Delta t) &= E(x_R - c(t + \Delta t)) = E((x_R - c\Delta t) - ct) \\ &= E(x_R - c\Delta t, t) \end{aligned}$$

Or

$$\begin{aligned} E(x_R, t + \Delta t) &= \frac{\Delta x - c\Delta t}{\Delta x} E(x_R, t) \\ &\quad + \frac{c\Delta t}{\Delta x} E(x_R - \Delta x, t) \end{aligned} \quad (6)$$

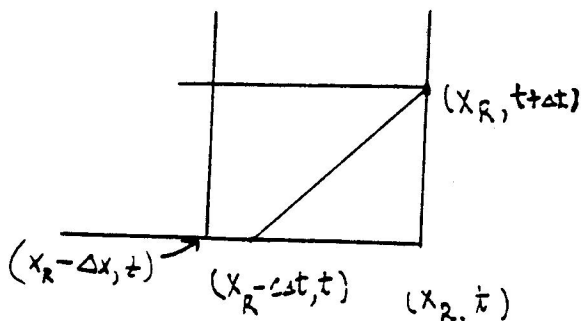


Fig. 5. Interpolation to get $E(x_R, t + \Delta t)$.

5. The Transmission Line Approximation

We can obtain a transmission line approximation of our problem by assuming that the electromagnetic field is that given by 1-D TEM Maxwell's equations.

$$\epsilon \frac{\partial E_y}{\partial t} = -\frac{\partial H_z}{\partial x} \quad (7a)$$

$$\mu \frac{\partial H_z}{\partial t} = -\frac{\partial E_y}{\partial x} \quad (7b)$$

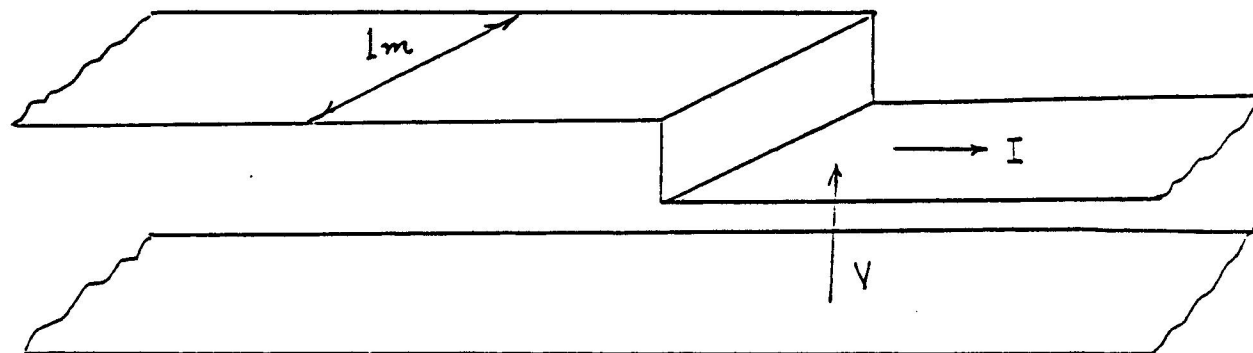


Fig. 6. A unit width two-line transmission line.

Referring to Figure 1 for the coordinates and Figure 6 for the direction of the voltage and current, we let

$$V = -h E_y$$

$$I = -H_z \cdot 1 \text{ m}$$

where h is the separation between the parallel planes.

(7b) and (7a) can be written as

$$\frac{\partial V}{\partial x} = -h\mu \frac{\partial I}{\partial t} \quad (8a)$$

$$\frac{\partial I}{\partial x} = -\frac{\epsilon}{h} \frac{\partial V}{\partial t} \quad (8b)$$

(8a) and (8b) are the familiar transmission-line equations with

$$L = h\mu \quad \text{henrys/m} \quad (9a)$$

$$C = \frac{\epsilon}{h} \quad \text{farad/m} \quad (9b)$$

The wave velocity is

$$v = (\sqrt{LC})^{-1} = \frac{1}{\sqrt{\mu\epsilon}}$$

and the characteristic impedance is

$$Z_0 = \sqrt{\frac{L}{C}} = \sqrt{\frac{\mu}{\epsilon}} h = \eta h ; \eta = \sqrt{\frac{\mu}{\epsilon}}$$

where η is the "characteristic" impedance of a plane TEM wave. For the purpose of analysis, we take $x=0$ at the discontinuity as shown in Figure 7.

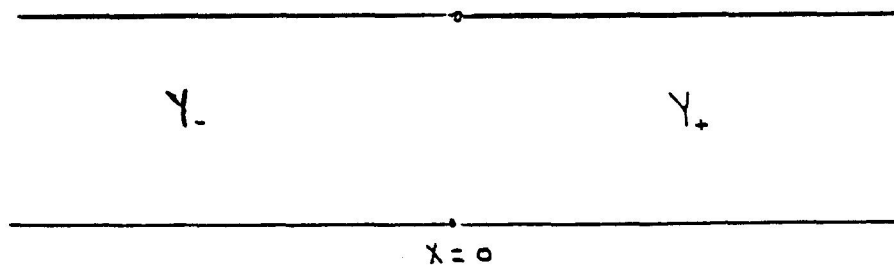


Fig. 7. Two different transmission lines connected at $x=0$.

Our crude approximation is equivalent to the wave propagation in two different transmission lines connected at $x=0$. The symbols in Figure 7 are

$$Z_- = Y_-^{-1}, \text{ the characteristic impedance for } x < 0,$$

$$Z_+ = Y_+^{-1}, \text{ the characteristic impedance for } x > 0,$$

If we use the superscript + to denote a positive traveling wave and the superscript - to denote a negatively traveling wave, we get at $x=0$.

$$V = V^+ + V^-$$

$$I = I^+ + I^- = (1/Z_-)(V^+ - V^-)$$

For $x=0_+$, we have

$$V = Z_+ I$$

as there is only an outgoing wave to the right. Combining

$$(V^+ + V^-) \Big|_{x=0_-} = V \Big|_{x=0_+} = Z_+ I \Big|_{x=0_+}$$

$$= Z_+ I \Big|_{x=0_-} = \frac{Z_+}{Z_-} (V^+ - V^-) \Big|_{x=0_-}$$

yields

$$V^- = V^+ \frac{Z_+ - Z_-}{Z_+ + Z_-} = \mathcal{R} V^+ \quad (10a)$$

At $x=0_+$, we have

$$V^+ \Big|_{x=0_+} = (Z_+ I^+) \Big|_{x=0_+} = (V^+ + V) \Big|_{x=0}$$

$$V^+ \Big|_{x=0_+} = (1 + \mathcal{R}) V^+ \Big|_{x=0} = \mathcal{T} V^+ \Big|_{x=0} \quad (10b)$$

where \mathcal{R} and \mathcal{T} are the reflection and transmission coefficients, respectively, at $x=0$.

$$\mathcal{R} = \frac{Z_+ - Z_-}{Z_+ + Z_-} \quad (11a)$$

$$\mathcal{T} = 1 + \mathcal{R} = \frac{2Y_-}{Y_- + Y_+} \quad (11b)$$

If we calculate (or measure) the reflection coefficient at a position $n\lambda$ to the left of $x=0$, we get the same value as given in (11a). And, if we calculate (or measure) the transmission coefficient at a position $n\lambda$ to the right of $x=0$, we would get the same \mathcal{T} .

6. The Transmission Line Approximation with Approximate Account for Fringing at the Discontinuity

A more refined approximation would be to use the transmission line approximation for the dominant TEM mode with a shunt capacitor at $x=0$ to account for the fringing of the electric field at the discontinuity ($x=0$). Figure 8 shows such an admittance.²

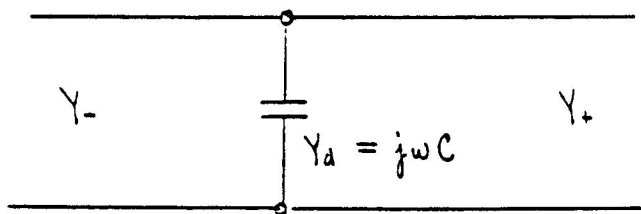


Fig. 8. Shunt admittance at the discontinuity.

For the two semi-infinite transmission lines connected together as shown in Figure 8, the boundary conditions at $x=0$ are

$$\begin{aligned} V(0_-,t) &= V^+(0_-,t) + V^-(0_-,t) = V(0_+,t) \\ I(0_-,t) &= Y_-(V^+(0_-,t) - V^-(0_-,t)) = (Y_d + Y_+) V(0_+,t) \end{aligned}$$

with

$$V^-(0_-,t) = \mathcal{R} V^+(0_-,t) ; V(0_+,t) = \mathcal{T} V^+(0_-,t) .$$

We find that

$$\mathcal{R} = \frac{Y_- - Y_+ - Y_d}{Y_- + Y_+ + Y_d} ; \quad (11c)$$

$$\mathcal{T} = 1 + \mathcal{R} = \frac{2Y_-}{Y_- + Y_+ + Y_d} . \quad (11d)$$

Also, if

$$V^+(x,t) = \text{Re} (e^{j\omega t} e^{-jkx} e^{+jkx_L} e^{-j\pi/2}) \text{ with } x_L = n\lambda$$

then

$$V^-(x,t) = \text{Re} (\mathcal{R} e^{j\omega t} e^{+jkx_L} e^{jkx} e^{j\pi/2}) .$$

For $\mathcal{R} = |\mathcal{R}| e^{j\theta_r}$ we get

$$V^-(x_L,t) = |\mathcal{R}| \sin(\omega t + \theta_r)$$

Both $|\mathcal{R}|$ and θ_r can be obtained from the time history of

$$E^r(x_L,t) = E(x_L,t) - E^i(x_L,t)$$

We can then go back to (11d)

$$Y_d + Y_- + Y_+ = \frac{2Y_-}{1+R}$$

or

$$Y_d = \frac{2Y_-}{1+R} - Y_- - Y_+ \quad (12)$$

From (12) we can get C as required in Figure 8.

In Appendix A we give more details to compute Y_d and hence C from our numerical scheme.

7. Computational Results

We take $h = 1$ cm and $\Delta x = \Delta y = 1/8$ cm. This would allow 32 zones per wavelength. The left calculational boundary is 2λ from the discontinuity and the right calculational boundary is 11λ from the discontinuity. The left boundary condition is imposed at $x = -2\lambda$ and the right boundary condition is imposed at $x = 11\lambda$. For the time interval of calculation, the effect of the right boundary is not felt at the left boundary, as we only wish to test the effect of the change of grid sizes. At $t=0$ we set the electric and magnetic fields equal to zero. This will give us the initial condition. For $t \geq 0$ we set

$$E_y^i \Big|_{x_L = -2\lambda} = \sin \omega t$$

In Figure 9a-c we show

$$E_y^r \Big|_{x_L = -2\lambda} \quad \text{for } t \geq 0.$$

Using Tables 1a-c we can calculate the time difference, Δt , between the cross-over points of the incident and reflected E_y for different values of h_+/h_- . Since ω is known, we can then calculate the phase angle between these E_y from $\theta_r = \omega \Delta t$. We then derive the shunt capacitance as shown in Appendix A.

In the last column of Table 2 we give the reflection coefficient based on equation (A.4). The last column of Table 3 is based on the exact static formula [equation (13) below] due to the fact that the electric field lines at the neighborhood of the discontinuity are curved (fringing).

A static approximation for C shown in Figure 8 can be obtained. It is the excess capacitance over what occurs when the field lines are uniformly distributed and straight across. The formula is³

$$C = \frac{\epsilon}{\pi} \left\{ \frac{(\alpha^2 + 1)}{\alpha} \ln \frac{(1 + \alpha)}{(1 - \alpha)} - 2 \ln \left(\frac{4\alpha}{1 - \alpha^2} \right) \right\} \text{ f/meter width} \quad (13)$$

where $\alpha = h_+ / h$.

8. Conclusions

The sets of calculations of the reflection coefficients and capacitances for the infinite parallel plates with a finite discontinuity show that using grids of different sizes in different regions gives meaningful results. This approach will save considerable running time and require less memory than a finer grid throughout would need. In addition, it will enable smaller objects to be modeled more accurately.

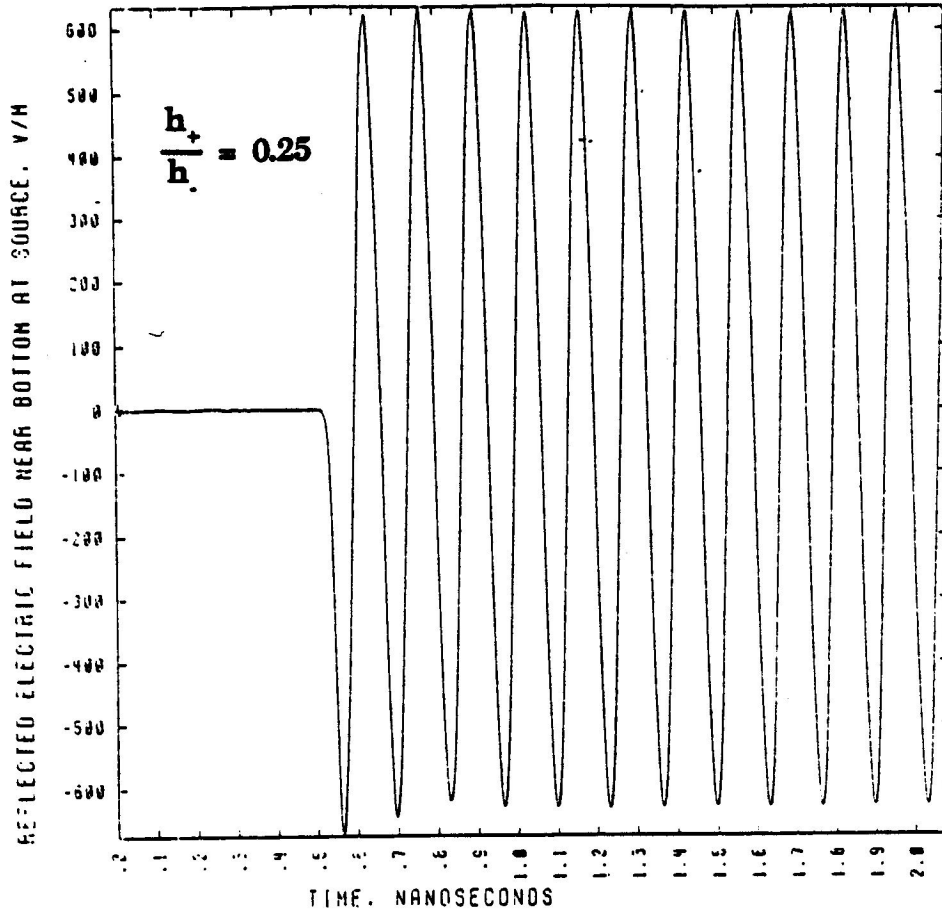


Fig. 9a

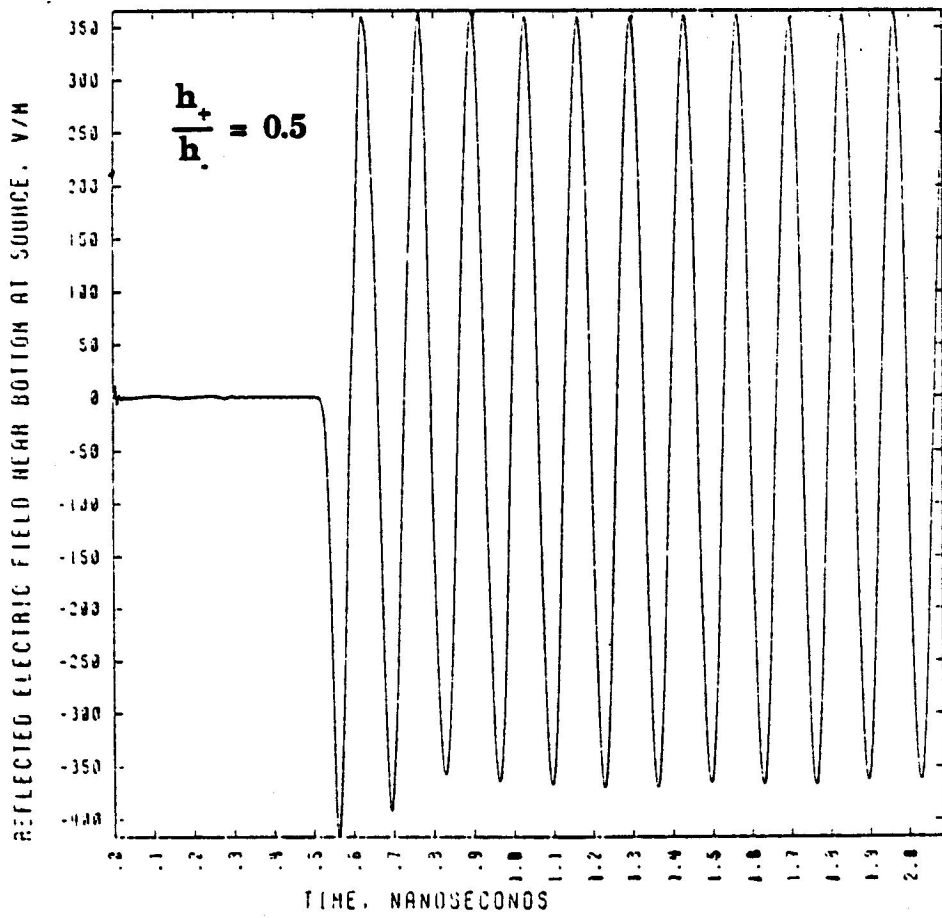


Fig. 9b

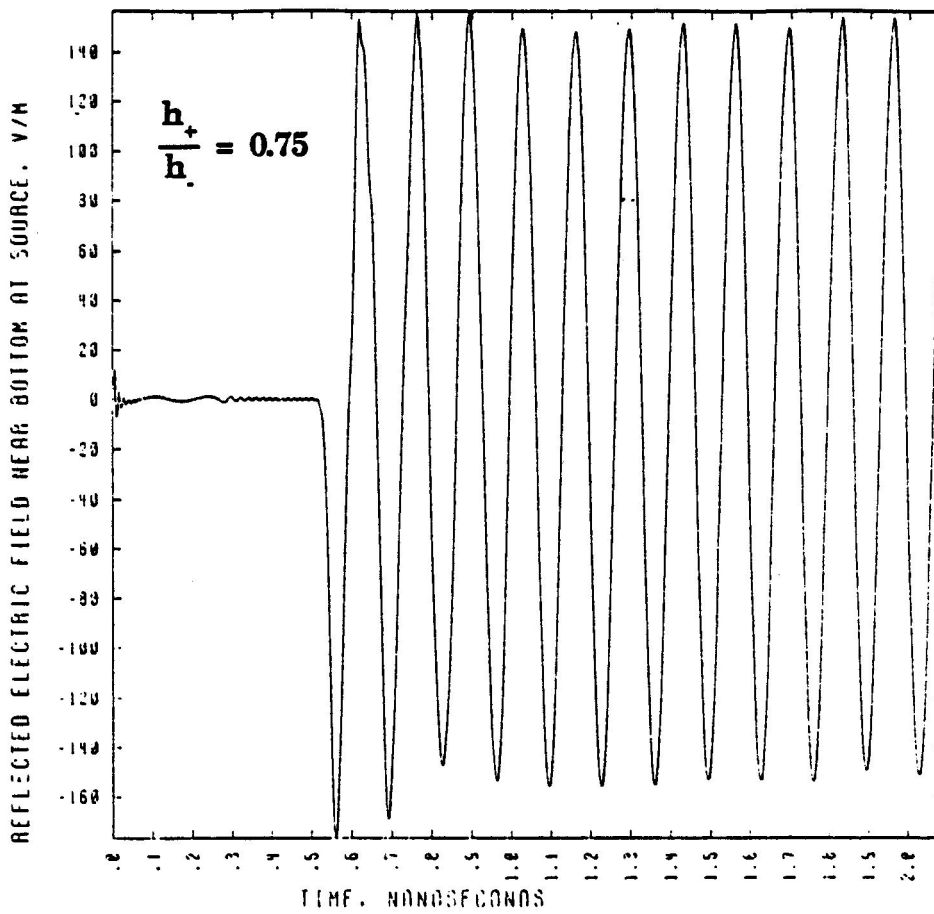


Fig. 9c

Figure 9. Reflected y-component of the electric field 2λ away from the discontinuity.

Fig. 9a: $h_+/h_- = .25$

Fig. 9b: $h_+/h_- = .50$

Fig. 9c: $h_+/h_- = .75$

The incident electric field at $x = -2\lambda$ is $E^i(-2\lambda, t) = 1000 \sin \omega t$ for $t \geq 0$.

Time (ns)	E_y^i , Incident	E_y^r , Reflected
1.9957333	-1.9509e+02	4.8245e+01
1.99791667	-9.8016e+01	-1.3807e+01
2.00000	+1.3923e-03	-7.5750e+01

Table 1a: $h_+/h_- = .25$

1.99375000	-2.9028e+02	1.0602e+01
1.99583333	-1.9509e+02	-2.4998e+01
1.999791667	-9.8016e+01	
2.000000	1.392923e-03	

Table 1b: $h_+/h_- = .50$

1.99375000	-2.9028e+02	1.6992e+00
1.99583333	-1.9509e+02	-1.2897e+01
1.999791667	-9.8016e+01	
2.00000	1.392923e-03	

Table 1c: $h_+/h_- = .75$

Table 1a,b,c. The incident and reflected E_y at $x = -2\lambda$. The left boundary of the calculational grid is at $x = -2\lambda$ and the right boundary of the calculational grid is at $x = +11\lambda$.

Calculated $|R|$

h_+/h_-	Calculated R			Transmission-Line Approx. R
	Uniform Coarse Grid	Mixed Grid	Uniform Fine Grid	
.25	.629	.627	.627	$(4-1)/(4+1)$
.50	.363	.362	.362	$(2-1)/(2+1)$
.75	.151	.150	.151	$(4-3)/(4+3)$

Table 2. Calculated and transmission-line-approximation reflection coefficients.

Calculated $C \times 10^{12}$ f/m

h_+/h_-	Calculated $C \times 10^{12}$ f/m			From Equation (13)
	Uniform Coarse Grid	(Mixed Grid)	Uniform Fine Grid	
.25	5.20	5.1	5.22	5.75
.50	2.31	2.27	2.29	2.21
.75	.59	.566	.570	5.73

Table 3. Calculated shunt capacitance and the static approximation based on Equation (13).

ACKNOWLEDGMENT

We appreciate Dr. Hans Kruger's encouragement.

REFERENCES

1. Yee, K. S., "Numerical Solution of Initial Boundary Value Problems Involving Maxwell's Equation in Isotropic Media", IEEE Transactions on Antennas and Propagation. Vol. Ap-14, No. 3, pp.302-307, May 1966.
2. Yee, K. S., "A Subgridding Method for the Finite Difference Time Domain Algorithm to Solve Maxwell's Equations", UCRL-96772, Lawrence Livermore National Laboratory, April, 1987. Submitted to IEEE Trans. Microwave Theory and Techniques.
3. Ramo, Whinnery, and Van Duzer, Fields and Waves in Communication Electronics, John Wiley and Sons, p. 598, 1965.

APPENDIX A
Calculation of the Shunt Capacitance
from the Numerical Output

From the text we have the incident wave at $x_L = n\lambda$

$$E^i(x_L, t) = \sin \omega t \quad t > 0 \quad (\text{A.1})$$

[Equation (5a)]

The reflected wave is

$$E^r(x, t) = \text{Re} \{ \mathcal{R} e^{j[kx - j\pi/2 + j\omega t]} \}$$

with

$$\mathcal{R} = |\mathcal{R}| e^{j\theta_r} \text{ and } x = -n\lambda$$

$$\begin{aligned} E^r(x, t) &= |\mathcal{R}| \cos(\omega t + \theta_r - \pi/2) = |\mathcal{R}| \sin(\omega t + \theta_r) \\ &= -|\mathcal{R}| \sin(\omega t + \Delta_r) \end{aligned} \quad (\text{A.2})$$

where

$$\Delta_r = \theta_r - \pi \text{ (or } \theta_r = \pi + \Delta_r)$$

In our numerical examples, Δ_r is a small number. Δ_r can be obtained directly from the E^r vs. ωt plot. From equation (12)

$$Y_d = \frac{2 Y_c}{1 + \mathcal{R}} = Y_c - Y_+ \quad (\text{A.3})$$

Let

$$\mathcal{R} = |\mathcal{R}| \cos \theta_r + j |\mathcal{R}| \sin \theta_r = -|\mathcal{R}| \cos \Delta_r - j |\mathcal{R}| \sin \Delta_r$$

$$\begin{aligned}
Y_d &= \frac{2Y_-(1 + \mathcal{R}^*)}{(1 + \mathcal{R})(1 + \mathcal{R}^*)} - Y_- - Y_+ \\
&= \left\{ \frac{2Y_-(1 - |\mathcal{R}| \cos \Delta_r)}{(1 - |\mathcal{R}| \cos \Delta_r)^2 + |\mathcal{R}|^2 \sin^2 \Delta_r} - Y_- - Y_+ \right\} \\
&\quad + \frac{j 2Y_- |\mathcal{R}| \sin \Delta_r}{(1 - |\mathcal{R}| \cos \Delta_r)^2 + |\mathcal{R}|^2 \sin^2 \Delta_r}
\end{aligned}$$

The value $|\mathcal{R}|$ can be read off directly from the computer output, and Δ_r can be obtained from a numerical interpolation. We also recall that

$$Y_- = \frac{1}{\sqrt{\frac{\mu}{\epsilon}} h_-} = \frac{1}{377} \frac{1}{h_-} \quad \text{for free space.}$$

For the transmission line approximation,

$$\mathcal{R} = \frac{Z_+ - Z_-}{Z_+ + Z_-} = \frac{h_+ - h_-}{h_+ + h_-} \quad (\text{A.4})$$

APPENDIX B Symbols and "Pseudo" FORTRAN Flow Chart

In this appendix, we show the names of some variables and a "pseudo" FORTRAN flow chart. The electric field components in zone 1 will be $E1x$, $E1y$; the horizontal zone boundaries will be $I1L$, $I1R$, etc. The vertical boundaries will be $J1B$, $J1T$, etc. A pseudo flow chart outlining the steps of calculations, interpolations, etc. is shown in steps (1)-(13).

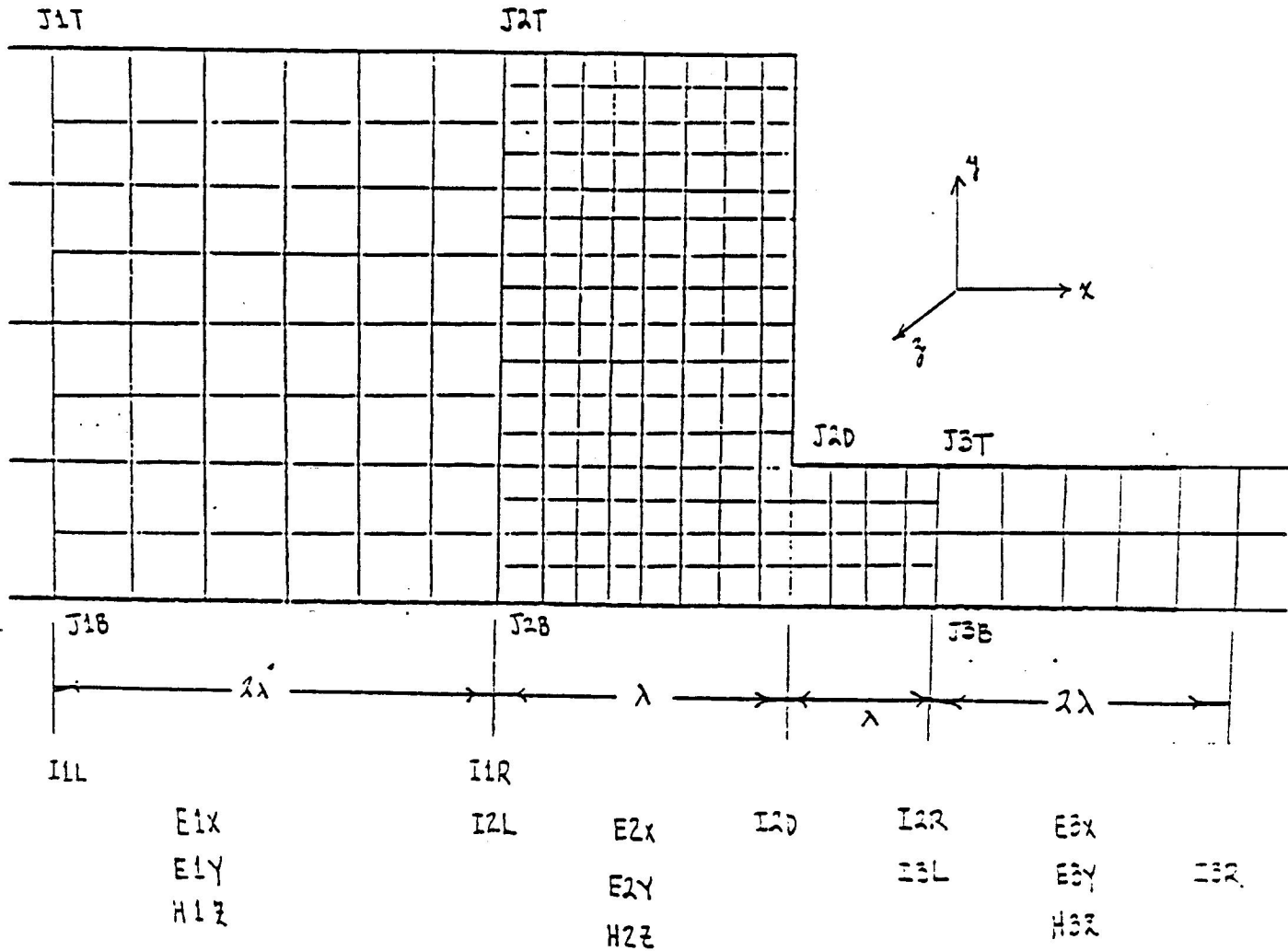
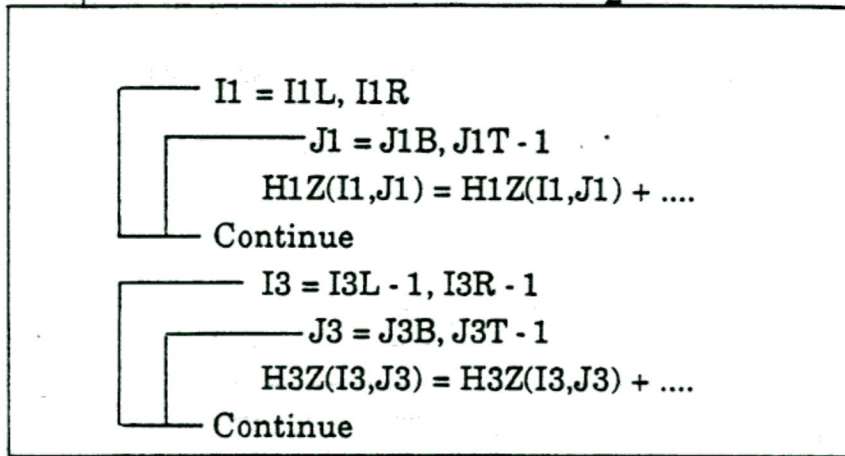


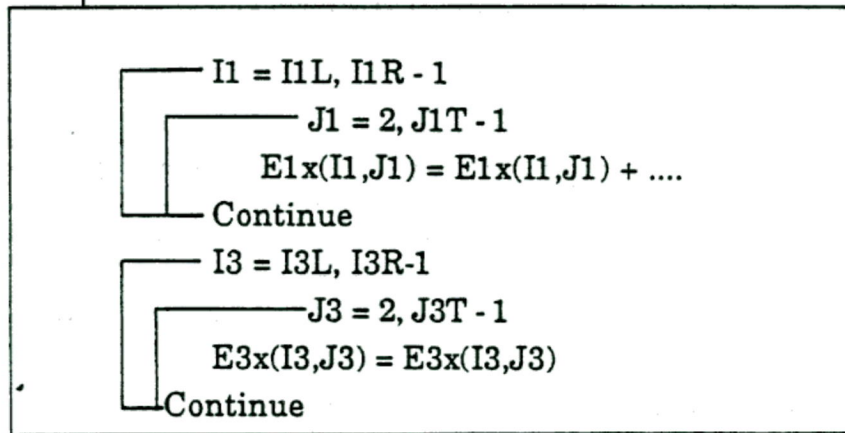
Fig. B.1. The variable zones, indices and variables.

Back from (13)

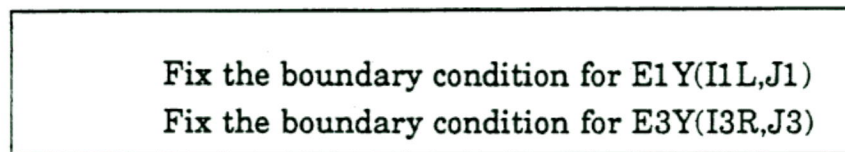
(1) Use $\Delta T1$, advance to $t = \frac{\Delta T1}{2}$



(2) Use $\Delta T1$, advance to $t = \Delta T1$



Fix to $t = \Delta T1$



(3) **At the interface**
Saving the old values for interpolation

J1 = J1B, J1T - 1
E1YT(J1) = E1Y(I1R, J1)
Continue

J3 = J3B, J3T - 1
E3YT(J1) = E3Y(I3L, J3)
Continue

to t = 0

(4) **At the interface**
Interpolate and extrapolate to t = 0

E2Y(I2L, 1) = E1Y(I1R, 1)
E2Y(I2L, J2T-1) = E1Y(I1R, J1T-1)
E2Y(I2R, 1) = E3Y(I3L, 1)
E2Y(I2R, J2D-1) = E3Y(I3L, J3T-1)

K = 2, J1T-1
E1Y(I2L, 2*K-1)
= .75*E1Y(I1R, K)
+ .25*E1Y(I1R, K-1)
E2Y(I2L, 2*(K-1)) = .25*E1Y(I1R, K)
+ .75*E1Y(I1R, K-1)
Continue

K = 2, J3T-1
E2Y(I2R, 2*K-1) = .75*E3Y(I3L, K) + .25*E3Y(I3L, K-1)
E2Y(I2R, 2*(K-1)) = .25*E3Y(I3L, K) + .75*E3Y(I3L, K-1)
Continue

(5) Use ΔT_2 , advance H2Z to $t = \frac{\Delta t_2}{2} = \frac{\Delta t_1}{4}$

I2 = I2L, I2D-1

J2 = J2B, J2T-1

H2Z(I2,J2) = H2Z(I2,J2) + ...

Continue

I2 = I2D, I2R-1

J2 = J2B, J2D-1

H2Z(I2,J2) = H2Z(I2,J2) + ...

Continue

(6) Use Δt_1 , advance E1Y and E3Y to $t = \Delta t_1$

I1 = I1L+1, I1R

J1 = J1B, J1T-1

E1Y(I1,J1) = E1Y(I1,J1) + ...

Continue

I3 = I3L, I3R-1

J3 = J3B, J3T-1

E3Y(I3,J3) = E3Y(I3,J3) + ...

Continue

(7) Time average values for E1Y
and E3Y at the interface

$$\text{to } t = \Delta t_2 = \frac{\Delta t_1}{2}$$

J1 = J1B, J1T-1

$$E1YT(J1) = .5 * E1YT(J1) + .5 * E1Y(I1R, J1)$$

Continue

J3 = J3B, J3T-1

$$E3YT(J3) = .5 * E3YT(J3) + .5 * E3Y(I3L, J3)$$

Continue

(8) Spatial average to get E2Y
at the interface

$$\text{to } t = \Delta t_2$$

$$E2Y(I2L, 1) = E1YT(1)$$

$$E2Y(I2L, J2T-1) = E1YT(J1T-1)$$

$$E2Y(I2R, 1) = E3YT(1)$$

$$E2Y(I2R, J2D-1) = E3YT(J3T-1)$$

K = 2, J1T-1

$$E2Y(I2L, 2 * K - 1) = .75 * E1YT(K) + .25 * E1YT(K-1)$$

$$E2Y(I2L, 2 * (K-1)) = .25 * E1YT(K) + .75 * E1YT(K-1)$$

Continue

K = 2, J3T-1

$$E2Y(I2R, 2 * K - 1) = .75 * E3YT(K) + .25 * E3YT(K-1)$$

$$E2Y(I2R, 2 * (K-1)) = .25 * E3YT(K) + .75 * E3YT(K-1)$$

Continue

(8a)

Advance the interior E2x, E2Y to

$$t = \Delta t_2$$

(9) Replacing the calculated values in
(1) by spatial average (tempor.) to $t = \frac{\Delta t_2}{2}$

J1 = 1, J1T - 1

$$\begin{aligned} H1Z(I1R, J1) = & .25*(H2Z(I2L, 1+2*(J1-1)) \\ & + H2Z(I2L+1, 1+2*(J1-1)) \\ & + H2Z(I2L, 2*J1) + H2Z(I2L+1, 2*J1)) \end{aligned}$$

Continue

J3 = 1, J3T - 1

$$\begin{aligned} H3Z(I3L-1, J3) = & .25*(H2Z(I2R-1, 1+2*(J3-1)) \\ & + H2Z(I2R-2, 1+2*(J3-1)) \\ & + H2Z(I2R-1, 2*J3) \\ & + H2Z(I2R-2, 2*J3)) \end{aligned}$$

Continue

(10) Use Δt_2 , advance H2Z to $t = \frac{3}{2} \Delta t_2$

I2 = I2L, I2D-1

J2 = J2B, J2T-1

$$H2Z(I2, J2) = H2Z(I2, J2) + \dots$$

Continue

I2 = I2D, I2R-1

J2 = J2B, J2D-1

$$H2Z(I2, J2) = H2Z(I2, J2) + \dots$$

Continue

to (11)

(11) Time average of (9) and (10). This replaces the calculated boundary values by (1) for

$t = \frac{1}{2} \Delta t_1$. These values are then advanced by

(1) to a new time $t = \frac{3}{2} \Delta t_1$

J1 = 1, J1T-1

H1Z(I1R, J1) = .5*H1Z(I1R, J1)
+ .5*.25*(H2Z(I2L, 1+2*(J1-1))
+ H2Z(I2L+1, 1+2*(J1-1))
+ H2Z(I2L, 2*J1) + H2Z(I2L+1, 2*J1))

Continue

J3 = 1, J3T-1

H3Z(I3L-1, J3) = .5*H3Z(I3L-1, J3)
+ .5*.25*(H2Z(I2R-1, 1+2*(J3-1))
+ H2Z(I2R-2, 1+2*(J3-1))
+ H2Z(I2R-1, 2*J3)
+ H2Z(I2R-2, 2*J3))

Continue

to (12)

(12) Spatial average to get E2Y at the interface to $t = \Delta t_1 = 2\Delta t_2$

$$E2Y(I2L,1) = E1Y(I1R,1)$$

$$E2Y(I2L,J2T-1) = E1Y(I1R,J1T-1)$$

$$E2Y(I2R,1) = E3Y(I3L,1)$$

$$E2Y(I2R,J2D-1) = E3Y(I3L,J3T-1)$$

— K = 2, J1T-1

$$E2Y(I2L,2*K-1) = .75*E1Y(I1R,K) + .25*E1Y(I1R,K-1)$$

$$E2Y(I2L,2*(K-1)) = .25*E1Y(I1R,K) + .75*E1Y(I1R,K-1)$$

— Continue

— K = 2, J3T-1

$$E2Y(I2R,2*K-1) = .75*E3Y(I3L,K) + .25*E3Y(I3L,K-1)$$

$$E2Y(I2R,2*(K-1)) = .25*E3Y(I3L,K) + .75*E3Y(I3L,K-1)$$

— Continue

(13)

Advance the interior E2Y, E2x to $t = 2\Delta t_2 = \Delta t_1$

Back to (1)

APPENDIX C
The Finite Difference Equations

The finite difference equations used in this report are derived from the integral forms of Maxwell's equations, which are

$$\oint \vec{E} \cdot d\vec{\ell} = -\frac{\partial}{\partial t} \iint \mu \vec{H} \cdot d\vec{S} \quad (C.1)$$

$$\oint \vec{H} \cdot d\vec{\ell} = \frac{\partial}{\partial t} \iint \epsilon \vec{E} \cdot d\vec{S} \quad (C.2)$$

For the TM wave appropriate to our problem, we have

$$\vec{E}(x,y,z,t) = \hat{x} E_x(x,y,t) + \hat{y} E_y(x,y,t) \quad (C.3)$$

$$\vec{H}(x,y,z,t) = \hat{z} H_z(x,y,t) \quad (C.4)$$

and there is no z dependence.

Using (C.1), we have

$$\begin{aligned} & -\mu \frac{H_z^{n+1/2}(i+1/2, j+1/2) - H_z^{n-1/2}(i+1/2, j+1/2)}{\Delta t} \Delta x \Delta y \\ & = \Delta x (E_x^n(i+1/2, j) - E_x^n(i+1/2, j+1)) \\ & + \Delta y (E_y^n(i+1, j+1/2) - E_y^n(i, j+1/2)) \end{aligned}$$

resulting in

$$\begin{aligned} H_z^{n+1/2}(i+1/2, j+1/2) &= H_z^{n-1/2}(i+1/2, j+1/2) - \frac{\Delta t}{\mu \Delta y} (E_x^n(i+1/2, j) - E_x^n(i+1/2, j+1)) \\ & - \frac{\Delta t}{\mu \Delta x} (E_y^n(i+1, j+1/2) - E_y^n(i, j+1/2)) \end{aligned}$$

Using (C.2), we have

$$\epsilon \frac{E_x^{n+1}(i+1/2,j) - E_x^n(i+1/2,j)}{\Delta t} \Delta y \cdot 1 =$$

$$1 \cdot \left(H_z^{n+1/2}(i+1/2,j+1/2) - H_z^{n+1/2}(i+1/2,j-1/2) \right)$$

$$\epsilon \frac{E_y^{n+1}(i,j+1/2) - E_y^n(i,j+1/2)}{\Delta t} \Delta x \cdot 1 =$$

$$1 \cdot \left(H_z^{n+1/2}(i-1/2,j+1/2) - H_z^{n+1/2}(i+1/2,j+1/2) \right)$$

resulting in

$$E_x^{n+1}(i+1/2,j) = E_x^n(i+1/2,j) + \frac{\Delta t}{\epsilon \Delta y} \left(H_z^{n+1/2}(i+1/2,j+1/2) - H_z^{n+1/2}(i+1/2,j-1/2) \right)$$

$$E_y^{n+1}(i,j+1/2) = E_y^n(i,j+1/2) + \frac{\Delta t}{\epsilon \Delta x} \left(H_z^{n+1/2}(i-1/2,j+1/2) - H_z^{n+1/2}(i+1/2,j+1/2) \right)$$

G.R. Haack
 Electronics Research Laboratory
 Defence Science and Technology Organisation Salisbury
 GPO Box 2151
 Adelaide South Australia 5001

ABSTRACT

The Numerical Electromagnetics Code (NEC) is a computer code for analysing the electromagnetic response of an arbitrary structure consisting of wires and surfaces in free space or over a ground plane. It is based on the application of the Method of Moments to solve the electric field integral equation. A practical application of NEC which involved calculation of the impedance of a vertically polarised HF log-periodic antenna and comparison with measurements is described. A technique for improving the accuracy of the numerical calculations is discussed in addition to methods for accurately measuring impedances of antennas employing balanced two-wire transmission line feeders.

1. INTRODUCTION

This paper describes the author's experience in a practical application of NEC which involved calculation of the impedance of a vertically polarised HF log-periodic antenna (LPA), and comparison with measurements. The LPA considered is a proprietary design which was originally designed for use in broadband high-gain, steerable linear arrays for HF transmitters and receivers.

2. NUMERICAL MODELLING OF AN HF LOG-PERIODIC ANTENNA

For broadband linear arrays the elements of the array must be very closely spaced at the low frequency end of the operating band to minimise grating lobes at the upper frequency limit. At such close spacings the mutual impedances between elements of such an array have a significant effect on the impedance of each element which may vary substantially with frequency and steer angle. The LPA investigated here employs a novel element construction for the high-frequency radiators, and varying design parameters, σ and τ along the structure in an attempt to deal with mutual effects in an optimum manner.

As a first step towards investigating mutual impedance effects in a linear array of LPAs, an attempt was made to develop a model of a single LPA for use with NEC. An essential requirement for such a model, if it is to be useful for analysing arrays of, say, 8 or more LPAs, is that the number of wire segments be kept to a minimum so that computer core storage and processing time requirements do not limit the size of the array to be analysed.

A schematic of the LPA under investigation is shown in Figure 1. The construction is largely conventional in that guyed front and rear masts with catenary wires are used to support the radiating dipole elements which are fed by a two-wire balanced transmission line. (Guy wires and other wires supporting the radiating elements are not shown in Figure 1.) A balun at the feed point of the LPA permits connection to a 50 ohm coaxial system. The

arrangement used for coupling the low frequency conventional dipole radiators to the two-wire feeder is shown in Figure 2. The high frequency radiators, commonly referred to as 'extended aperture elements', are shown in Figure 3, and differ from the low frequency dipoles by virtue of having an additional closely-spaced wire parallel to each of the driven arms of the dipole of approximately double the length of each half of the dipole. An additional unusual feature of the LPA is that the element spacings and lengths do not conform to a true log-periodic geometry with constant σ and τ along its length, and the wire diameters are equal for all elements rather than proportional to the element length.

The model initially chosen for the single LPA is as shown in Figure 1. No attempt was made to model in detail the complex structure connecting the two-wire feed to the dipole elements, each driven element being represented by a single wire with crossed transmission lines connected between the centres of adjacent pairs of elements. The parasitic elements associated with the 'extended aperture elements' were simply modelled as two wires with the same spacing, length and centre-gap as the actual antenna.

No attempt was made to include catenary or guy wires, partly to minimise the number of wires required for the model, and also because their effect was considered to be small due to insulators being inserted at relatively close spacings to suppress induced currents on these portions of the structure. Comparison of calculated results using this model with NEC and measured impedances were encouraging, but showed that an improved numerical model would be required if close agreement of measurements and calculation were to be achieved. As shown in the Smith Chart plots of Figure 4, the magnitude of the measured and calculated impedances are similar, but the phase angle of the reflection coefficient is in error by about 0.15λ for the frequency range shown. (The frequency range covered in these plots is near the lower end of the operating band.) Note that this is an expanded Smith Chart with a maximum VSWR of 2.5:1.

It was reasoned that the most significant source of error was likely to be due to the simplified model used for the region connecting the dipoles and the two-wire feeder. This problem has been considered in detail (R.W.P. King, The Theory of Linear Antennas; Chapter 11, Harvard Univ. Press, 1958) for various configurations of two-wire lines feeding dipoles, however extensions of these techniques to the problem considered here appears somewhat intractable. An alternative approach which was also considered was to model the region near the junction of the two-wire feeder and a single driven element using NEC. This approach was not pursued, as the geometry is such that wire junctions with 90° bends, abrupt changes in wire radii and multiple wire junctions would be involved. Reports from other NEC users suggest that such configurations should be avoided where possible.

In order to further simplify the problem of obtaining a simple LPA model for use with NEC, a single 'extended aperture element' was fabricated and its impedance measured. The impedance of the single 'extended aperture element' near resonance was also calculated using NEC with the simple model shown in Figure 5. The calculated and measured impedances are shown in Figure 6. It is seen that the calculated impedance of the 'extended aperture' element near resonance is of the order of 200 ohms, which is substantially greater than a simple dipole (~ 70 ohms). The measured impedance is similar to that calculated, however the former has a significantly greater capacitive

reactance at all frequencies. This is attributed, to a first order, to the capacitance between the two halves of the assembly connecting the driven elements of the dipole to the two-wire feeder, no attempt having been made to accurately model this region.

If a parallel capacitance is added to the calculated impedance to match the measured impedance near resonance, the new 'calculated' impedance agrees more closely with the measured impedance as shown in Figure 7. An independent measurement of the static (dc) capacitance between the two halves of the centre portion of the dipole assembly was found to agree quite closely with that calculated above (4.5 pF calculated from the difference between measured and calculated impedances near resonance, and 5 pF static capacitance measured).

By adding a similar capacitance in parallel with the feedpoint of each element in the LPA model, the plots of measured and 'calculated' impedance become as shown in Figure 8. It can be seen that the agreement is substantially improved compared with the original calculations. Figure 9 compares measured and calculated impedances over a band 10 MHz wide above the low frequency operating limit. The agreement is very close. The narrow blip near the centre of the measured curve is unexplained; it is not evident in the calculated curve, however this may be due to the 'removal' of low frequency elements in the model of the LPA as the frequency increases.

3. THE MEASUREMENT PROBLEM

When comparing measured and calculated impedances of antennas it is necessary to consider the possible sources of error in the measurements. This is particularly important for antennas fed by two-wire transmission lines since most impedance measurement systems operate with 50 ohm coaxial transmission line test ports, and a balun must therefore be used to enable measurement of balanced impedances. Since the perfect balun does not exist, measurement errors will normally be introduced.

However, there are techniques that can be used to minimise such errors. For example, if the vector accuracy enhancement techniques as described in HP Application Note 221A, June 1980 are applied to an automated 50 ohm coaxial network analyser followed by an imperfect balun, then most of the significant errors due to system imperfections can be eliminated by calibrating the system with three standard terminations on the two-wire terminals of the balun. The terminations normally used for calibration are a short-circuit, open-circuit, and a resistance equal to the two-wire terminal impedance of the balun. This latter impedance is the reference impedance for all measurements made following calibration. The first two standard impedances usually are easily realised at HF, however the matched two-wire line termination may present some difficulties. The latter problem may be alleviated by fitting coaxial connectors to each of the balanced output ports of the balun and terminating each of these ports with high-quality coaxial resistors each equal in value to half the desired two-wire impedance. Since coaxial resistors are available in a range of resistance values, calibration at the characteristic impedance at most two-wire transmission lines is possible. The main source of error with this technique is the discontinuity between the coaxial connectors and the two-wire transmission line, which should be small at HF frequencies.

A further source of errors in the above is the rejection of unbalanced voltages at the 'balanced' output terminals of the balun. These errors cannot be easily quantified.

4. CONCLUSION

The results presented show that accurate results can be obtained for complex structures provided that steps are taken to accurately model the feed region of centre-driven elements. A technique for accurate impedance measurement of antennas driven by two-wire balanced transmission lines was also outlined.

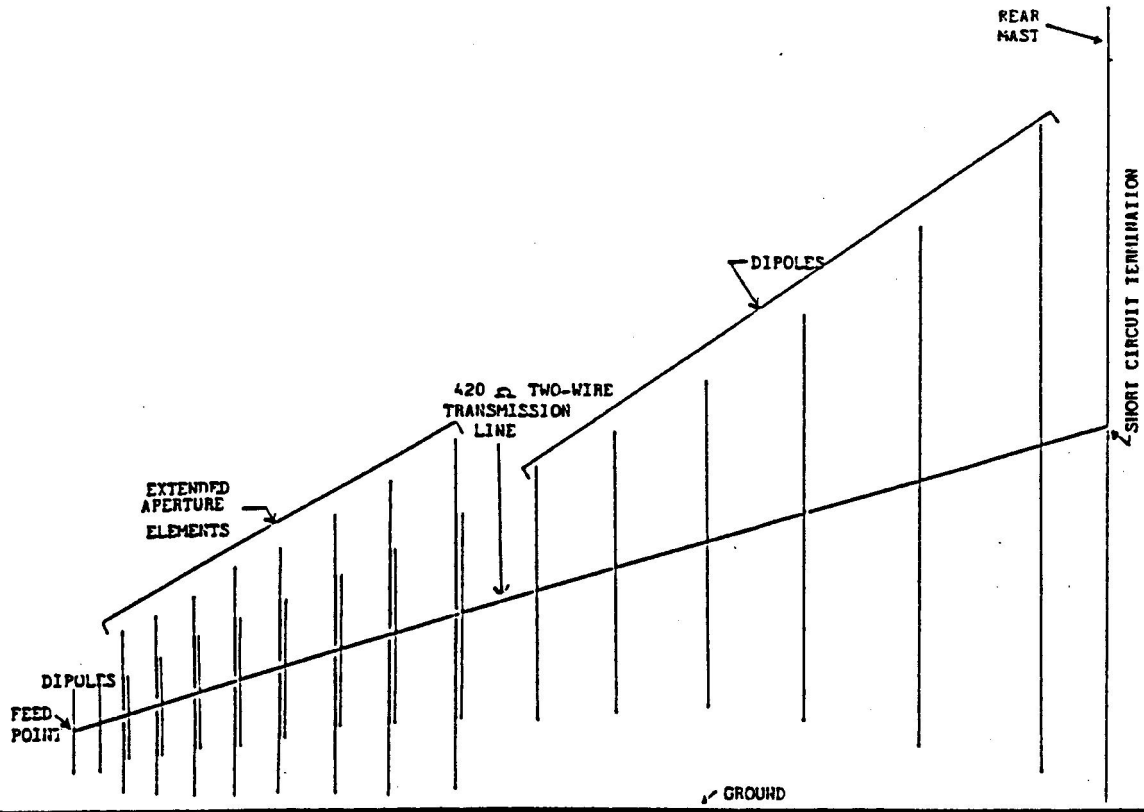


FIGURE 1 SCHEMATIC OF VERTICAL LPA
(APPROX 1/200TH FULL SIZE)

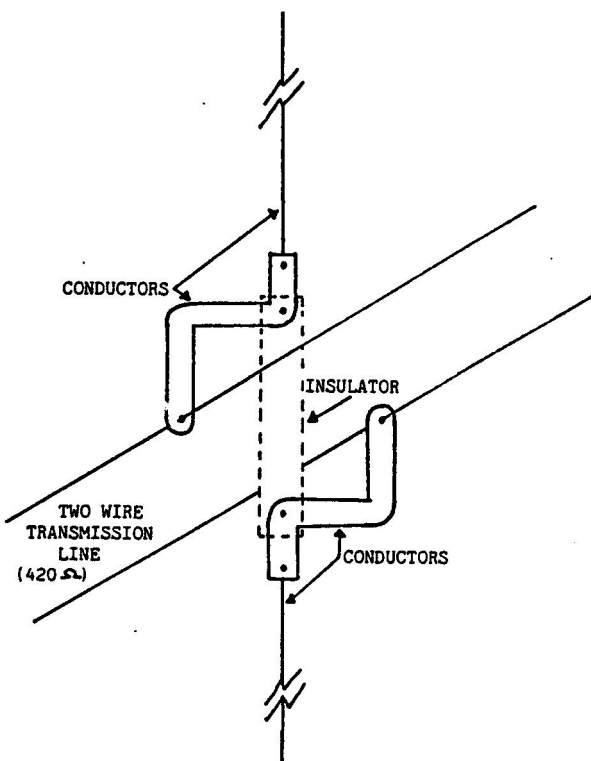


FIGURE 2 DETAILS OF DIPOLE TO TWO-WIRE TRANSMISSION
LINE CONNECTION

IMPEDANCE OR ADMITTANCE COORDINATES

—○— MEASURED
 —*— CALCULATED

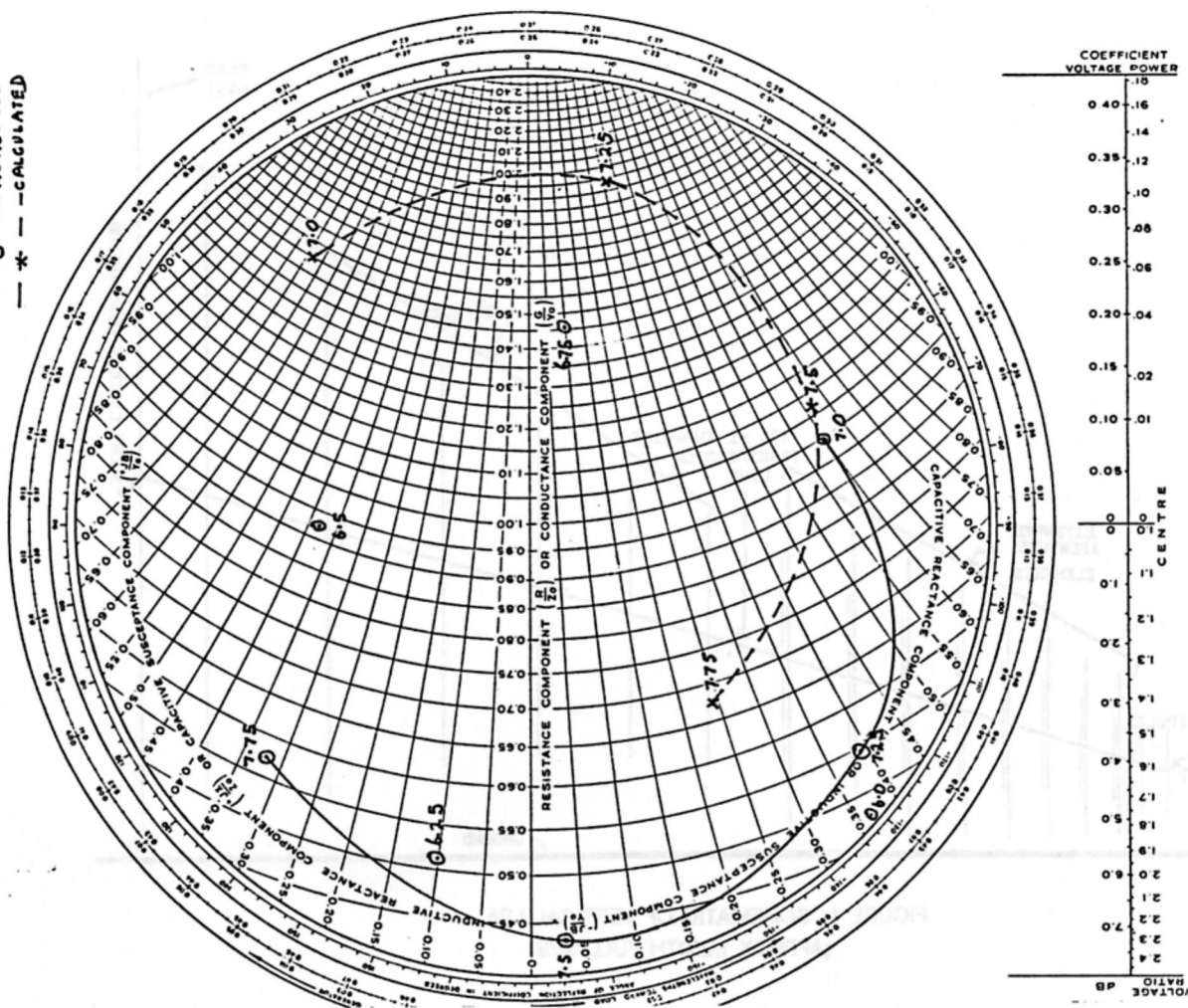


FIGURE 4 INITIAL COMPARISON OF MEASURED AND CALCULATED IMPEDANCES OF VERTICAL LPA (FREQUENCIES IN MHz)

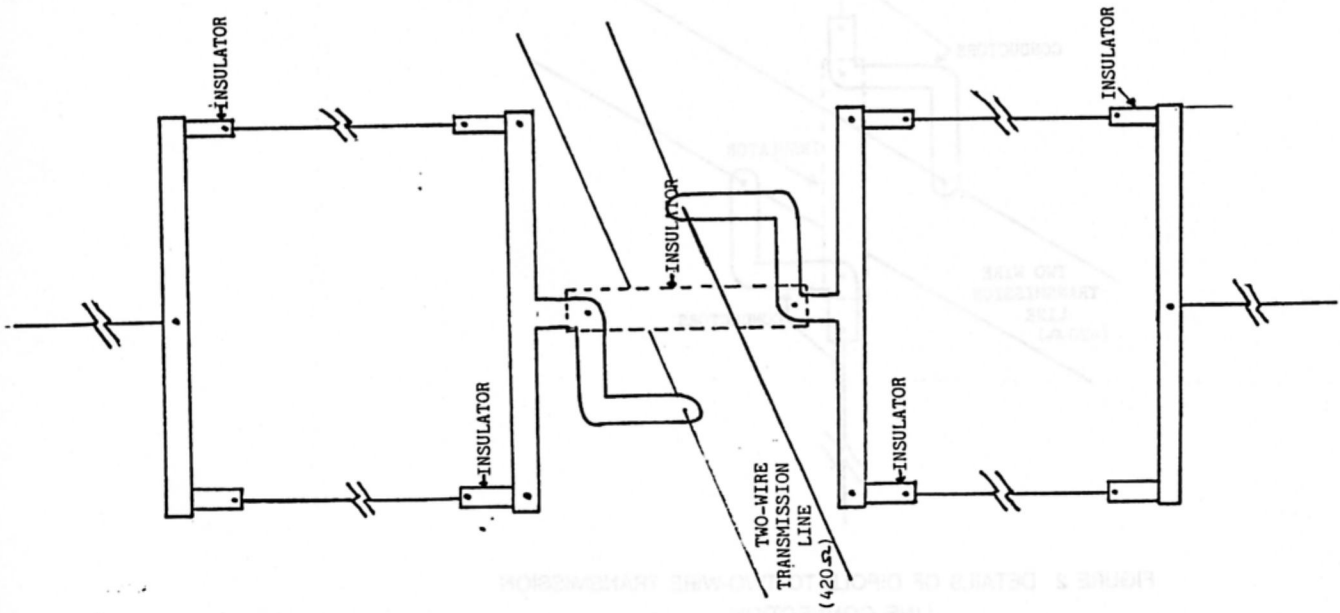


FIGURE 3 DETAILS OF "EXTENDED APERTURE" ELEMENT TO TWO-WIRE TRANSMISSION LINE CONNECTION

IMPEDANCE OR ADMITTANCE COORDINATES
 ○ — MEASURED
 × — CALCULATED

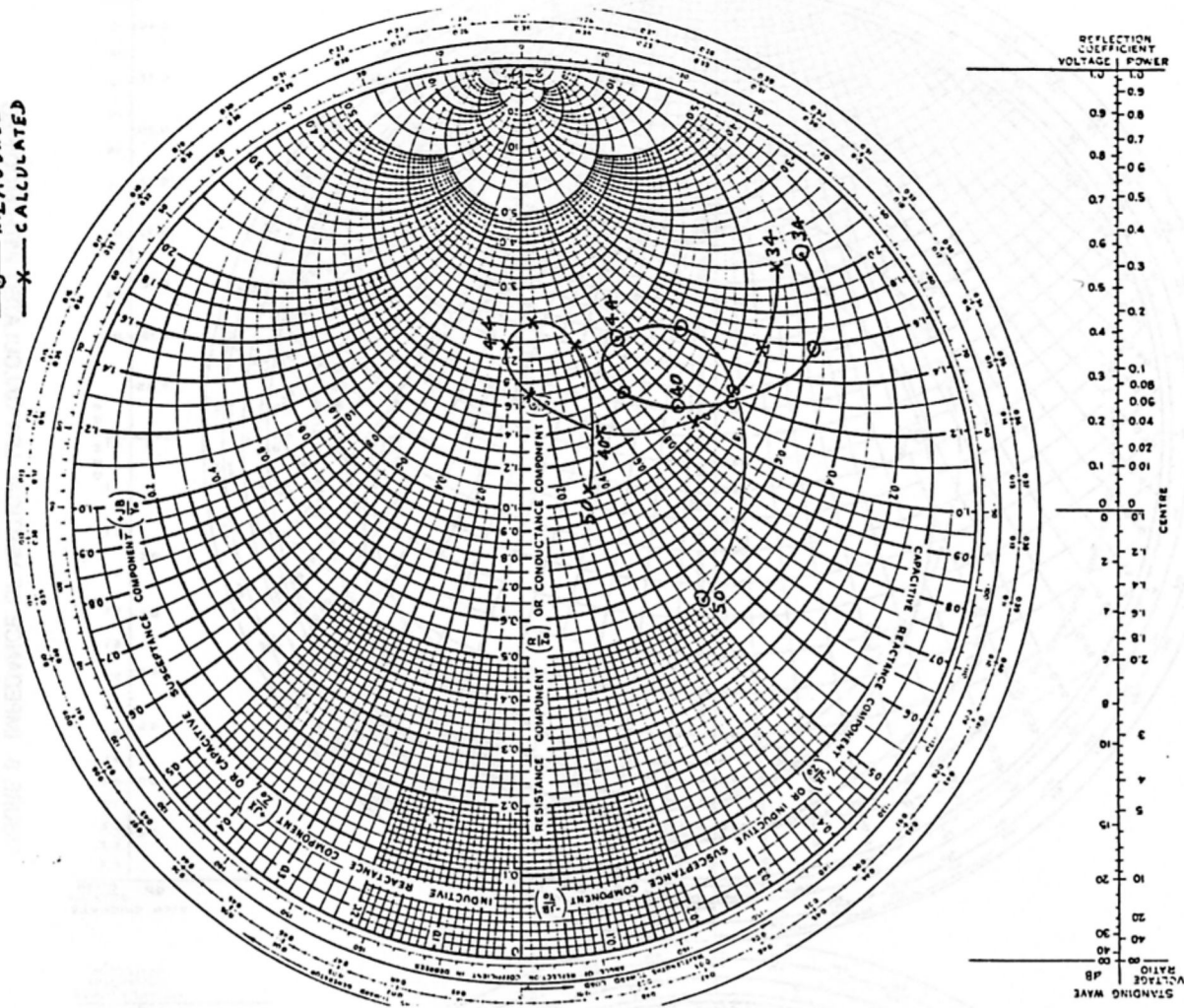


FIGURE 6 INITIAL COMPARISON OF MEASURED AND CALCULATED IMPEDANCES FOR SINGLE "EXTENDED APERTURE" ELEMENT (FREQUENCIES IN MHz)

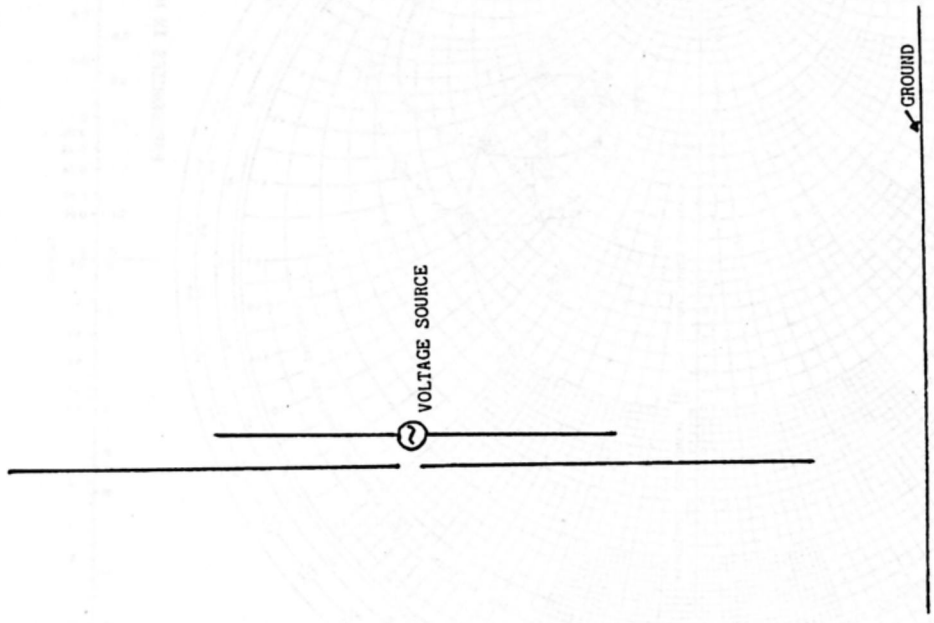


FIGURE 5 MODEL OF "EXTENDED APERTURE" ELEMENT FOR NEC

IMPEDANCE OR ADMITTANCE COORDINATES

—○— MEASURED
—*— CALCULATED

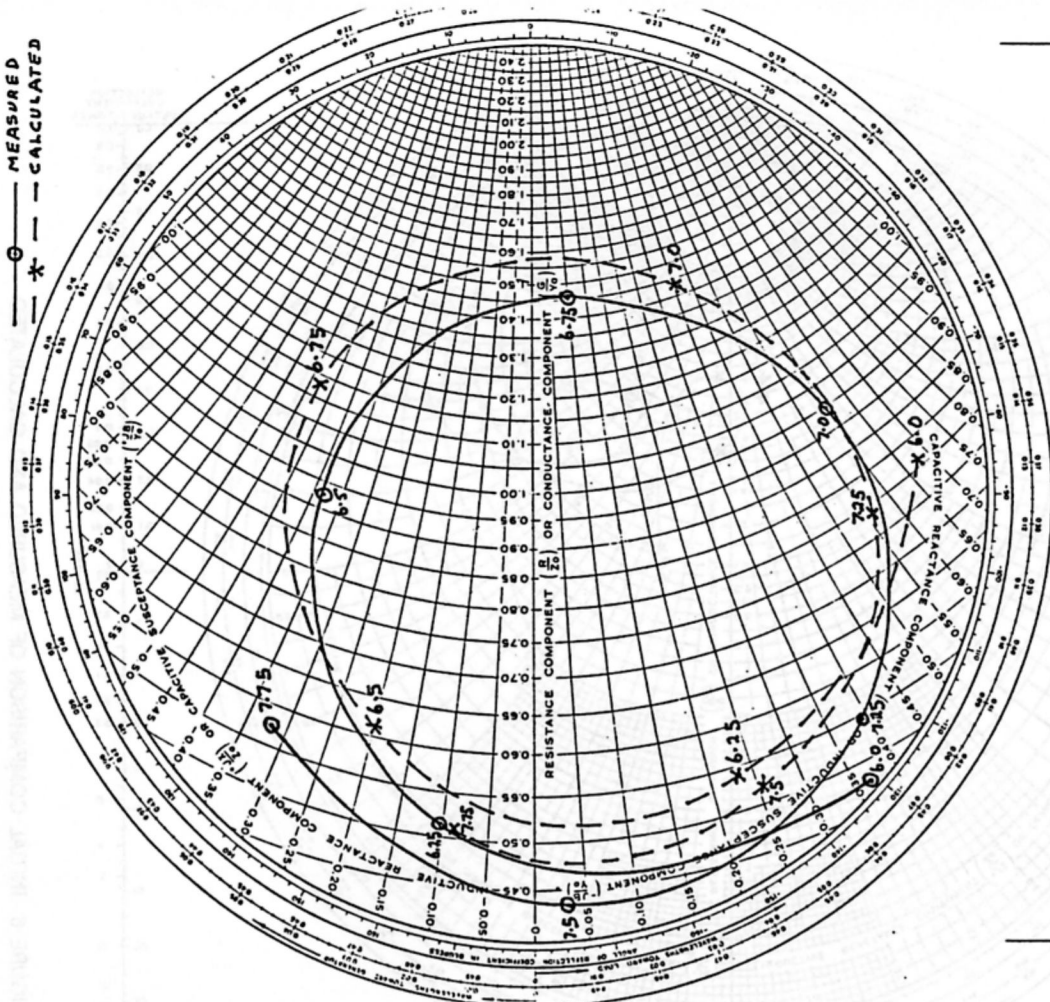


FIGURE 8 IMPEDANCE OF VERTICAL LPA CALCULATED WITH MODIFIED TRANSMISSION LINE LENGTHS & IMPEDANCES (FREQUENCIES IN MHz)

IMPEDANCE OR ADMITTANCE COORDINATES

—○— MEASURED
—□— CALCULATED

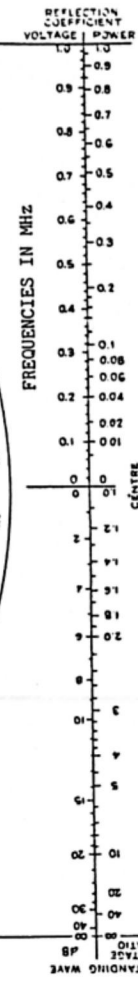
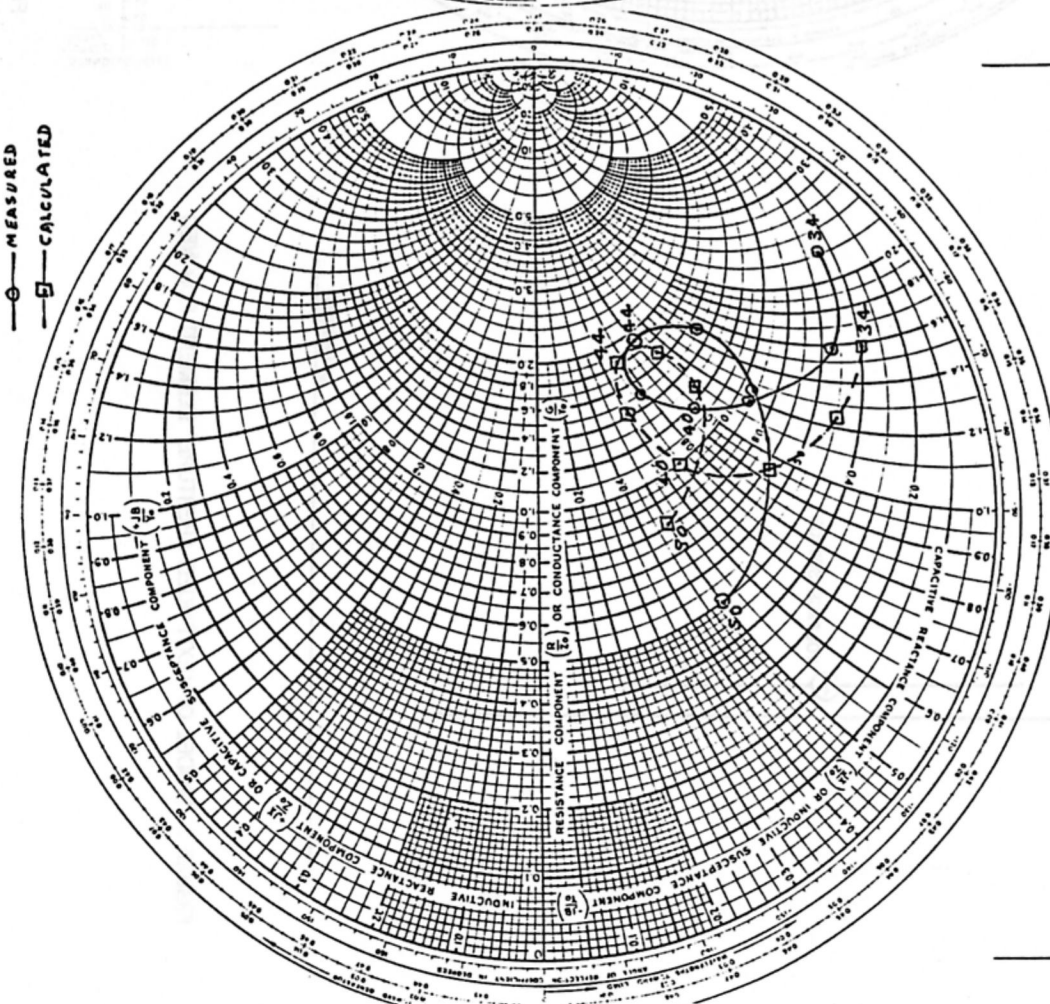


FIGURE 7 COMPARISON OF MEASURED AND CALCULATED IMPEDANCES FOR SINGLE "EXTENDED APERTURE" ELEMENT WITH SHUNT CAPACITANCE IN PARALLEL WITH FEED POINT

VERTICAL LPA

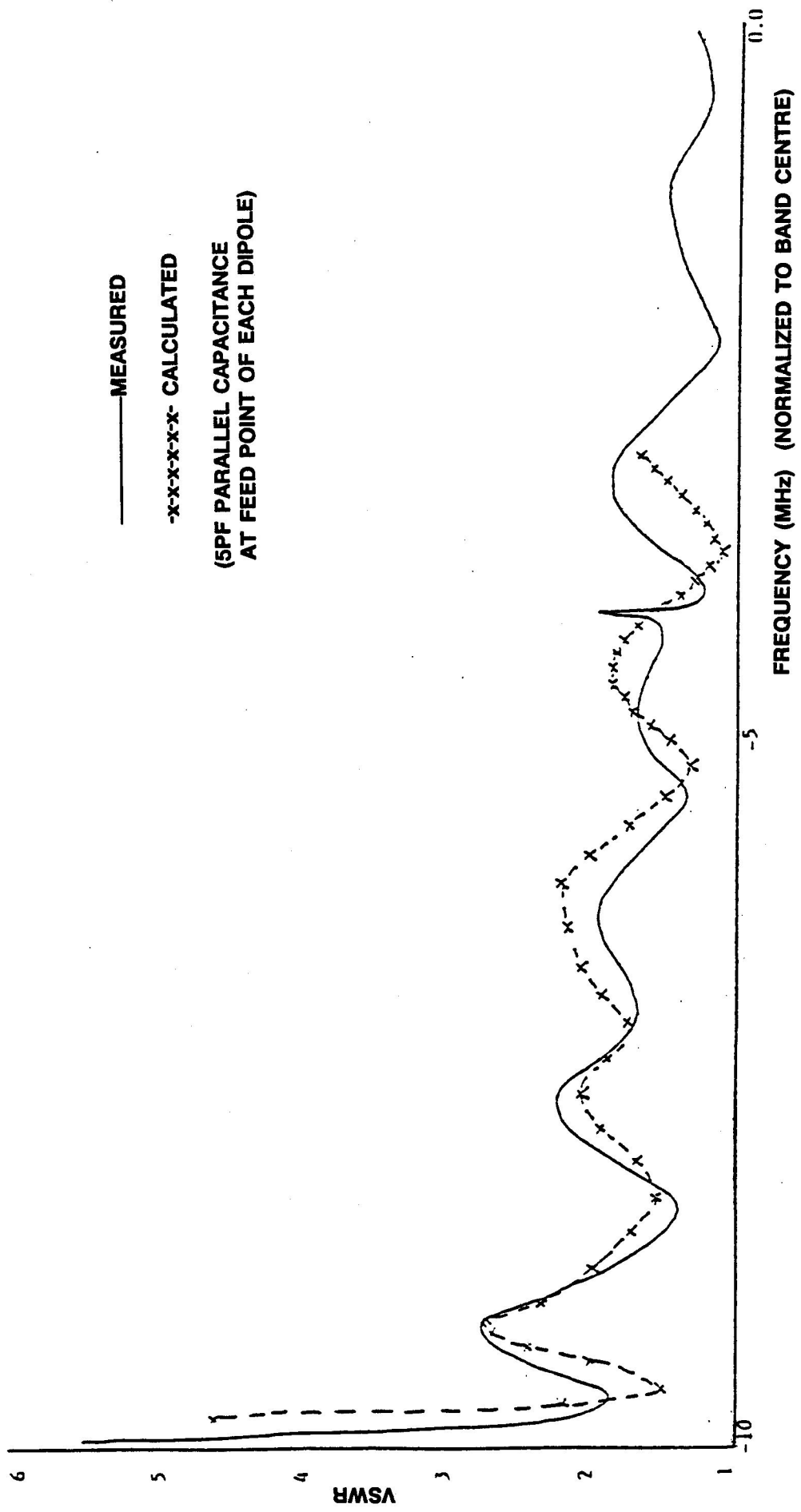


FIGURE 9 COMPARISON OF MEASURED AND CALCULATED VSWRS FOR VERTICAL LPA

Wan-xian Wang

Space Astronomy Laboratory, University of Florida
Gainesville, FL 32609

ABSTRACT

The higher order terms of eigenvalues in spheroidal differential equation are developed by using power-series expansion and asymptotic ones for both prolate and oblate wave functions, these important multipole expansions greatly facilitate and improve the computations of the electromagnetic scattering by different kinds of spheroids with various size parameters, refractive indices, and aspect ratios.

I. INTRODUCTION

The prolate and oblate spheroidal eigenvalues λ_{mn} are usually calculated following Bouwkamp's method¹ while restricted to the case of small value of size parameter c ($= \kappa(a^2-b^2)^{1/2}$, where κ is wave number, a is semi-major axis, and b is semi-minor axis) and large number n . For large value of c (say > 15) and/or small number n , the asymptotic expansions must be employed; J. Meixner^{2,3} had performed the asymptotic developments of prolate and oblate spheroidal eigenvalues up to c^{-5} , respectively. However, for moderate value of c and the intermediate number n , there appears a gap between Bouwkamp's and the asymptotic expansions because of the orders of the included terms being not high enough for these expansions.

The author has pushed the power-series expansion forward to c^{16} term, and the prolate and oblate asymptotic developments till c^{-6} , respectively. Thus the correct arrangement of the eigenvalues λ_{mn} from small value through large value of c and from small number through large number n is formed in increasing order by correspondingly selecting one of these two expansions. The developments of the analytical expressions of the spheroidal eigenvalues, together with further improvements on calculating the spheroidal radial functions, have made it feasible to compute the scattering coefficients for different kinds of spheroids within very wide range.

The angular differential equation of the spheroidal wave functions can be written in the form

$$(1 - \eta^2) \frac{d^2 S_{mn}}{d\eta^2} - 2\eta \frac{dS_{mn}}{d\eta} + \left(\lambda_{mn} - c^2 \eta^2 - \frac{m^2}{1 - \eta^2} \right) S_{mn} = 0 \quad (1)$$

where η is angular coordinate in the spheroidal system, $-1 \leq \eta \leq 1$;

S_{mn} are the spheroidal angle functions of order m and degree n ;

λ_{mn} are the eigenvalues of the spheroidal differential equation;

m and n are positive integers with $n \geq m$.

This equation is for prolate spheroidal wave functions. By replacing c by $-ic$ in Eq. (1) we would have the equation for oblate one. For small value of c , the following expression of the eigenvalues λ_{mn} in the form of continued fraction can be obtained by using three-term recursion relation of the expansion coefficients, $d_r^{mn}(c)$, of the spheroidal angle functions S_{mn} with respect to the associated Legendre functions P_{m+r}^m (where r is the summation index):⁴

$$\lambda_{mn} = \gamma_{n-m}^m - \frac{\beta_{n-m}^m}{\gamma_{n-m-2}^m - \lambda_{mn}} - \frac{\beta_{n-m-2}^m}{\gamma_{n-m-4}^m - \lambda_{mn}} \dots - \frac{\beta_{n-m+2}^m}{\gamma_{n-m+2}^m - \lambda_{mn}} - \frac{\beta_{n-m+4}^m}{\gamma_{n-m+4}^m - \lambda_{mn}} \dots \quad (2)$$

$$\text{where } \gamma_r^m = (m+r)(m+r+1) + \frac{1}{2}c^2 \left[1 - \frac{4m^2-1}{(2m+2r-1)(2m+2r+3)} \right] \quad (r \geq 0) \quad (2-1)$$

$$\beta_r^m = \frac{r(r-1)(2m+r)(2m+r-1)c^4}{(2m+2r-1)^2(2m+2r-3)(2m+2r+1)} \quad (r \geq 2) \quad (2-2)$$

Substituting in Eq. (2) the power-series expansion

$$\lambda_{mn} = \sum_{k=0}^{\infty} l_{2k}^{mn} c^{2k} \quad (3)$$

and then developing the continued fraction by raising consecutively each partial denominator up to the associated numerator with the use of binomial expansion, we can find the coefficients l_{2k}^{mn} by equating the power of c^{2k} . The coefficients in the book by C. Flammer⁵ were given till l_{10}^{mn} ; it might be remarked that he obtained the coefficient

ℓ_{10}^{mn} as given below, but apart from a sign error in the third term of the second part (the numerator $6n-25$ instead of the correct $6n+25$).⁶ In most cases, the coefficients up to ℓ_{12}^{mn} are often used, the coefficients ℓ_{14}^{mn} and ℓ_{16}^{mn} are just applied to some certain size parameters of moderate value of c and intermediate numbers n . To save space the coefficients derived by author are not fully listed; ℓ_{14}^{mn} and ℓ_{16}^{mn} can be found from author's paper.⁷

The power-series expansion of the spheroidal eigenvalues λ_{mn} is as follows:

$$\lambda_{mn} = \sum_{k=0}^{\infty} \ell_{2k}^{mn} c^{2k} \quad (4)$$

where

$$\ell_0^{mn} = n(n+1) \quad (4-1)$$

$$\ell_2^{mn} = \frac{1}{2} \left[1 - \frac{4m^2-1}{(2n-1)(2n+3)} \right] \quad (4-2)$$

$$\ell_4^{mn} = \frac{\beta_0}{2(2n-1)} - \frac{\beta_2}{2(2n+3)} \quad (4-3)$$

$$\ell_6^{mn} = -\frac{\beta_0(4m^2-1)}{4(2n-1)^2} \left[\frac{4}{(2n-5)(2n-1)(2n+3)} \right] + \frac{\beta_2(4m^2-1)}{4(2n+3)^2} \left[\frac{4}{(2n+7)(2n+3)(2n-1)} \right] \quad (4-4)$$

$$\ell_8^{mn} = -\frac{\beta_0(4m^2-1)}{4(2n-1)^2} \left[\frac{\ell_4^{mn}}{(4m^2-1)} - \frac{8(4m^2-1)}{(2n-5)^2(2n-1)^3(2n+3)^2} - \frac{\beta_{-2}}{4(4m^2-1)(2n-3)} \right] \\ - \frac{\beta_2(4m^2-1)}{4(2n+3)^2} \left[\frac{\ell_4^{mn}}{(4m^2-1)} + \frac{8(4m^2-1)}{(2n+7)^2(2n+3)^3(2n-1)^2} + \frac{\beta_4}{4(4m^2-1)(2n+5)} \right] \quad (4-5)$$

$$\ell_{10}^{mn} = -\frac{\beta_0(4m^2-1)}{4(2n-1)^2} \left[\frac{\ell_6^{mn}}{(4m^2-1)} - \frac{4\ell_4^{mn}}{(2n-5)(2n-1)^2(2n+3)} + \frac{16(4m^2-1)^2}{(2n-5)^3(2n-1)^5(2n+3)^3} \right. \\ \left. + \frac{\beta_{-2}(6n-19)}{2(2n-9)(2n-5)(2n-3)(2n-1)^2(2n+3)} \right] \\ - \frac{\beta_2(4m^2-1)}{4(2n+3)^2} \left[\frac{\ell_6^{mn}}{(4m^2-1)} - \frac{4\ell_4^{mn}}{(2n+7)(2n+3)^2(2n-1)} - \frac{16(4m^2-1)^2}{(2n+7)^3(2n+3)^5(2n-1)^3} \right. \\ \left. - \frac{\beta_4(6n+25)}{2(2n+11)(2n+7)(2n+5)(2n+3)^2(2n-1)} \right] \quad (4-6)$$

$$\begin{aligned}
\ell_{12}^{mn} = & -\frac{\beta_0(4m^2-1)}{4(2n-1)^2} \left\{ \frac{\ell_8^{mn}}{(4m^2-1)} - \frac{(\ell_4^{mn})^2}{2(4m^2-1)(2n-1)} - \frac{4\ell_6^{mn}}{(2n-5)(2n-1)^2(2n+3)} + \frac{12(4m^2-1)\ell_4^{mn}}{(2n-5)^2(2n-1)^4(2n+3)^2} \right. \\
& - \frac{32(4m^2-1)^3}{(2n-5)^4(2n-1)^7(2n+3)^4} - \frac{\beta_{-2}}{(4m^2-1)(2n-3)} \left[\frac{(4m^2-1)^2 d_1}{(2n-9)^2(2n-5)^2(2n-1)^4(2n+3)^2} \right. \\
& \left. \left. - \frac{(10n-13)\ell_4^{mn}}{16(2n-3)(2n-1)} + \frac{\beta_{-2}}{32(2n-3)(2n-1)} + \frac{\beta_{-4}}{96(2n-5)(2n-3)} \right] \right\} \\
& - \frac{\beta_2(4m^2-1)}{4(2n+3)^2} \left\{ \frac{\ell_8^{mn}}{(4m^2-1)} + \frac{(\ell_4^{mn})^2}{2(4m^2-1)(2n+3)} - \frac{4\ell_6^{mn}}{(2n+7)(2n+3)^2(2n-1)} + \frac{12(4m^2-1)\ell_4^{mn}}{(2n+7)^2(2n+3)^4(2n-1)} \right. \\
& + \frac{32(4m^2-1)^3}{(2n+7)^4(2n+3)^7(2n-1)^4} + \frac{\beta_4}{(4m^2-1)(2n+5)} \left[\frac{(4m^2-1)^2 d_2}{(2n+11)^2(2n+7)^2(2n+3)^4(2n-1)^2} \right. \\
& \left. \left. + \frac{(10n+23)\ell_4^{mn}}{16(2n+5)(2n+3)} + \frac{\beta_4}{32(2n+5)(2n+3)} + \frac{\beta_6}{96(2n+7)(2n+5)} \right] \right\} \quad (4-7)
\end{aligned}$$

where $\beta_{-4} = \beta_{n-m-4}/c^4$, $\beta_{-2} = \beta_{n-m-2}/c^4$, $\beta_0 = \beta_{n-m}/c^4$,
 $\beta_2 = \beta_{n-m+2}/c^4$, $\beta_4 = \beta_{n-m+4}/c^4$, $\beta_6 = \beta_{n-m+6}/c^4$.

and $d_1 = (2n-1)^2 + 2(2n-1)(2n-9) + 3(2n-9)^2$
 $d_2 = (2n+3)^2 + 2(2n+3)(2n+11) + 3(2n+11)^2$

The power-series expansion of the oblate eigenvalues λ_{mn} is obtained from Eq. (4) by simply replacing c^2 by $-c^2$.

III. ASYMPTOTIC DEVELOPMENT OF THE PROLATE SPHEROIDAL EIGENVALUES

Let us set

$$S_{mn} = (1 - \eta^2)^{\frac{m}{2}} u_{mn} \quad (5)$$

substitute this expression in Eq. (1), and make the transformation

$$\eta = (2c)^{-\frac{1}{2}} x \quad (6)$$

there results

$$\left(1 - \frac{x^2}{2c}\right) \frac{d^2 u_{mn}}{dx^2} - \frac{(m+1)}{c} x \frac{du_{mn}}{dx} + \left(K - \frac{x^2}{4}\right) u_{mn} = 0 \quad (7)$$

$$\text{where constant } K = \frac{\lambda_{mn} - m(m+1)}{2c} \quad (7-1)$$

First of all, developing u_{mn} and K in the asymptotic forms of size parameter c :

$$u_{mn} = u_0 + u_1 c^{-1} + u_2 c^{-2} + u_3 c^{-3} + \dots + u_k c^{-k} \quad (8-1)$$

$$K = \alpha_0 + \alpha_1 c^{-1} + \alpha_2 c^{-2} + \alpha_3 c^{-3} + \dots + \alpha_k c^{-k} \quad (8-2)$$

and substituting them in Eq. (7), we can determine the terms u_0, u_1, u_2, \dots of eigenfunctions u_{mn} by a series of differential equations of the second order, namely —

$$u_0'' + \left(\alpha_0 - \frac{x^2}{4}\right)u_0 = 0 \quad (9-1)$$

$$u_1'' + \left(\alpha_0 - \frac{x^2}{4}\right)u_1 = -\alpha_1 u_0 + \frac{1}{2} \left[x^2 u_0'' + 2(m+1)xu_0' \right] \quad (9-2)$$

$$u_2'' + \left(\alpha_0 - \frac{x^2}{4}\right)u_2 = -\alpha_1 u_1 - \alpha_2 u_0 + \frac{1}{2} \left[x^2 u_1'' + 2(m+1)xu_1' \right] \quad (9-3)$$

.....

$$u_k'' + \left(\alpha_0 - \frac{x^2}{4}\right)u_k = -\alpha_1 u_{k-1} - \alpha_2 u_{k-2} - \dots - \alpha_k u_0 + \frac{1}{2} \left[x^2 u_{k-1}'' + 2(m+1)xu_{k-1}' \right] \quad (9-k+1)$$

Let

$$\alpha_0 = p + \frac{1}{2} \quad (10)$$

where p is a positive integer or zero. The solution of Eq. (9-1) is

$$u_0 = D_p(x) \quad (11)$$

where $D_p(x)$ is parabolic cylinder function. For simplicity, we just denote it by D_p .

In the first approximation of K , we have

$$K = \alpha_0 = p + \frac{1}{2} \quad (12)$$

It implies that

$$\lambda_{mn} = (2p + 1)c \quad \text{while } c \rightarrow \infty \quad (13)$$

According to the asymptotic property of the eigenvalues λ_{mn} , we find that

$$\lambda_{mn} = [2(n - m) + 1]c \quad \text{while } c \rightarrow \infty \quad (14)$$

The foregoing suggests that

$$p = n - m \quad (15)$$

Next we define the operator⁸

$$\nabla D_p = x^2 D_p'' + 2(m+1)x D_p' \quad (16)$$

Utilizing the recursion relation of the parabolic cylinder functions:

$$D_p' + \frac{x}{2} D_p - p D_{p-1} = 0 \quad (17)$$

we obtain

$$\nabla D_p = C_{1,p} D_{p+4} + C_{2,p} D_{p+2} + C_{3,p} D_p + C_{4,p} D_{p-2} + C_{5,p} D_{p-4} \quad (18)$$

where

$$C_{1,p} = \frac{1}{4} \quad (18-1)$$

$$C_{2,p} = -m \quad (18-2)$$

$$C_{3,p} = -\frac{2p^2+2p+3}{4} - m \quad (18-3)$$

$$C_{4,p} = m|p|_2 \quad (18-4)$$

$$C_{5,p} = \frac{|p|_4}{4} \quad (18-5)$$

with $|p|_2 = p(p-1)$, and $|p|_4 = p(p-1)(p-2)(p-3)$.

Again, we define the operator

$$\Delta u_r = u_r'' + \left(p + \frac{1}{2} - \frac{x^2}{4}\right) u_r \quad (19)$$

where $r = 1, 2, \dots, k$.

Remembering that

$$\Delta D_p = 0 \quad (20)$$

we find that D_p term will not appear in the solution u_r of Eqs. (9-2), (9-3),

Furthermore we set

$$u_r = \sum_{\ell \neq 0} A_{2\ell} D_{p+2\ell} \quad (21)$$

then

$$\Delta u_r = \sum_{\ell \neq 0} (-2\ell) A_{2\ell} D_{p+2\ell} = \sum_{\ell \neq 0} B_{2\ell} D_{p+2\ell} \quad (22)$$

where we have expressed the right-hand sides of Eqs. (9-2), (9-3), ... in the forms

of $\sum_{\ell \neq 0} B_{2\ell} D_{p+2\ell}$.

Hence the coefficients $A_{2\ell}$ are found to be

$$A_{2\ell} = -\frac{B_{2\ell}}{2\ell} \quad (23)$$

Now we can solve Eqs. (9-2), (9-3), ...

From Eq. (9-2), we get

$$\alpha_1 = \frac{C_{3,p}}{2} = -\frac{2p^2+2p+3}{8} - \frac{m}{2} \quad (24)$$

By assuming

$$q = 2p + 1 \quad (25)$$

we have

$$\alpha_1 = -\frac{q^2+5+8m}{16} \quad (26)$$

The term u_1 of the eigenfunctions u_{mn} is found in the form

$$u_1 = \frac{1}{2} \left[f_1^D{}_{p+4} + f_2^D{}_{p+2} + f_3^D{}_{p-2} + f_4^D{}_{p-4} \right] \quad (27)$$

where

$$f_1 = -\frac{1}{16} \quad (27-1)$$

$$f_2 = \frac{m}{2} \quad (27-2)$$

$$f_3 = \frac{m}{2} |p|_2 \quad (27-3)$$

$$f_4 = \frac{1}{16} |p|_4 \quad (27-4)$$

Similarly we can obtain the other coefficients α_r of the eigenvalues λ_{mn} and the terms u_r of the eigenfunctions u_{mn} by the successive substitutions. The expression of terms u_r will be lengthy and lengthy while r increases; therefore I only list the coefficients α_r .

$$\alpha_2 = -\frac{q(q^2+11-32m^2)}{2^7} \quad (28)$$

$$\alpha_3 = -\frac{5(q^4+26q^2+21)-384m^2(q^2+1)}{2^{11}} \quad (29)$$

$$\alpha_4 = -\frac{(33q^5+1594q^3+5621q)-128m^2(37q^3+167q)+2048m^4q}{2^{15}} \quad (30)$$

$$\alpha_5 = -\frac{(63q^6+4940q^4+43327q^2+22470)-128m^2(115q^4+1310q^2+735)+24576m^4(q^2+1)}{2^{17}} \quad (31)$$

$$\alpha_6 = - \left[(527q^7 + 61529q^5 + 1043961q^3 + 2241599q) - 32m^2(5739q^5 + 127550q^3 + 298951q) + 2048m^4(355q^3 + 1505q) - 65536m^6q \right] 2^{-21} \quad (32)$$

$$\alpha_7 = - \left[(9387q^8 + 1536556q^6 + 43711178q^4 + 230937084q^2 + 93110115) - 1536m^2(2989q^6 + 112020q^4 + 648461q^2 + 270690) + 196608m^4(175q^4 + 1814q^2 + 939) - 12582912m^6(q^2 + 1) \right] 2^{-26} \quad (33)$$

Therefore the eigenvalues λ_{mn} are in the form:

$$\lambda_{mn} = qc - \frac{1}{8}(q^2 + 5 - 8m^2) + \sum_{r=2}^7 2\alpha_r c^{-r+1} + o(c^{-7}) \quad (34)$$

Correspondingly the eigenfunctions u_{mn} are in the form:

$$u_{mn} = \sum_{r=0}^6 u_r c^{-r} + o(c^{-7}) \quad (35)$$

As E.L.Ince said: "If anyone had the courage to push the development on a stage or two further he would greatly enhance the value of an important expansion. But any reader who attempts to verify the results given above will realize that the work involved would be tremendous".⁹

The expression of the eigenvalues λ_{mn} of the prolate spheroidal differential equation can be converted to that of the eigenvalue Λ of the Mathieu differential equation, as follows:

$$\begin{aligned} \Lambda = & -2h^2 + 2qh - \frac{1}{8}(q^2 + 1) - (q^3 + 3q)2^{-7}h^{-1} - (5q^4 + 34q^2 + 9)2^{-12}h^{-2} - (33q^5 + 410q^3 + 405q)2^{-17}h^{-3} \\ & - (63q^6 + 1260q^4 + 2943q^2 + 486)2^{-20}h^{-4} - (527q^7 + 15617q^5 + 69001q^3 + 41607q)2^{-25}h^{-5} \\ & - (9387q^8 + 388780q^6 + 2845898q^4 + 4021884q^2 + 506979)2^{-31}h^{-6} + o(h^{-7}) \end{aligned} \quad (36)$$

where

$$h = \frac{c}{2} \quad (36-1)$$

$$\Lambda = \lambda_{mn} + \frac{1}{4} - \frac{1}{2}c^2 \quad (36-2)$$

herein the author has developed one more high order term h^{-6} .

IV. ASYMPTOTIC DEVELOPMENT OF THE OBLATE SPHEROIDAL EIGENVALUES

The oblate spheroidal differential equation for angle functions S_{mn} is expressed as

$$(1 - \eta^2) \frac{d^2 S_{mn}}{d\eta^2} - 2\eta \frac{dS_{mn}}{d\eta} + \left(\lambda_{mn} + c^2\eta^2 - \frac{m^2}{1 - \eta^2} \right) S_{mn} = 0 \quad (37)$$

Referring to C. Flammer's book, and using three-term recursion relation of the expansion coefficients, A_s^{mn} , of the oblate spheroidal angle functions S_{mn} with respect to the Laguerre functions $L_{\nu+s}^{(m)}$ (where $\nu = \frac{1}{2}(n-m)$ if $(n-m)$ is even, and $\nu = \frac{1}{2}(n-m-1)$ if $(n-m)$ is odd, and s is the summation index), we have the following expression of the eigenvalues Λ_{mn} in the form of transcendental equation:

$$\Lambda_{mn} = \frac{Q_0^2}{\Lambda_{mn} + P_{-1}} - \frac{Q_{-1}^2}{\Lambda_{mn} + P_{-2}} - \dots + \frac{Q_1^2}{\Lambda_{mn} + P_1} - \frac{Q_2^2}{\Lambda_{mn} + P_2} - \dots \quad (38)$$

where

$$Q_s = (s+\nu)(s+\nu+m) \quad (38-1)$$

$$P_s = 2s(2\nu+m+1-2c+s) \quad (38-2)$$

The eigenvalues Λ_{mn} are related to the eigenvalues λ_{mn} by

$$\lambda_{mn} = -c^2 + 2qc - \frac{1}{2}(q^2+1-m^2) + \Lambda_{mn} \quad (39)$$

where

$$q = n + 1 \quad \text{while } (n-m) \text{ even} \quad (39-1)$$

$$q = n \quad \text{while } (n-m) \text{ odd} \quad (39-2)$$

Substituting in Eq. (38) the inverse power-series with respect to size parameter c :

$$\Lambda_{mn} = \sum_{i=1}^{\infty} \ell_i c^{-i} \quad (40)$$

and then expanding the continued fraction by doing same procedure as power-series expansion discussed in Section II, we can get the coefficients ℓ_i . The eigenvalues λ_{mn} of the oblate spheroidal differential equation would be:

$$\begin{aligned} \lambda_{mn} = & -c^2 + 2qc - \frac{1}{2}(q^2+1-m^2) - q(q^2+1-m^2)2^{-3}c^{-1} - [(5q^4+10q^2+1)-2m^2(3q^2+1)+m^4]2^{-6}c^{-2} \\ & - q[(33q^4+114q^2+37)-2m^2(23q^2+25)+13m^4]2^{-9}c^{-3} - [(63q^6+340q^4+239q^2+14) - \\ & 10m^2(10q^4+23q^2+3)+3m^4(13q^2+6)-2m^6]2^{-10}c^{-4} - q[(527q^6+4139q^4+5221q^2+1009)- \\ & m^2(939q^4+3750q^2+1591)+5m^4(93q^2+127)-53m^6]2^{-13}c^{-5} - [(9387q^8+101836q^6+ \\ & 205898q^4+86940q^2+3747)-12m^2(1547q^6+9575q^4+8657q^2+701)+6m^4(1855q^4+5078q^2+939)- \\ & 12m^6(167q^2+85)+51m^8]2^{-17}c^{-6} + 0(c^{-7}) \end{aligned} \quad (41)$$

In order to obtain the accurate spheroidal eigenvalues, we should substitute the expression of spheroidal eigenvalues with higher order terms for Bouwkamp's or asymptotic expansion, as the initial values, into Eq. (2). Since the terms in the multipole expansion have been developed in such a high order that the initial eigenvalues will be immediately bound within the convergence circles. Therefore, the final eigenvalues λ_{mn} can be easily reached by iterated procedures at very fast convergence rates.

The spheroidal eigenvalues λ_{mn} , the spheroidal angular functions S_{mn} , and the spheroidal radial functions R_{mn} , together with the boundary conditions matching, make the computational electromagnetic scattering problems solvable.

REFERENCES

1. C.J. Bouwkamp, "On Spheroidal Wave Functions of Order Zero", J. Math. Phys., 26, 79 (1947).
2. J. Meixner, "Asymptotische Entwicklung der Eigenwerte und Eigenfunktionen der Differentialgleichungen der Sphäroidfunktionen und der Mathieuschen Funktionen", Z. angew. Math. Mech., 28, 304 (1948).
3. J. Meixner and F.W. Schäfke, "Mathieusche Funktionen und Sphäroidfunktionen", Springer-Verlag, Berlin (1954).
4. J.A. Stratton, P.M. Morse, L.J. Chu, J.D.C. Little, and F.J. Corbató, Spheroidal Wave Functions, The Massachusetts Institute of Technology Press (1956)
5. C. Flammer, Spheroidal Wave Functions, Stanford University Press (1957).
6. Wan-xian Wang, "Corrections and Developments on the Theory of Scattering by Spheroid — Comparison with Experiments", presented at 1986 CRDEC Scientific Conference on Obscuration and Aerosol Research, Aberdeen, MD (June 1986).
7. Wan-xian Wang, "Power-Series Expansion of the Eigenvalues for Spheroidal Differential Equation", presented at 1986 CRDEC Scientific Conference on Obscuration and Aerosol Research, Aberdeen, MD (June 1986).
8. R. Sips, "Représentation Asymptotique des Fonctions de Mathieu et des Fonctions d'onde Sphéroidales", Trans. Amer. Math. Soc., 66, 93 (1949).
9. E.L. Ince, "Researches into the Characteristic Numbers of the Mathieu Equation", Royal Soc. Edinburgh Proc., 46, 316 (1926).

K T Wong and P S Excell
Schools of Electrical & Electronic Engineering, University of Bradford,
West Yorkshire, BD7 1DP, U.K.

Abstract

Experiences of modelling a log-periodic antenna (tapered transmission line type) using NEC are reported. The antenna is required as a component of a near-field EMC test range, and hence computation of the near fields was the primary objective although some discussion of impedance is presented.

Measurements of the near field of the real antenna were undertaken on a planar measurement range having the ability to scan planes at varying distances from the antenna. The measurements show good agreement with the predictions of NEC.

Introduction

As part of a programme to investigate design parameters for low-cost compact ranges for EMC testing [1,2], the use of an array of seven broadband elements in a hexagonal array is being investigated. The elements currently being evaluated are log-periodic dipole antennas of a standard type intended to operate over the range from 850 to 1800 MHz (Jaybeam Limited, type 7085). These antennas are of a standard design (Fig. 1), constructed from metal rods and having a tapered (V-shape) transmission line. For ease of construction, all of the radiating elements are made of rods of the same cross-sectional diameter, although this deviates from the ideal for log-periodic antennas.

In order to facilitate rapid prediction of the behaviour of arrays of these antennas, a single example was modelled using NEC [3], concentrating on the near-field distributions, and validated by making direct measurements of the near fields of a real antenna using a three-dimensional Cartesian probe-scanning system in an anechoic chamber [4].

The NEC Model

The radiating elements of the antenna shown in Fig. 1 are cylindrical rods, all having the same constant cross-sectional diameter (9 mm), and the transmission line is a pair of tubes with constant square cross-section (12 mm wide). To model this antenna with NEC, the radiating elements can be represented by wires. The transmission line elements may also be represented by wires, in which case they are modelled by circular wires with a cross-sectional perimeter equal to that of the square (i.e. 7.64 mm radius).

Since the width of the tubes is a relatively large fraction of a wavelength at the upper limit of the operating frequency range, and since the tubes

come relatively close together at the feed point, some consideration was given to a more detailed model of the square tubes.

A wire grid model could be used, constructed from eight parallel longitudinal wires connected by a sequence of transverse squares of wire: this approach was rejected due to the very large number of segments that would be required. A representation using surface patches was tried but the results were very unsatisfactory (severe errors in the polarisation of the computed near field) and the approach was abandoned.

The upper and lower halves of the antenna are not mirror images of each other and hence reflection cannot be used to simplify data input. It is, however, possible to model one half of the antenna and then rotate it through 180° about the main lobe axis to generate the lower half.

With the wire model of the transmission line it is not possible to satisfy the criterion for the ratio of segment length (Δ) to wire radius (a) unless the extended thin-wire kernel is used, due to the intricacy of the structure. Even so, it is impossible to avoid Δ/a ratios of somewhat less than the desirable minimum of two in a few segments at the upper limit of the operating frequency range.

The vertical rod joining the ends of the transmission line tubes at the rear of the antenna was modelled as a cylindrical wire, and a segment containing a voltage generator was connected to the front ends of the two transmission line tubes. No attempt was made to model the support structure beyond the vertical rod.

Physical measurements with a planar near-field probe scanner

Near field measurements were carried out in an anechoic chamber containing a probe positioner capable of measuring the field at any point in a cubical volume. In the present case, measurements were performed on two planes oriented normally to the nominal antenna boresight direction at distances of 400 and 800 mm from the feed point of the antenna. The electric field probe used was an electrically-short dipole (46 mm overall length), connected to a coaxial cable via a broadband balun. In practice, it was found that the performance of the balun was not ideal, leading to a certain amount of residual 'boresight error' in the probe at most frequencies. This effect was cancelled out by taking the average of two sets of measurements, the probe being rotated through 180° between each set. The fields were measured over symmetrical one-metre scan widths along the two principal transverse axes only (x and y co-ordinates). The sample spacing used was 100 mm at 850 and 1000 MHz and 50 mm at 1800 MHz. According to the Nyquist sampling criterion, these spacings will resolve evanescent modes with vector wave numbers having imaginary z-components of 25.9 m^{-1} , 23.4 m^{-1} and 50.2 m^{-1} respectively. At the minimum scanning distance of 400 mm, such modes will be attenuated by 90, 81 and 174 dB respectively, compared with their values on the nominal aperture plane passing through the feed point of the antenna. It is thus concluded that the sample spacings used are adequate to resolve the detailed structure of the near field distribution at the distances chosen.

Computation using NEC

Using the input data set generated as described above, NEC was run on an Amdahl 5890-300 computer. The total number of segments used at the three frequencies of interest (for the single wire representation of the transmission line) is shown in Table 1, together with the corresponding CPU times.

Comparison of results

Figures 2 to 4 show the computed and measured results. Only the magnitude of the dominant x-component of the electric field is shown, as this is the most useful for comparison purposes, being directly proportional to the probe output voltage. All of the results shown are normalised to give 0 dB amplitude and 0° phase in the centre of the distribution at $Z = 400$ mm.

Comparison of the predicted and measured amplitude distributions shows reasonably good agreement, the maximum discrepancy being around 1 dB. The agreement observed between the phase measurements and the NEC predictions is excellent, even in the regions of rapid phase change at the higher frequencies: the maximum phase discrepancy being about 10°.

Table 2 gives a comparison of the VSWR, as calculated from the input impedance predicted by NEC, and the corresponding typical values given by the antenna manufacturer. These figures show remarkably good agreement at lower frequencies, but this deteriorates at the upper end of the range.

Conclusions

The results of computation of the near fields of a log-periodic dipole antenna, using NEC, have been presented and compared with measurements on a real antenna obtained using a planar near-field probe positioner.

Although some doubts were entertained concerning the validity of use of a cylindrical wire model for the square tubes forming the transmission line, the agreement between the measured results and the NEC predictions using the wire representation is very good, showing a maximum error of about 1dB in the amplitude and 10° in the phase. Attempts to use a more detailed model for the transmission line were unsuccessful.

The antenna VSWR deduced from the NEC predictions of the impedance shows good agreement with the manufacturer's typical data for the real antenna although the agreement deteriorates at the upper end of the nominal operating band of the antenna.

Work on the modelling and testing of arrays of these antennas is proceeding.

References

1. Excell, P S and Gunes Z F: 'The compact range principle applied to electromagnetic susceptibility testing', IERE Conf. Pub. No. 56, 'Electromagnetic Compatibility', 1982, pp. 317-322.

2. Excell, P S: 'Assessment of errors in radiative susceptibility and emission testing in a compact range', IERE Conf. Pub. No. 60, 'Electromagnetic Compatibility, 1984, pp. 33-38.
3. Burke, G J and Poggio, A J: 'NEC-Method of Moments', NOSC TD116, 1981.
4. Rousseau, M and Excell, P S: 'Computation of the field distribution in a broadband compact range for EMC applications', IEE Conf. Pub. No. 274, 'Antennas & Propagation', 1987, pp.395-398.

Acknowledgements

This work forms a part of a project funded by the UK Science and Engineering Research Council. The planar probe positioner and its control system were built by Moshe Rousseau.

Listing of NEC input deck for LPDA at 1000MHz

(NEC modified for free-format input)

CM CALCULATE THE NEAR FIELDS OF A LPDA, WITH THE TRANSMISSION LINE
 CM REPRESENTED BY A SERIES OF CIRCULAR RODS, THE ENDS
 CM OF THE RODS COINCIDING WITH THE RADIATING ELEMENTS.

CM FREQUENCY = 1000 MHZ

CM RADIUS OF CIRCULAR RODS = 7.64 MM

CE

GW 101	1	0	0.012	-0.040	0	0.01545	-0.06728	0.00764
GW 102	1	0	0.01545	-0.06728	0	0.01777	-0.08564	0.00764
GW 103	1	0	0.01777	-0.08564	0	0.02040	-0.10647	0.00764
GW 104	1	0	0.02040	-0.10647	0	0.02341	-0.13028	0.00764
GW 105	1	0	0.02341	-0.13028	0	0.02654	-0.15509	0.00764
GW 106	1	0	0.02654	-0.15509	0	0.03030	-0.18485	0.00764
GW 107	2	0	0.03030	-0.18485	0	0.03456	-0.21858	0.00764
GW 108	2	0	0.03456	-0.21858	0	0.03888	-0.25281	0.00764
GW 109	2	0	0.03888	-0.25281	0	0.04383	-0.29200	0.00764
GW 110	2	0	0.04383	-0.29200	0	0.04935	-0.33565	0.00764
GW 111	2	0	0.04935	-0.33565	0	0.05537	-0.38327	0.00764
GW 112	2	0	0.05537	-0.38327	0	0.06238	-0.43883	0.00764
GW 113	4	0	0.06238	-0.43883	0	0.07542	-0.54201	0.00764
GW 1	1	0	0.01545	-0.06728	-0.023	0.01545	-0.06728	0.0045
GW 2	1	0	0.01777	-0.08564	0.026	0.01777	-0.08564	0.0045
GW 3	2	0	0.02040	-0.10647	-0.031	0.02040	-0.10647	0.0045
GW 4	2	0	0.02341	-0.13028	0.034	0.02341	-0.13028	0.0045
GW 5	2	0	0.02654	-0.15509	-0.038	0.02654	-0.15509	0.0045
GW 6	2	0	0.03030	-0.18485	0.043	0.03030	-0.18485	0.0045
GW 7	2	0	0.03456	-0.21858	-0.048	0.03456	-0.21858	0.0045
GW 8	3	0	0.03888	-0.25281	0.054	0.03888	-0.25281	0.0045
GW 9	3	0	0.04383	-0.29200	-0.061	0.04383	-0.29200	0.0045
GW 10	3	0	0.04935	-0.33565	0.068	0.04935	-0.33565	0.0045
GW 11	3	0	0.05537	-0.38327	-0.076	0.05537	-0.38327	0.0045
GW 12	4	0	0.06238	-0.43883	0.084	0.06238	-0.43883	0.0045
GM 100	1	0	0 0 180	0 0 0	0 0			
GW 9999	1	0	-0.012	-0.040	0	0.012	-0.040	0.00732
GW 999	5	0	-0.07542	-0.54201	0	0.07542	-0.54201	0.0125
GE	0 0	0 0 0	0 0 0	0 0				
EK	0 0 0 0 0	0 0 0 0 0						
FR	0 0 0 0	1000	0 0 0 0 0					
EX	0 9999	1 01 1	0 50 0 0 0					
NE	0	11 11	2 -0.5 -0.5	0.4	0.1 0.1	0.4		
EN	0 0 0 0 0	0 0 0 0 0						

Table 1: Total CPU Times on Amdahl 5890 - 300

Frequency (MHz)	No. of Segments in model	CPU time (s)
850	102	5.27
1000	106	5.42
1800	153	15.27

Table 2: Comparison of VSWRs derived from NEC with Manufacturer's
Typical Data

Frequency (MHz)	VSWR	
	NEC	Mfr
850	3.8	3.4
1000	3.0	3.0
1100	3.5	2.7
1400	3.3	3.3
1800	2.0	3.5
2000	1.9	3.3

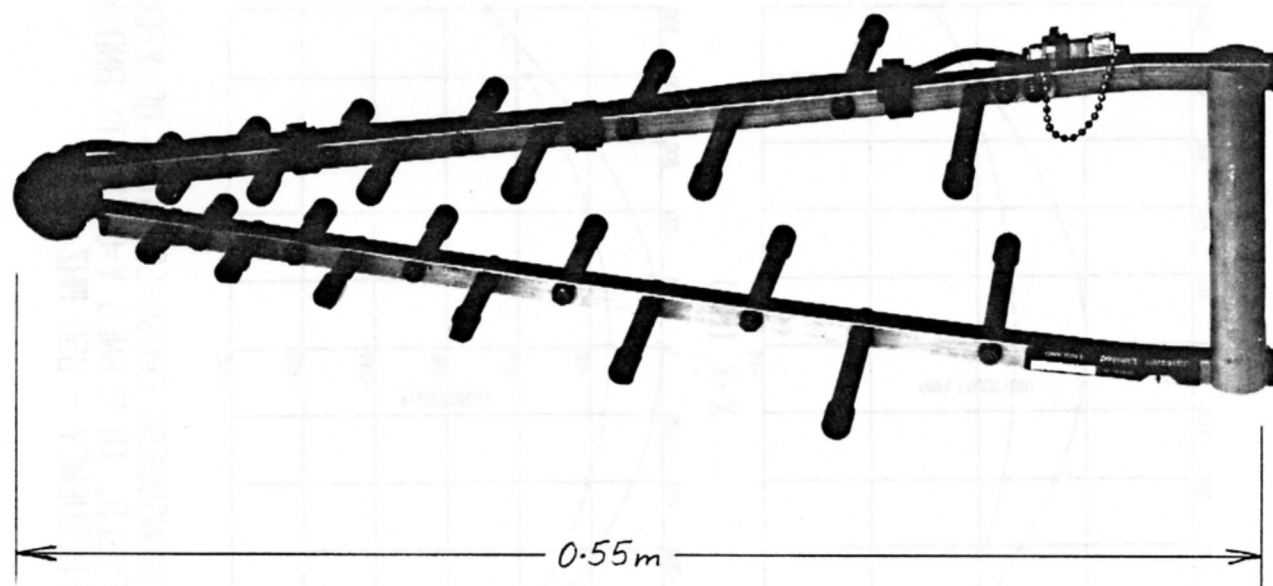


Fig. 1: The log-periodic dipole antenna

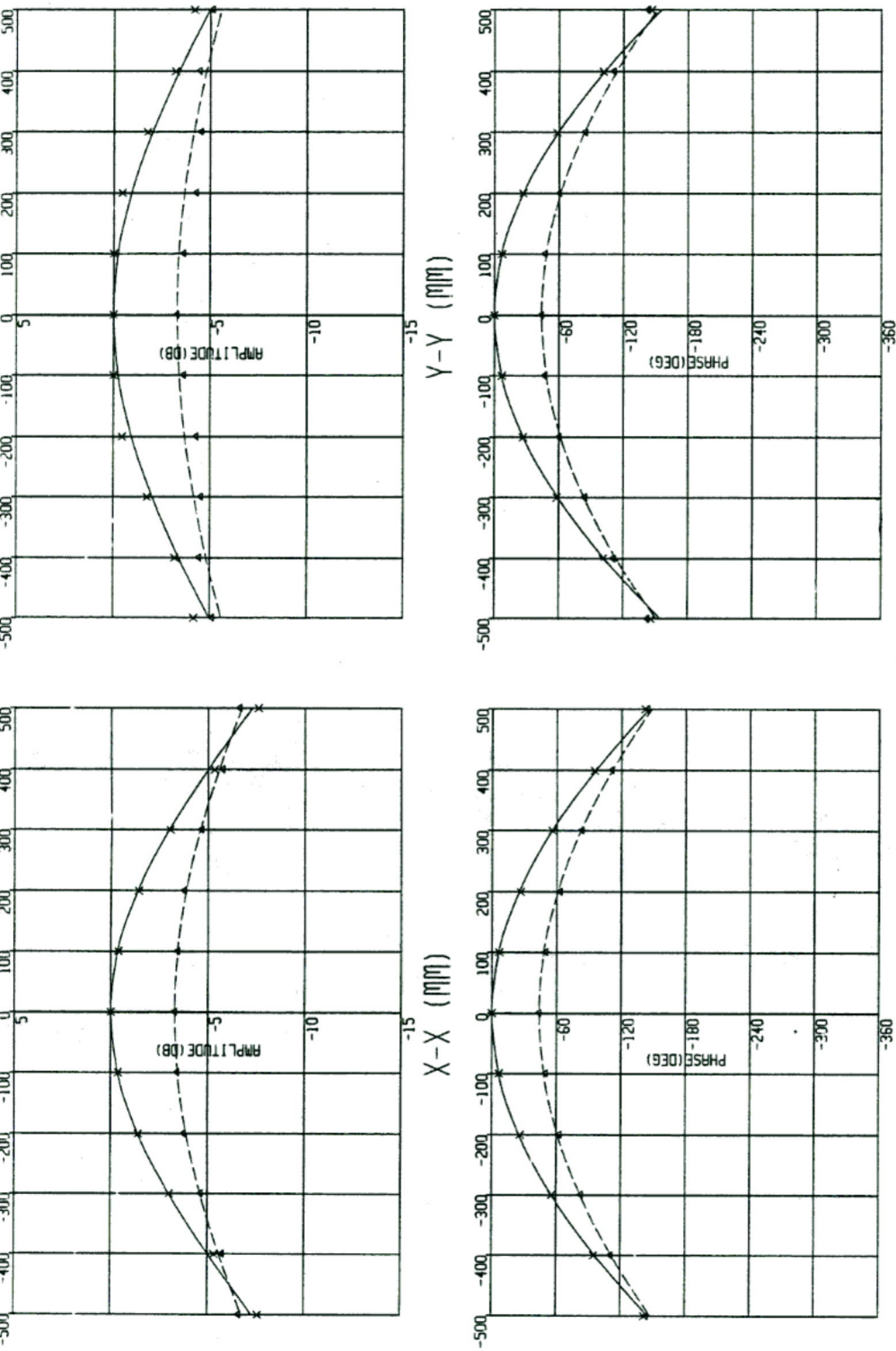


FIG. 2 : TRANSVERSE CROSS-SECTIONS OF X-COMPONENT OF NEAR ELECTRIC FIELD, IN PLANES Y=0 (LEFT) AND X=0 (RIGHT).
 FREQUENCY = 850 MHz

x	MEASUREMENT, Z=400 mm
—	NEC, Z=400 mm
△	MEASUREMENT, Z=800 mm
- - -	NEC, Z=800 mm

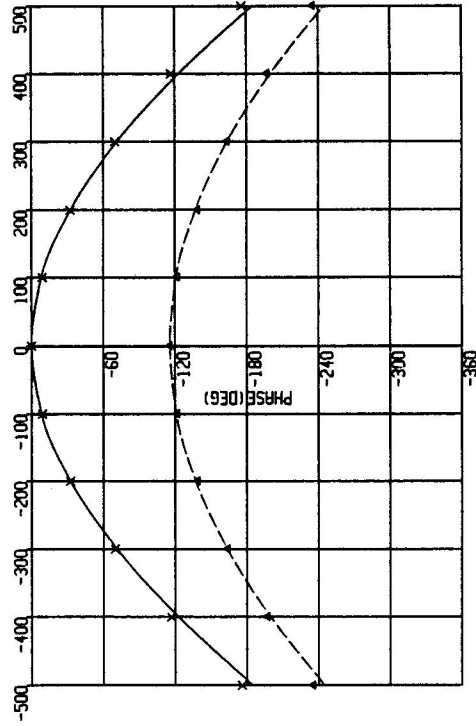
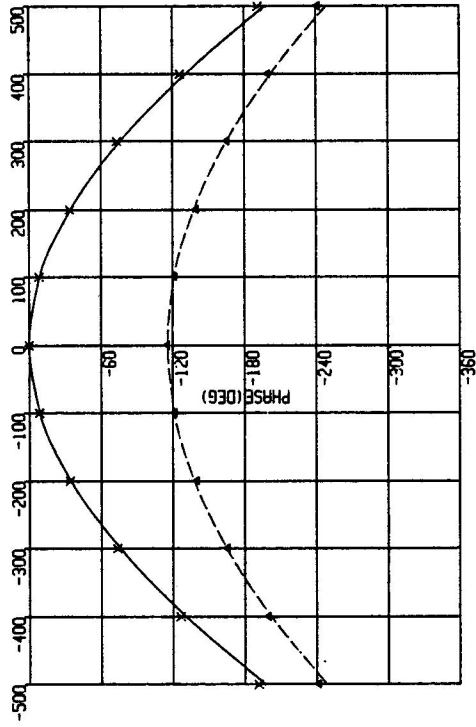
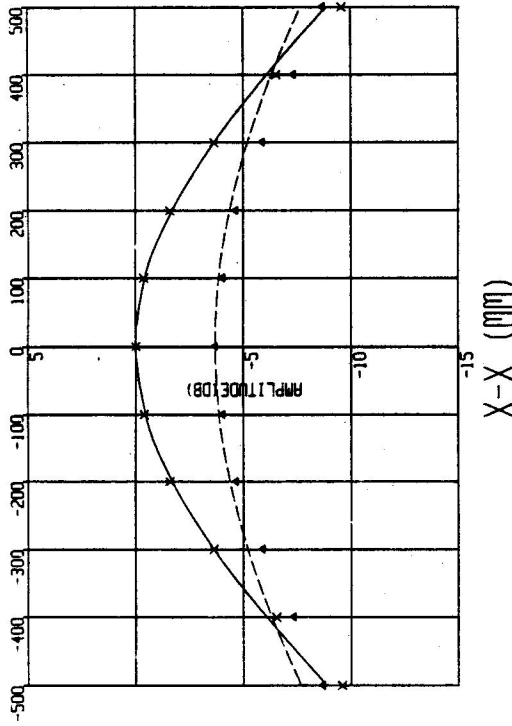
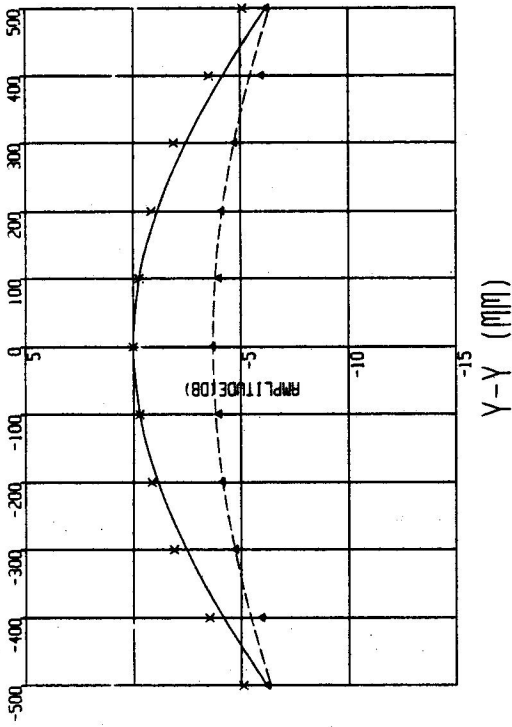


FIG. 3 : TRANSVERSE CROSS-SECTIONS OF X-COMPONENT OF NEAR ELECTRIC FIELD, IN PLANES Y=0 (LEFT) AND X=0 (RIGHT).
 FREQUENCY = 1000 MHz

x	MEASUREMENT, Z=400 MM
—	NEC, Z=400 MM
△	MEASUREMENT, Z=800 MM
- - -	NEC, Z=800 MM

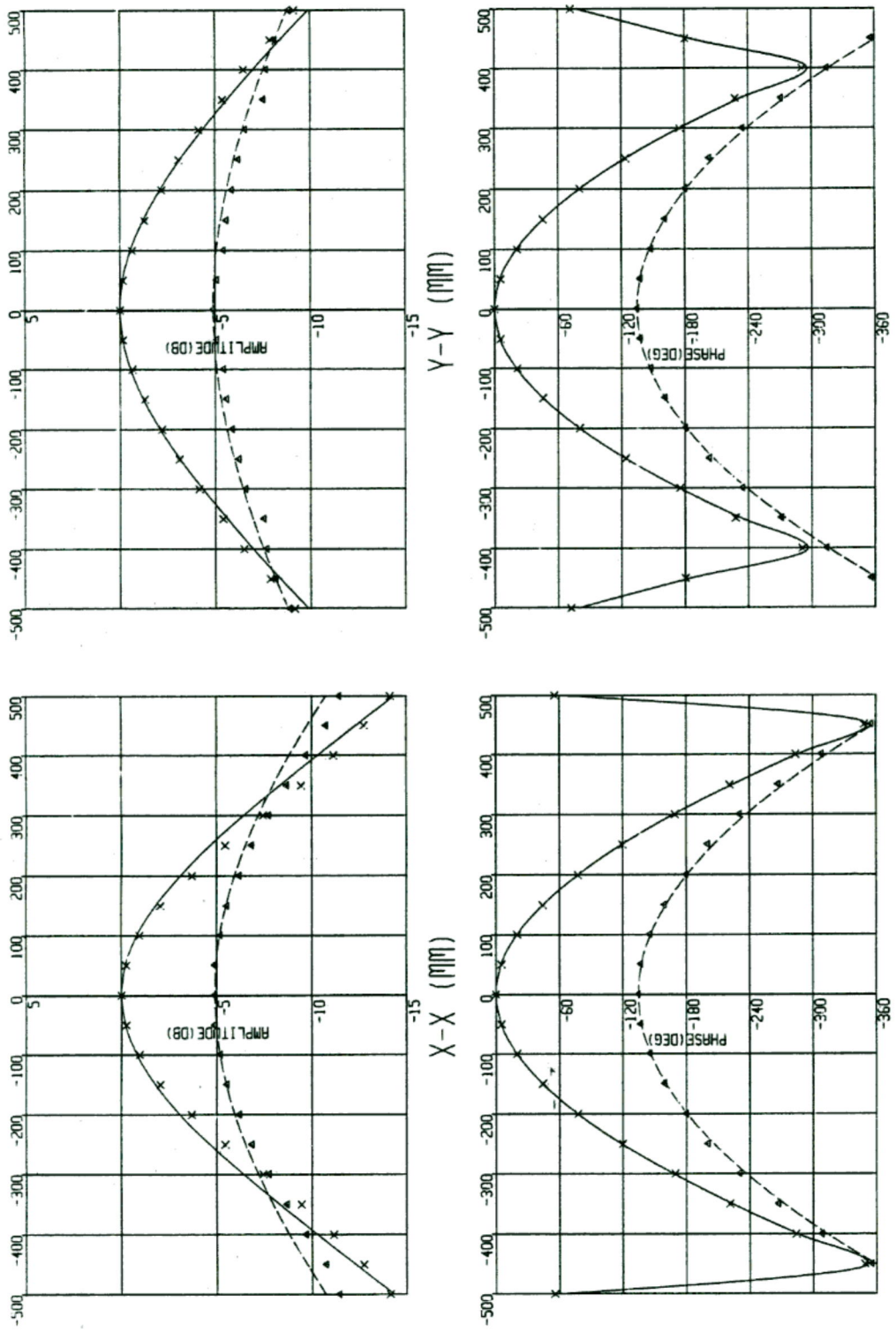


FIG. 4 : TRANSVERSE CROSS-SECTIONS OF X-COMPONENT OF NEAR ELECTRIC FIELD, IN PLANES Y=0 (LEFT) AND X=0 (RIGHT). FREQUENCY = 1800 MHz

x	MEASUREMENT, Z=400 MM
Δ	MEASUREMENT, Z=800 MM
—	NEC, Z=400 MM
- - -	NEC, Z=800 MM

THE APPLICATION OF THE CONJUGATE
GRADIENT METHOD TO THE SOLUTION OF
OPERATOR EQUATIONS - AN UNCONVENTIONAL PERSPECTIVE

Tapan K. Sarkar
Ercument Arvas
Department of Electrical Engineering
Syracuse University
Syracuse, New York 13244-1240

ABSTRACT: This narrative presents an alternate philosophy for the accurate solution of operator equations, you might say "both singular and nonsingular" in general. In this approach, we try to solve the exact operator equation in an approximate way, quite differently from the matrix methods which try to solve the approximate operator equation in an exact fashion. The advantage of this new philosophy is that convergence is assured and a priori error estimates are available. The conjugate gradient methods are numerical methods which provide a means to reach this new goal, as opposed to an efficient means of just solving matrix equations, which some researchers have assumed them to be. We thereby take the position that there is a heaven-and-hell difference between the application of the conjugate gradient method to solve an operator equation and its application to the solution of matrix equations.

1. THE BASIC PHILOSOPHY: The objective is to solve the operator equation $AX = Y$, where A is the known integro-differential operator and X is the unknown to be solved for the known excitation Y . The actual problem setting is in an infinite dimensional space, which in simple terms means that we have an infinite number of unknowns to be solved for. Historically, the matrix methods, starting with Method of Moments, have first projected the original problem posed in an infinite dimensional space to a finite dimensional space (described by the moment matrix) and then have tried to solve the approximate finite dimensional problem exactly using Gaussian elimination and, in recent times, with the iterative methods, particularly the conjugate gradient method. Unfortunately, this basic philosophy lacks mathematical rigor. The area in which this manifests itself is a complete lack of theoretical convergence analysis of the sequence of solutions for an arbitrary operator equation. Whatever convergence analysis exists for matrix methods is generated from numerical experimentation of a particular problem. Hence, there is no guarantee that as the number of unknowns is increased, there is a monotonic convergence of the sequence of approximate solutions [1-2].

What we have tried to do over the years is to usher in a new concept and also point out the deficiencies of the conventional matrix methods. The approach taken by us and Van den Berg [3] are philosophically the same and similar to the work of Hayes [4]. The basic philosophy is simple: Let us not discretize the problem right from the beginning or assume a set of known expansion functions by projecting the operator to a finite dimensional space. Let us see if we can develop a theoretical solution symbolically in an exact fashion. It is at this stage, that our philosophies differ radically from the conventional matrix methods viewpoint. First let us see if we can find a solution to the exact operator equation - let it be in a symbolic fashion. By developing the solution in this way, we have an absolute guarantee to begin with, namely that as the degree of approximation is increased, we indeed have

a monotonic convergence of the solution and that in the limit our solution converges to the exact solution. So in our method, we start with the "blessings" of convergence and, unlike matrix methods, we do not have to "tweak" the expansion functions sometimes in midstream to generate meaningful results. Now we observe that the computer cannot generate the exact solution or, for that matter, follow the exact recipe to reach the solution as it cannot handle an infinite number of unknowns. Therefore, we try to approximate the exact solution.

In summary, the matrix methods first approximate the operator equation and then seek to solve it exactly, whereas in our approach we try to solve exactly the operator equation by utilizing an iterative method, say one of the conjugate gradient methods [5-7] (there are various versions of the conjugate gradient method) and then approximate the exact recipe numerically, yielding an approximate solution. The reward of following the latter procedure is that there is an unconditional guarantee of monotonic convergence to the true solution, as the number of unknowns is increased without "tweaking" any expansion or weighting functions. No such statements can be made for matrix methods, indicating that there are some fundamental differences, in reality, between these two procedures - differences which are not tautological.

In the next section we show how to utilize this new operator form to generate solutions.

2. THE ACT:

Consider the following integral equation:

$$\int_0^1 f(x') \cos \pi(x-x') dx' = \sin \pi x ; 0 \leq x \leq 1 \quad (1).$$

The objective is to solve for $f(x)$. Before we start number crunching let us take a few moments to "meditate" over the problem. The first question that is raised is: does a solution to this problem exist? The existence of the solution of an operator equation is given by the Fredholm Alternative Theorem, which states that a solution to $AX = Y$ exists, iff Y is orthogonal to every non-trivial solution of the homogeneous adjoint equation $A^*u = 0$, where A^* is the adjoint operator. Hence for a solution to exist all u must be orthogonal to Y . If this condition is violated then a solution to the problem does not exist. In this example, we have a self-adjoint operator, since

$$\langle Au; v \rangle = \int_0^1 dx v(x) \int_0^1 dx' u(x') \cos \pi(x-x') = \langle u; A^*v \rangle; \text{ so } A=A^*. \quad (2)$$

By expanding the kernel

$$\cos \pi(x-x') = \cos \pi x \cos \pi x' + \sin \pi x \sin \pi x'$$

it is seen that there is an infinite set of nontrivial solutions to the adjoint homogeneous equation. Hence, unless Y is orthogonal to all such solutions u , we are just wasting our time trying to solve this problem. It is seen that $\sin \pi x$ is orthogonal to all such solutions ($\sin m\pi x$ and $\cos m\pi x$ for

$m > 1$ and m odd) of the homogeneous equation and hence the solution to the problem exists. However, the solution is not unique, as a solution to the homogeneous equation can be added to any solution creating a different solution.

But, what has "existence" got to do with electromagnetics? All electromagnetics problems do not have solutions! Consider the problem of electromagnetic scattering from a closed conducting structure at a frequency corresponding to the internal resonant frequency of the same structure. This problem has been recently addressed quite exhaustively!!!. Now the simple truth is that the above problem, when represented by an electric field integral equation, has for the homogeneous equation a nontrivial solution, and unless the excitation is orthogonal to every solution of the homogeneous equation, a solution to the problem does not exist according to the Fredholm alternative. Therefore, instead of trying to solve a problem which is not solvable mathematically, we think we ought to pose the problem in a different way. Yet, methods are still being researched as how to solve this unsolvable problem! An interested reader should look at the development of the modified Green's function as discussed on pp.215-218 of Stakgold[8].

Next, questions about uniqueness, ill-conditioning and the like are addressed. The operator in (1) has a nontrivial solution to the homogeneous equation and it is a positive semidefinite operator. Hence, any matrix methods utilized to solve this equation will fail as the matrix is singular. The strength of the conjugate gradient method lies in the fact that it can solve singular operator equations and the user does not have to worry about the nature of the equation. But, now comes the question: what is the meaning of the solution if the operator is singular? It turns out that the conjugate gradient method will yield the minimum norm solution, if the iteration was started with a zero initial guess. The minimum norm solution implies that of all the possible solutions of this equation, the conjugate gradient method will yield a solution which has the least energy. The solution procedure for a positive semidefinite operator will start with $x_0 = 0$ and residual $r_0 = Y - AX = \sin \pi x$. Since the operator is self-adjoint, $P_0 = r_0 = \sin \pi x$.

We update $x_1 = x_0 + a_0 p_0$, where $a_0 = \|r_0\|^2 / \langle Ap_0; p_0 \rangle = 2$ and $x_1 = 2 \sin \pi x$ and $r_1 = 0$ and hence $2 \sin \pi x$ is the minimum norm solution. It can be shown that another solution $q = (-\pi^3/4)x(x-1)$ also satisfies (1). However,

$$\|x_1\|^2 = \int_0^1 |x_1|^2 dx > \int_0^1 |q|^2 dx$$

and the second solution is not minimum norm. So if we have an ill-conditioned problem, in this case perfectly singular, we can find the minimum norm solution through the use of iterative methods. Direct methods do not work well for ill-conditioned, singular problems. Observe that we have utilized the conjugate gradient method to solve the operator equation directly as first suggested by Hayes [4].

In electromagnetics problems, for example, evaluation of Ap_0 and $\|x_1\|^2$ cannot be done analytically. Hence, we have to evaluate these quantities numerically. It is at this point that we introduce numerical

approximations. An additional advantage of handling it in this way is that one can have a grasp on the numerical value of the discretization error. The discretization error in the evaluation of $A p_0$ and $\|x_1\|$ can be minimized by simply taking more samples of the functions of interests. For such situations, the residual $AX_n - Y$ will never go to zero as $n \rightarrow \infty$. Whatever is left will be the discretization error.

3. EPILOGUE: For illustrative purposes, it is educational to look into the philosophical differences of first discretizing the operator equation and then finding an exact solution to the problem, as opposed to first finding a symbolically exact solution and then finding an approximation to that. In the conventional matrix methods, let us assume that the elements of the matrix have been integrated with sufficient degree of accuracy (even if one chooses a Galerkin procedure) and the final error is always zero as the matrix equation has been solved to the machine precision using either Gaussian elimination or conjugate gradient or by any other method.

Now in the conjugate gradient solution of the operator equation, there are two errors. First the error in the generation of the sequence of the approximation, i.e. $\|x_{\text{exact}} - X_n\|$ after m iterations and, secondly, the discretization error made in the evaluation of AX_n . If we perform a large number of iterations, presumably $\|x_{\text{exact}} - X_n\| \rightarrow 0$, whereas the operator $(AX_n - Y)$ would not be zero due to discretization error. So by applying the conjugate gradient method directly to the solution of the operator equation, it is seen that the final error may never become zero, unlike that of matrix methods. The global residual error provides an estimate of the discretization error (i.e. we have obtained X_{exact} subject to the stated discretization error). If this error is large, finer discretization may be preferred. Also no "tweaking" of the expansion functions is involved when one applies the conjugate gradient method directly to the solution of the operator equation. This is the same philosophy in Van den Berg's approach.

Another point to make: What is the difference between applying the iterative method to the solution of the matrix equation, where each element of the matrix is evaluated at each iteration and the storage decreases from N^2 to $6N$, as opposed to applying the conjugate gradient method directly to the solution of the operator equation? It is interesting to note that the application of the conjugate gradient method directly to the solution of an operator equation may sometimes even be computationally more efficient than computing the matrix elements once and using them at each iteration, particularly, when the scatterer geometry fits into an FFT (Fast Fourier Transform) grid [6-7]. However, for an arbitrarily shaped structure, it may not be efficient in some instances to use FFT to perform the evaluation of the convolution. In that case, application of an iterative method directly to the solution of an operator-application of an iterative method directly to the solution of an operator equation may be rather time consuming. However, in spite of this disadvantage, the reward of applying the conjugate gradient method directly to the solution of the operator equation lies in the fact that not only does one have a handle on the discretization error, but also he can solve a problem to a "global" prespecified degree of accuracy.

CONCLUSION: An alternate philosophy is presented for solving operator equations. In this new philosophy the exact system is solved in an approximate numerical fashion as opposed to solving an approximate matrix

equation in an exact way. The advantage of this new philosophy is that convergence to the exact solution is guaranteed and a priori error estimates are available. The conjugate gradient method therefore just turns out to be a method which accomplishes our desired objective of formulating and evaluating a symbolic exact solution of the problem. The use of the conjugate gradient method is distinctly different from its use in solving moment-method matrix equations, sometimes in an efficient way. The basic difference between these two philosophies is the stage at which numerical discretization is made. Our claim is that the new philosophy just presented not only guarantees absolute convergence but also an estimate of the numerical discretization error incurred in the actual solution of the problem.

REFERENCES:

- [1] T. K. Sarkar, "The conjugate gradient method as applied to electromagnetic field problems", IEEE Trans. Antennas and Propagation Newsletter, Aug. 1986, pp. 5-14.
- [2] T. K. Sarkar, "Reply to comments on "Application of FFT and conjugate gradient method for the solution of electromagnetic scattering from electrically large and small conducting bodies", IEEE Trans. Antennas and Propagation", vol. AP-35, No. 5, May 1987, pp. 608-609.
- [3] P. M. Van den Berg, "Iterative computational techniques in scattering based upon the integrated square error criterion", IEEE Trans. Antennas and Propagation", vol. AP-32, No.10, October 1984, pp. 1063-1071.
- [4] R. M. Hayes, "Iterative methods of solving linear problems in Hilbert space", in contributions to the solution of systems of linear equations and the determination of eigenvalues", O. Taussky, ed. NBS Appl. Math. Ser., vol. 39, pp. 71-104, 1954.
- [5] T. K. Sarkar and E. Arvas, "On a class of finite step iterative methods (conjugate directions) for the solution of an operator equation arising in electromagnetics", IEEE Trans. Antennas and Propagation, vol. AP-33, No.10, October 1985, pp. 1058-1066.
- [6] T. K. Sarkar, "On the application of the Generalized BiConjugate gradient method", Journal of Electromagnetic Waves and Applications, Vol. 1, No.3, July 1987, pp. 223-242.
- [7] T. K. Sarkar, E. Arvas and S. M. Rao, "Application of the fast fourier transform and conjugate gradient method for the solution of electromagnetic scattering from electrically large and small conduction bodies", IEEE Trans. Antennas and Propagation, vol. AP-34, No.5, May 1986, pp. 635-640.
- [8] I. Stakgold, "Green's Functions and Boundary Value Problems", J. Wiley & Sons, New York, 1973.

1988 INSTITUTIONAL MEMBERS

MARTIN MARIETTA AEROSPACE

Research Library 1565
P.O. Box 179
Denver, CO 80201

KATHREIN INC.

William A. Wickline, President
26100 Brush Ave. Suite 319
Euclid, OH 44132

THE PILLSBURY COMPANY

Research & Development Laboratories
311 Second St. Southeast
Minneapolis, MN 55414

DEPARTMENT OF THE NAVY

Base Library Bldg. 437
485 EIG/EIEUS
Griffiss AFB, NY 13441

IMAGINEERING LIMITED

E.A. Bogdanowicz, Senior Vice-President
95 Barber Greene Rd.
Suite 112
Don Mills, Ontario, Canada M3C 3E9

DEPARTMENT OF THE ARMY

US Army Foreign Science & Technology Center
220 Seventh St. NE.
Charlottesville, VA
22901-5396



**Leadership in Computational
Electromagnetics
-Giving Shape to Imagination**

Advanced Systems Technology
Orgn. 91-60 Bldg. 256
3251 Hanover Street, Palo Alto, CA 94304-1191
(415) 424-3390

TECHNOLOGY FOR COMMUNICATIONS INTERNATIONAL

President—John W. Ballard
Vice President Broadcast and Communications Division—Gerald E. Solberg
1625 Stierlin Road, Mountain View, CA 94043, Phone: 415/962-5200
Vice President Information Systems Division—Don Webster
34175 Ardenwood Boulevard, Fremont, CA 94536-7800, Phone: 415/795-7800
Broadcast and Communications Division products include ultra-high gain steerable HF antenna arrays used in OTH radar and communications as well as an extensive line of broadband HF antennas, accessories and transportable tactical antennas for military applications. High power short and medium wave broadcast antennas are offered, together with transmission lines and transformers.
Information Systems Division products include HF, VHF and UHF signal acquisition, signal recognition and classification, and emitter location systems, applications for shore stations, mobile platforms and tactical transportable units.
TCI offers all its products on a turn-key basis.

CELWAVE

Rt. 79, Marlboro, NJ 07728

(201) 462-1880

Antenna System Products
Base Station Antennas
Cavity Devices
Tx-Combiners
Rx-Multicouplers
and Components
Cable
Mobile Antennas
Portable Antennas
Marine Antennas
and Accessories

Communicate With Us

Ford Aerospace & Communications Corporation, Western Development Laboratories Division in Palo Alto, California has immediate openings for you to join us on some of the most exciting projects in the communications industry. We have large, multi-year contracts in spacecraft construction.

Explore these opportunities to join us:

Space Systems Operation Microwave Design Engineers

Responsibilities will include analysis, development and design of satellite and ground communication systems. This position requires a minimum of 5 years of experience in microwave transponder/subsystem design. Familiarity with all aspects of communication systems preferred. TT&C transponder design or microwave circuit design capabilities are desirable. BSEE or equivalent, MS preferred.

Transponder Engineer

You will provide direction in the areas of RF communication system design and development, analyze component nonconformances and prepare review design inputs and other technical reports. Requires a BSEE or equivalent, MSEE preferred, and 8 years' experience in microwave, RF and communication theory. Expertise in allocating system requirements to the component level desired. Familiarity with satellite communication systems, TT&C transponders, modulation, demodulation and digital techniques a plus.

For the above positions, respond to Dept. RP-ACES12.

Satcom Terminals Operation Principal Engineer

If you would like a technical challenge as well as a program challenge, consider this position. A BSEE

or equivalent, MSEE preferred, and a minimum of 15 years' experience in satellite communication and Satcom Network Control Systems Design and Development are required. Systems design and integration of communications hardware for antenna, RF, baseband and network access subsystems are necessary. This position will require project leadership with responsibility for program schedules, costs and technical performance.

For the above position, respond to Dept. RP-ACES12.

Special Programs Operation Systems Design and Development Engineer

Working with phased array antenna systems and their RF components, you will conduct trade studies, select approaches, conduct customer design reviews and briefings, and prepare proposals and white papers. You will supervise the work of other engineers. Requires a BSEE/Physics or equivalent, and at least 10 years of experience, including 6 years in antenna subsystem design and development in microwave frequencies.

For the above position, respond to Dept. PF-ACES12.

Now.

To find out more, send your resume, indicating appropriate department, to Ford Aerospace & Communications Corporation, Western Development Laboratories Division, Professional Staffing, 3939 Fabian Way, M/S D04, Palo Alto, CA 94303-4697. An equal opportunity employer. Principals only, please.



Ford Aerospace &
Communications Corporation

Western Development Laboratories Division
U.S. Citizenship May Be Required.

ANTENNA / MICROWAVE CAREER OPPORTUNITIES

MANAGER OF ANTENNA SYSTEMS

• Lead antenna development of state-of-the-art communication networks. M.S.E.E. required, 15-plus years of design, development and test experience with microwave antenna systems; including reflectors, arrays and their associated beamforming networks. Salary starting at mid 60s.

ANTENNA TEST MANAGER

• Lead company's indoor and outdoor antenna test operations. Management experience and ability to specify purchases of test equipment. Salary open.

MICROWAVE ANTENNA ENGINEERS

• B.S.E.E. with 2-plus years experience to work with advanced design and development with phased array antenna RF microwave system design. Expertise desired in radiation, wideband components, power dividers and phase shifter circuitry. Familiarity with antenna testing and RCS measurement. Salary 30s to 70s.

COMMERCIAL ANTENNA DESIGN

• Project Engineer — design development of parabolic antennas for satellite, broadcast, and TVRO. Frequency C, Ku, band. Citizenship not required. Salary 40K++.

SENIOR SCIENTIST

• Ph.D. Satellite communication specialist to conduct R&D involving antenna, propagation, link analysis problems. Strong analysis, computer modeling and simulation experience. Salary open.

ENGINEERING MANAGER

• Lead the technical direction of a small, aggressive company. R&D, plus specialty antenna design, RCS and radome projects are the challenges that await the best. Salary 65K+.

E. J. Dort & Associates

Search Consultants / Antenna, Microwave & Communications

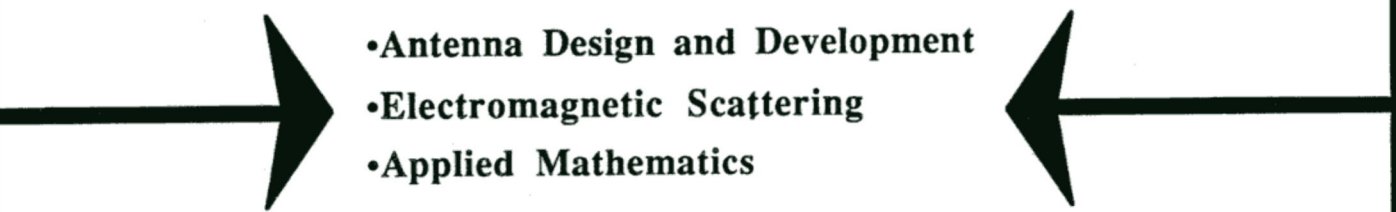
2100 Westpark Drive • Suite 201

Research Triangle Park, NC 27713

Call or Write for many other opportunities worldwide

Telephone (919) 544-1894

ATLANTIC AEROSPACE ELECTRONICS CORPORATION

- 
- Antenna Design and Development
 - Electromagnetic Scattering
 - Applied Mathematics

The Antenna Development Group at ATLANTIC AEROSPACE is seeking highly-qualified, self-motivated individuals to work in the above areas. An advanced degree is preferred.

ATLANTIC AEROSPACE, an employee-owned corporation, offers a technically-challenging environment and the opportunity to work with nationally-renowned founding members. An excellent compensation package includes competitive salary, liberal bonus pool, and the opportunity for equity (stock) participation. ATLANTIC AEROSPACE is a new company, being formed in 1985, but already has over 50 technical employees with the majority holding advanced degrees.

please contact: Dr. James R. Rogers (tel. 301-220-1501)
Atlantic Aerospace Electronics Corporation
6404 Ivy Lane, Suite 300
Greenbelt, Maryland 20770-1406

(Greenbelt is conveniently located between Washington, D.C. and Baltimore, Maryland.)

U. S. Citizenship is required
Atlantic Aerospace Electronics Corporation is an Equal Opportunity Employer